THE ACCURACY AND REPEATABILITY OF LODOX STATSCAN OSTEOMETRIC MEASUREMENTS

Bontle Mamabolo

A dissertation submitted to the School of Anatomical Sciences, Health Science Faculty,University of the Witwatersrand, for the degree of Masters of Science.

Johannesburg

2021

The financial assistance of the National Research Foundation (NRF) towards this research is hereby acknowledged. Opinions expressed and conclusions arrived at, are those of the author and not necessarily to be attributed to the NRF.

DECLARATION

I Bontle Mamabolo declare that this thesis is my own unaided work. It is being submitted for the degree of Master's of Science in Medicine at the University of the Witwatersrand, Johannesburg. It has not been submitted before for any degree or examination at any other University.

_____

Bontle Mamabolo

10th day of May 2021 at The University of the Witwatersrand, Faculty of Health Sciences, Johannesburg

PUBLICATIONS AND PRESENTATIONS ARISING FROM THESIS

Publication:

- Mamabolo, B., Alblas, A., Brits, D. (2020) Modern imaging modalities in forensic anthropology and the potential of low-dose x-rays. Forensic Imaging 23: 200406 (https://doi.org/10.1016/j.fri.2020.200406).

Presentation:

- An abstract entitled "The Accuracy and Repeatability of the Lodox Statscan Osteometric Measurements" was accepted for an oral presentation at the 48th Annual Conference of the Anatomical Society of Southern Africa (ASSA), Durban, South Africa. Regrettably this conference has been postponed due to the COVID-19 pandemic.
- A teaser of this research was presented during the virtual Word Anatomy Day (WAD) hosted by the Anatomical Society of Southern Africa (ASSA) (14 October 2020).

ABSTRACT

The rise of the use of radiographic imaging techniques in forensic science, propelled forensic anthropologists to explore virtual imaging modalities, in order to estimate biological profiles. This includes low-dosage X-ray (Lodox), which is currently operational in South African medico-legal laboratories.

This research aimed to compare the repeatability and accuracy of osteometric measurements taken from Lodox images of macerated bones, with that of the corresponding dry bone material. A total of 50 full-body Lodox images with corresponding dry bones were selected from the Kirsten Skeletal Collection. Forty-six standard osteometric measurements were collected from the Lodox images and the corresponding dry bone. The sample was equally distributed by sex and consisted of adults, aged 23-49. Where applicable, the left and right skeletal elements were both collected, resulting in 84 measurements collected from three datasets; the skull (n=9), pectoral girdle and upper limb (n=36), as well as the pelvic girdle and lower limb (n=39).

Using technical error of measurement (TEM), Lodox measurements were deemed repeatable (intra-observer rTEM < 1.5% and inter-observer rTEM < 2.0%), with exceptions of the intra- and inter-observer results of the; maximum ramus height, minimum ramus breadth, maximum length of clavicle, physiological length of ulna, maximum vertical diameter of the head of humerus, maximum diameter of the femoral head and the maximum and minimum diameter of the clavicle, humerus, radius, ulna, femur and fibula.

Using percentage differences, 72.6% of the measurements collected had percentage differences less than 10%. This consisted of the long bone measurements along the scan direction/y-axis. No significantdifference ($p>0.05$) was noted with 25% of the measurements collected. Most of these measurements were small midshaft measurements collected along the

x-axis.

Majority of the measurements were deemed repeatable; however, these measurements were not accurate, likely due to the use of 2D images.

Keywords: Virtual Anthropology; low-dosage X-rays (Lodox); Metric assessment

ACKNOWLEDGEMENTS

The completion of this thesis would not have been made possible if it was not for the help and timeless effort of a group of people.

My greatest gratitude is to my supervisors, Prof. Desiré M. Brits and Dr. Amanda Alblas. Thank you for your time, patience, guidance and for encouraging me through this. I will be eternally grateful for the knowledge that you imparted to me, the motivation and kindness.

I would like to extend my warmest thank you to Dr. A. Alblas and her family for opening up their home to me during the course of my stay in Cape Town, while I was collecting my data. Thank you for being warm and welcoming, for the good food, great conversations and lovely memories.

I would like to thank Ms Amy Spies, a PhD student at the School of Anatomical Sciences, Faculty of Health Science, University of the Witwatersrand and Ms Rachel Pieterse, a master's student from the Department of Biomedical Sciences, Faculty of Medicine and Health Science, Stellenbosch University, for being the second investigators for the Lodox and dry bone inter-observer repeatability of this study, respectively. Your time and valued efforts do not go unnoticed.

I would like to give a token of my appreciation to the masters' students at Stellenbosch University under Dr. A. Alblas' supervision for welcoming me into your Department, offering your help throughout my data collection and for your friendships. A special thank you to Stephanie Lathe for getting all the samples that I needed ready and helping me look for samples that I could not find.

I would like to extend gratitude to the statistical assistance received from the University of the Witwatersrand.

Lastly, I would like to thank my family and friends for their words of encouragement and

motivating me to completion. A special note of thanks to my friend Rethabile Maboa for helping me when I needed it the most.

TABLE OF CONTENTS

LIST OF FIGURES

LIST OF TABLES

ABBREVIATIONS

2D	Two-dimensional
3D	Three-dimensional
ABS	Anterior breadth of sacrum
AHS	Anterior height of sacrum
ASISS	Anterior superior iliac spine to symphysion
BLF	Bicondylar breadth of femur
BS	Breadth of scapula
CT	Computed Tomography
cm	Centimetres
DCP	Data Collection Procedures
DeBT	Distal epiphyseal breadth of tibia
DICOM	Digital Imaging and Communications in Medicine
DVS	Digital Viewing Station
EBF	Epicondylar breadth of femur
EBH	Epicondylar breadth of humerus
FOL	Length of foramen magnum
FOB	Breadth of foramen magnum
HMB	Height of mandibular body
HREC	Health Research Ethics Committee
HS	Height of scapula

IOD	Image object distance
KSC	Kirsten Skeletal Collection
L	Left
Lodox	Low-dosage X-Ray
LT	Length of tibia
Max	Maximum
MDC	Maximum diameter of clavicle at midshaft
mDC	Minimum diameter of clavicle at midshaft
MDF	Maximum midshaft diameter of femur
mDF	Minimum midshaft diameter of femur
MDFh	Maximum diameter of femur head
MDFib	Maximum diameter of fibula at midshaft
MDH	Maximum diameter of humerus at midshaft
mDH	Minimum diameter of humerus at midshaft
MDR	Maximum diameter of radius at midshaft
mDR	Minimum diameter of radius at midshaft
MDRh	Maximum diameter of radial head
MDU	Maximum diameter of ulna at midshaft
mDU	Minimum diameter of ulna at midshaft
MIB	Minimum innominate breadth
Min	Minimum
MInh	Maximum innominate height

ML	Mandibular length
MLC	Maximum length of clavicle
MLF	Maximum length of femur
MLFib	Maximum length of fibula
MLH	Maximum length of humerus
MLR	Maximum length of radius
MLU	Maximum length of ulna
mm	Millimetres
MPeBT	Maximum proximal epiphyseal breadth of tibia
mRB	Minimum ramus breadth
MRh	Maximum ramus height
MRI	Magnetic Resonance Imaging
MT	Maximum midshaft diameter of tibia
mT	Minimum midshaft diameter of tibia
MVDhH	Maximum vertical diameter of the head of humerus
n	Sample number
NECSA	South African Nuclear Energy Corporation
OID	Object image distance
PLU	Physiological length of ulna
R	Right
SD	Standard deviation
SID	Subject image distance

SUDI	Sudden unexpected death in infants
TDSS1	Transverse diameter of sacral segment 1
TEM	Technical error of measurement
TSDF	Transverse subtrochanteric diameter of femur
VSD	Virtual skeletal database
WIB	Minimum iliac breadth
ZYG	Bizygomatic breadth

CHAPTER 1: INTRODUCTION

Forensic anthropology is a subdiscipline of physical anthropology which aids in the identification of unknown human remains (Deadman, 1964; Krogman, 1962; Schulz *et al.,* 2005). Human remains of medico-legal significance, are often recovered in advanced stages of decomposition, mutilated, burnt and/or skeletonized (Deadman, 1964; Krogman, 1962; Schulz *et al.,* 2005). As a result of the state of these recovered human remains, primary forms of identification, such as; facial recognition, fingerprints and scars, cannot be used as a form of identification (Brogdon, 2006; Interpol, 2021). Thus, from these remains forensic anthropologists establish biological profiles (Dirkmaat *et al.,* 2009). A biological profile includes the estimation of the deceased individual's sex, age-at-death, ancestry, stature and other factors that circumstantially identify the individual (Dirkmaat *et al.,* 2009; Wiersema *et al.,* 2009). This information is given to law enforcement, who narrows down the possibilities of the unknown individual from a missing persons list (Dirkmaat, 2012).

To describe these biological parameters, skeletal collections of known individuals with known demographic information are needed as reference samples (Mann, 2013). Various skeletal collections exist worldwide, representing various populations (Krogman, 1962). These human skeletal collections include; the William M. Bass (Marks, 1995), Hamann-Todd (Kern & Wingate, 2006), Robert J. Terry Anatomical (Hunt & Albanese, 2005), Raymond A. Dart Collection (Dayal *et al.,* 2009), Pretoria Bone (L'Abbé *et al.,* 2005), Kirsten Skeletal (Alblas *et al.,* 2018), Lisbon (Cardoso, 2006), St. Bride (Scheuer & Black, 1995) and the Coimbra collections (Rocha, 1995), to name but a few. Human skeletal collections, however, need to represent modern populations, as outdated samples can no longer serve as reference samples, due to the impact of secular trends (Dirkmaat *et al.,* 2009).

Secular trends are genetic and non-genetic changes that occur over multiple generations

in a population (Albanese, 2010; Ousley & Jantz, 1998; Spradley *et al.,* 2008). These changes are the result and reflection of the changes of the living conditions of populations (Albanese, 2010), such as adjustments in nutrition and healthcare (Dirkmaat & Cabo, 2012), immigration, emigration and genetic admixing, which contribute to the continuously changing genetic landscape (Ousley & Jantz, 1998; Spradley *et al.,* 2008). In addition to the impact of secular trends and the continuously changing genetic landscape, not all populations are represented in skeletal collections (Colman *et al.,* 2017; Komar & Grivas, 2008; Ubelaker, 2008). Some skeletal collections do not have a representative distribution of sex, age and ancestry, which hampers research on the underrepresented individuals. An example would be the Raymond A. Dart Collection of Human Skeletons which comprises mostly of skeletal elements of older, black South African males, of the Zulu, Sotho and Xhosa tribes (Dayal *et al.,* 2009).

Similarly, forensic pathologists and anthropologists are also faced with issues pertaining to culture and religious beliefs of deceased individuals, as post-mortem examinations are not accepted by all (Goodman *et al.,* 2011; Gurley *et al.,* 2011; O'Sullivan *et al.,* 2018). For example, the Islamic population do not consent to cadaveric donation of the body as it involves mutilation (i.e. maceration) (Golmakani *et al.,* 2005) and some geographical regions, like India, are accustomed to cremating the body after death, due to religious reasons (Goodman *et al.,* 2011). As such, these individuals are not represented in skeletal collections.

To alleviate this problem, the Virtopsy, coined by Thali *et al.* (2007), or virtual autopsy project was founded (Thali *et al.,* 2009). The autopsy technique involves the non-invasive examination of deceased individuals, using virtual imaging modalities (Rosário *et al.,* 2012). Virtual autopsy is created to provide indestructible and objective evidence and is often used in conjunction with traditional autopsy in medico-legal investigations (Kahana & Hiss, 2005).

Currently, forensic anthropologists receive skeletal remains for examination from forensic pathologists or other legal entities. However, with the advancements and increased

popularity of virtual imaging modalities, forensic anthropologists might soon only receive virtual data for analyses. Thus, forensic anthropologists need to explore how they will utilise the data they receive. For forensic anthropologists to continue to describe the biological profiles from virtual material, virtual skeletal databases (VSD) need to be created (Colman *et al.,* 2017) so as to generate appropriate methodologies to assess the parameters of the biological profile, including; age-at-death, sex, ancestry, stature, etc.

A VSD eliminates the effects of secular trends, ethical and religious issues associated with maceration, the need for physical storage space and the time-consuming process of maceration associated with a physical skeletal collection (Colman *et al.,* 2017; Dedouit *et al.,* 2007). VSD eliminates secular trends by continuously providing reference samples relevant to the current living population. The objective of a VSD is to create and support the research community, which would in turn be able to collaborate and share information (Kistler *et al.,* 2013).

To capture human remains using imaging modalities, two types of non-contact imaging modalities are used, the reflective and transmissive imaging modalities (Carew & Errickson, 2019; Obertová *et al.,* 2019). Examples of reflective imaging modalities include; three-dimensional surface scanning and photogrammetry, to name but a few (Carew & Errickson, 2019). Transmissive imaging modalities include; sonography and three other commonly used techniques: Computed Tomography (CT), Magnetic Resonance Imaging (MRI) and X-rays (Bolton, 2010; Mehta *et al.,* 1997). Added to the transmissive imaging modalities, used to capture human remains, is the Low-dose X-Rays (Lodox) (Bolton, 2010; Mehta *et al.,* 1997). These radiological techniques have been used within the field of forensics to assist pathologists in medico-legal cases (Carew & Errickson, 2019; Clemente *et al.,* 2017). In forensic medicine, for example, these imaging modalities have been used to locate foreign objects within a deceased individuals' body, to identify peri-mortem fractures and to aid in positively

identifying deceased individuals (Bernitz & Verster, 2017; Kahana & Hiss, 2005; Kučerová *et al.,* 2014; Thali *et al.,* 2009).

Forensic radiology has become a key component in multi-disciplinary teams, which deal with casualty identification (Brough *et al.,* 2015). Forensic radiology has been classified as a sub-specialisation of forensic medicine, which makes use of radiological findings as evidence to answer legal questions (Walsh *et al.,* 2004). Forensic radiology captures the osseous skeleton (Bernitz & Verster, 2017), which allows forensic anthropologists to make use of these imaging modalities (Carew & Errickson, 2019; Clemente *et al.,* 2017). This giving rise to virtual forensic anthropology. Virtual forensic anthropology, therefore, merges radiological and anthropological techniques to aid in the estimation of biological profiles of deceased individuals (Guglielmi *et al.,* 2015). Forensic anthropologists often receive remains which are severely burnt and/or in advanced stages of decomposition, which means that the bones are often fragile. The use of virtual imaging modalities can aid in the reconstruction of bone without disrupting the remains and causing post-mortem damage (Dedouit *et al.,* 2007; Hishmat *et al.,* 2015). In addition to this, it allows for repetitive analyses of skeletal remains even after remains are burried (Grabherr *et al.,* 2009; Hishmat *et al.,* 2015).

To date, little work relating to virtual forensic anthropology has been completed in South Africa, mainly due to the availability and costs associated with virtual imaging modalities. Currently, a few South African medicolegal laboratories are equipped with low-dose X-ray (commonly known as Lodox) machines, which is frequently used in conjunction with autopsies. The use of Lodox in forensic anthropology is thus yet to be fully explored.

1.1 Aim

Therefore, the aim of this study was to assess the use of Lodox in forensic anthropology by comparing the accuracy and repeatability of two dimensional (2D) Lodox Statscan image measurements to three-dimensional (3D) dry bone measurements.

1.2 Objectives

To achieve this aim, three objectives were completed, which included:

i. To assess which of the 95 standard osteometric measurements from the most recent version of the Data Collection Procedures (DCP) for Forensic Skeletal Material 2.0 (Langley *et al.*, 2016) can be taken from the Lodox scan images.

ii. To determine the repeatability of the measurements collected from Lodox scan images.

iii. To evaluate the accuracy of the measurements collected from the Lodox scan images compared to the same measurements collected on the corresponding dry bones.

CHAPTER 2: LITERATURE REVIEW

2.1 Introduction

Certain imaging modalities are known to capture osseous tissue (Mehta *et al*., 1997; Obertová *et al.,* 2019). These techniques include non-contact reflective and transmissive imaging modalities (Obertová *et al.,* 2019). Reflective imaging modalities require remains to be macerated for osseous tissue to be detected. These include imaging modalities such as three-dimensional surface scanning and photogrammetry. Non-contact transmissive imaging modalities, however, depict osseous tissue while soft tissue is still attached and include: Sonography Computed Tomography (CT), Magnetic Resonance Imaging (MRI), X-rays, as well as, low-dosage X-rays (Bolton, 2010; Mehta *et al*., 1997; Obertová *et al.,* 2019).

A plethora of articles have been published illustrating the use of various imaging modalities in forensic anthropology with the advantage of reconstructing and documenting osseous tissue *in situ* to preserve fragile bones and reduce post-mortem damage (Dedouit *et al.*,2007; Hishmat *et al.,* 2015), while allowing repetitive analyses of the skeletal remains(Grabherr *et al.,* 2009; Hishmat *et al.,* 2015). Imaging modalities are also useful in victim identification, by allowing comparisons of bone lesions to existing ante-mortem virtual images (Dedouit *et al*., 2013; Guglielmi *et al.,* 2015) and through estimates of the biological profile (Franklin *et al*., 2016; Guglielmi *et al.,* 2015).

The use of imaging modalities such as X-rays and CT is well documented and for an in-depth review of these methods, the reader is referred to the works by Franklin *et al.* (2016), Garvin & Stock (2016) and Obertová *et al*. (2019).

2.2 Reflective Imaging Modalities

2.2.1 Three-dimensional Surface Scanning

Three-dimensional (3D) surface scanners make use of structured light or laser patterns to capture the 3D surface of an object (Garvin & Stock, 2016). To create a 3D model, images of the skeleton are taken at different angles and the scans are then merged (Garvin & Stock, 2016). Structured light scanning uses a combination of cameras and projectors, which are initially calibrated (Carew & Errickson, 2019). A scanner mounted with a camera, projects light onto a calibration board. A calibration board is a sheet with shapes of known dimensions (Errickson *et al.,* 2017). The calibration board is then replaced with the object of interest. This will result in the deformation of the lines originally projected on the calibration board, according to the geometry of the object of interest (Errickson *et al.*, 2017).

Laser surface scanning is frequently used to document human remains (Errickson *et al.*, 2017). To capture an object using laser surface scanning, a laser is projected onto the surface of the targeted object and then reflected to a detector. A distance is computed based on the position of the light on the detector. The distance computed is then used to build a series of geometric points into a 3D model of the object (Errickson *et al.,* 2017). These 3D models are used for illustration purposes in court and for teaching, in order to maintain the integrity of the actual bone (Johnson & Pandey, 2019). However, this technique has not directly contributed to anthropological case analyses (Johnson & Pandey, 2019).

Images of models developed using 3D surface scanners are of higher resolution than those prepared using CT with a slice thickness commonly used in clinical and forensic settings (Garvin & Stock, 2016). According to Cambridge Dictionary, higher resolution means that the image produced is of high quality and clearly shows the details of the image captured (Cambridge University Press, 2021). The technique is also suggested to be accurate and more

suitable in documenting detailed 3D models of bone, than multi-detector CT (Fahrni *et al.,* 2017; Sansoni*et al.,* 2009). The 3D models produced by 3D surface scanners can be printed as well (Filiault, 2012).In addition, it is less expensive, more accessible and due to its relatively small size, it is portable (Carew & Errickson, 2019; Garvin & Stock, 2016). The 3D surface scanners capture both the morphometry, geometry, texture and colour of bones, thus providing information on taphonomy, as well as, surface modification of bone (Errickson *et al.,* 2017; Sansoni *et al.,* 2009). It is also able to record most fractures and ballistic trauma (Ebert *et al*., 2016; Garvin & Stock, 2016; Thali *et al*., 2005). Furthermore, a study conducted by Filiault (2012), suggested that standard cranial osteological measurements taken from a 3D structured light scan were similar to dry bone measurements; with no significant differences between most of these measurements, including the maximum length, maximum breadth, bizygomatic breadth, basion-bregma, nasal height, nasal breadth, orbital breadth, orbital height, biorbital breadth, foramen magnum breadth, foramen magnum length and mastoid length to name but a few (Filiault, 2012). However, this was based on a single cranium scan and no intra- or inter-observer repeatability tests were conducted. Structured light scanning has been suggested to help reconstruct biological profiles as indicated in the study by Sholts *et al.* (2010), in which skull landmarks from 3D models were shown to be clearly visible resulting in accurate measurements taken from the scans.

Despite the pros mentioned above, 3D surface scanners can only document the visible parts of the bone, making it difficult for grooves and crevices to be captured (Ebert *et al*., 2016; Errickson *et al*., 2014; Garvin & Stock, 2016). Thus, making it difficult for bones with many grooves and crevices, such as the skull, os coxae and scapula to be accurately documented (Errickson *et al.,* 2017). In addition, sharp force trauma that has not occurred over a large surface area is generally recorded by 3D surface scanners (Gavin & Stock, 2016). Regrettably, data collection with structured light scanning can be disrupted by external light and as such

require a controlled environment (Carew & Errickson, 2019), along with high computational power to process thescanned data (McPherron *et al.,* 2009). Furthermore, data processing of this imaging modality has been proven to be difficult and advanced training is required (Obertová *et al*., 2019).

2.2.2 Photogrammetry

Photogrammetry makes use of a digital camera to document the size, shape, position and orientation of an object (Kraus, 2007). It was first used to create a topographic map compilation, in 1849, by Aime Laussedat, the father of photogrammetry (Birdseye, 1940). To produce an image, documentation of the subject takes place using single- or multiple camera photogrammetry (Carew & Errickson, 2019). Multiple overlapping images of an object are taken at different angles. These images are captured into a computer system, which calculates the position of certain homologous landmarks to produce a 3D model (Thali *et al.,* 2003).

Photogrammetry is inexpensive, easy to use and is highly accurate (Carew & Errickson, 2019). This technique can produce a photo-realistic appearance if a texture map is applied (Sansoni *et al*., 2009). In forensic medicine, it is found to be beneficial in documenting the external body (Urbanová *et al.,* 2015). Photogrammetry has shown to precisely identify cranial landmarks and the identification of these landmarks is found to be highly repeatable and reliable (Aldridge *et al.,* 2005). In the study conducted by Aldridge and colleagues (2005), a high repeatability referred to the ability to identify landmarks with a high degree of precision. The degree of error which measured precision, noted that most of the landmark distances had degree errors of less than 1 mm (Aldridge *et al.,* 2005). While, analysis of variance (ANOVA), was used to calculate the repeatability, finding the repeatability of most of the landmark distances to exceed 95% (Aldridge *et al.,* 2005). Similarly, a study conducted by Michienzi *et al.* (2018), showedthat the measurements taken from photogrammetry scans are more accurate

than standard images taken during autopsies. As suggested by Brüschweiler *et al.* (2003), this technique can also be used to document bone trauma and the possible instrument used to inflict the injury, according to the injuries' size, shape and angle.

The alignment, fusion and scaling of the images are done manually and thus, the image produced is subjective to the operator which can introduce error into the data set (Carew & Errickson, 2019; Errickson *et al.*, 2017; Sansoni *et al.*, 2009). This imaging modality, like all reflective imaging modalities, is sensitive to the presence of hair which may cause artifacts in the reconstructed image (Carew & Errickson, 2019). This is because photogrammetry systems are unable to capture hair, resulting in the loss of surface data of all areas covered by hair (Heike *et al.*, 2010). Details may be lost in photogrammetry, when thin bones, thin sharp fracture margins, shiny, wet, dark and translucent concavities are present on the bone. Like all reflective imaging modalities, photogrammetry only provides surface information and cannot detect structures deep to soft tissue. To date, the use of photogrammetry in forensic anthropology is still to be explored (Garvin & Stock, 2016).

Reflective imaging modalities, unlike transmissive imaging modalities, are not often used in medico-legal procedures (Ebert *et al.*, 2016; Urbanová *et al.*, 2015).

2.3 Transmissive Imaging Modalities

2.3.1 Sonography

Similar to MRI, sonography (also known as ultrasound) is a non-ionizing imaging modality (Franklin *et al.*, 2016). Non-ionizing imaging modalities are virtual imaging modalities which do not rely on radiation to generate images (Jacques & Christe, 2020). This technique uses ultrasound waves produced by electrical devices, known as transducers. Ultrasound waves are sent through the object of interest, which reflects the sound waves to the

transducers. Transducers generate electrical signals which are sent to the scanner. To document the object in the form of a 2D image, the scanner will calculate the distance from the object to the transducers, using the speed of sound and the time at which the echoes return (Abu-Zidan *et al.,* 2011).

A few studies pertaining to forensic anthropology and the use of sonography are available and mainly relate to the estimation of age in living individuals. This includes studies that assessed the ossification of the medial clavicle (Schulz *et al*., 2013), fusion of the iliac crest epiphysis (Schmidt *et al*., 2013) and ossification of the olecranon (Schulz *et al*., 2014).

This technique is inexpensive, easy to use and can be used to guide minimally invasive autopsies (van Rijn & Sieswerda-Hoogendoorn, 2012). Due to its limited penetration power, this imaging modality's potential to visualise bone structures is limited (Lento & Primack, 2008), especially in cases where the bone is buried deep under soft tissue (Lento & Primack, 2008).

2.3.2 Computed Tomography (CT)

This imaging modality was created by an English engineer, G.N Hounsfield in 1972 and makes use of collimated X-ray beams, that pass through an object, which is detected using a circular array of photomultiplier tubes (Hildebolt *et al.,* 1990; Swift & Rutty, 2006). Depending on the density of each tissue, a certain amount of the X-rays will be absorbed. The absorption pattern is then used to produce an image (Swift & Rutty, 2006).

Computed Tomography was first used in a clinical setting in 1972 (Swift & Rutty, 2006). It is seen as the golden standard, for scanning bones to produce 3D models, which are geometrically highly accurate (Rathnayaka *et al.,* 2012). In the clinical setting, these models are used to create surgical implants, which are fitted specifically to a patient (Schmutz *et al.,* 2010; 2011). The first reported post-mortem CT scan was only in 1983 (Kalender, 2011; Krantz

& Holtas, 1983). Portable post-mortem CT scans have been useful inmass fatality incidents (Rutty *et al*., 2007). Its use in forensic anthropology has become increasingly popular, as research has shown that linear osteological measurements (Colman *etal.*, 2017; Colman *et al.*, 2019; Franklin *et al*., 2013; Stull *et al*., 2014a) and angular measurements (Lopes *et al.*, 2008) collected from CT scans the same as dry bone specimens. In the identification of deceased individuals, CT can be employed in two ways; comparative orreconstructive (Dedouit *et al.*, 2013). Comparative identification consists of comparing ante- mortem abnormalities, variations or surgical procedures observed on the post-mortem CT scansto ante-mortem scans or records (Dedouit *et al.*, 2013; Guglielmi *et al*., 2015), while reconstructive CT involves taking images of the object at different angles to obtain a rendered 3D image of the object (Sree Ram *et al.*, 1998), which is often used in the estimation of a biological profile (Dedouit *et al*., 2013). This means that once a 3D image has been generated, standard methods used for the estimation of biological parameters from dry bone can be applied.

It produces cross-sections of bone with high visibility contrast between various soft tissues, which is greater than the imaging modality, X-rays, in addition to having a rapid processing time (Mehta *et al*., 1997; Stull *et al*., 2014a). It produces images in 2D, 3D or even both views (Obertová *et al.*, 2019) and both the shape and size of bone can be determined froma CT scans (Franklin *et al*., 2016). Studies assessing the use of CT scans for sex estimation include quantitative analyses of the sacrum (Franklin *et al*., 2014), scapula (Torimitsu *et al*., 2016), sternum (Franklin *et al.*, 2012), cranium (Mehta *et al*., 2015; Verhoff *et al*., 2008; Zhan *et al.*, 2019) and lower limb bones (Hishmat *et al.*, 2015). Qualitative analysis of the os coxae has also been used for sex estimation (Biwasaka *et al*., 2012). The estimation of age-at-death has been assessed from the cranium (Verhoff *et al*., 2008) and medial epiphysis of the clavicle (Franklin& Flavel, 2015). Stature estimation has also been described from measurements of lower limb bones (Hishmat *et al.*, 2015; Zhang *et al.*, 2019), cranium (Verhoff *et al*., 2008;

Zhan *et al.*, 2019) collected from CT scans. Metric and morphological analyses of CT scans of charred remains have also been explored to estimate age-at-death, sex and ancestry (Dedouit *et al*., 2007). CT has been described as a precise means of *in situ* trauma analysis with suggestions that physical reconstruction is not needed (Jalalzadeh *et al*., 2015). Fractures in small bones, such as the hyoid (Kempter *et al.*, 2009) and perinatal and neonatal bones (Arthurs *et al*., 2016; 2017) are also detected on CT images.

Even though CT scans are affected by metal artefacts such as projectiles, which degrade the quality of the image obtained (Bornik *et al*., 2018), reduction artefact algorithms can be employed to improve the image quality and retrieve lost data (Katsura *et al*., 2018). Despite CT producing images that are of high resolution, the high emission of radiation doses, make it undesirable for research of living populations (Verhoff *et al*., 2008). Collecting and analysing CT scans also requires extensive and specific training (Guglielmi & Nasuto, 2014). Furthermore, CT equipment is large and expensive (Bornik *et al*., 2018) and is rarely found in medicolegal laboratories in South Africa.

2.3.3 Magnetic Resonance Imaging (MRI)

Magnetic Resonance Imaging is a technique that was developed by Paul Lauterbur and Peter Mansfield in the 1980s (Swift & Rutty, 2006) and can be used to acquire images in any plane and provide information on both soft tissue and bone (Griffith & Genant, 2011).

It is a much safer technique to use when studying living populations, as the body is subjected to a strong magnetic frequency, instead of electromagnetic radiation (Franklin *et al*., 2014; Mehta *et al*., 1997). In forensic anthropology, a few studies have validated the accuracy and precision of long bone measurements collected from MRI scans and found that they are similar to their corresponding dry bone elements (Doyle & Winsor, 2011; Rathnayaka *et al*., 2012). A study which compared the osteological measurements collected from MRI scans and

their corresponding dry bone, indicated a mean difference of less than 2mm (Brits, 2016). Various studies have also focused on estimating characteristics of the biological profile from MRI scans. These include stature estimation from long bones in sub-adults (Brits *et al*., 2017) and adults (Brits *et al*., 2018), the sacral and coccygeal vertebrae (Pelin *et al.,* 2005) as well as age estimation studies focusing on the development of the medial clavicle (Hillewig *et al.,* 2011; 2013), ossification of the distal femur (Krämer *et al*., 2014), fusion of the distal tibial epiphysis and calcaneus (Saint-Martin *et al.,* 2013), radial epiphysis (Serin *et al*., 2016) and of the knee-joint (Dedouit *et al*., 2012). Hatipoglu and colleagues (2008) showed that landmarks of the cranium can be obtained from MRI scans, allowing craniometric data to be collected and used in estimating both age and sex (Hatipoglu *et al.,* 2008). However, MRI is not the preferred imaging modality for visualizing bone, as it documents structures by measuring nuclear magnetic resonance, given off by the excitement of protons, due to radio waves. These protons (hydrogen atoms) are found in soft tissue structures, as a result of high-water content (Carew & Errickson, 2019). Patients or participantswith metallic prostheses, foreign metal objects, etc. should not partake in MRI scans (Swift &Rutty, 2006), as metal objects, depending on their size, shape and type, experience a force which is exerted by the static magnetic field created by the MRI (Hargreaves *et al.,* 2011). This can cause the metal objects to produce variation in the frequency, loss of signals and displacement of the objects (Hargreaves *et al.,* 2011). This limits the use of MRI in the field of forensic medicine as the identification of prostheses and projectiles is frequently made throughthe use of imaging modalities. In addition, MRI does not provide sufficient bone detail; it is expensive, has a long acquisition time and is not frequently found within medical examiners or forensic medico-legal laboratories (Arthurs *et al*., 2017; Grabherr *et al.,* 2017).

2.3.4 X-Rays

X-rays were first discovered in 1895 by Wilhelm Conrad Roentgen. The technique involves the emission of electromagnetic radiation by an X-ray beam and depending on the density of various tissues, a certain amount of the radiation is absorbed with the remaining un-absorbed particles passing through a radiation-sensitive film to produce an image (Franklin *et al*., 2016). It allows for the external and internal visualization of bone and as such eliminates the need for the body to be dissected (Franklin *et al*., 2016). This technique provides excellent resolution and can differentiate bone boundaries (Mehta *et al*., 1997).

A year following the use of X-rays' in the clinical setting, it was used in detecting bullets lodged in the head of a deceased individual, introducing its use in forensic medicine (Franklin *et al*., 2016). Since then X-rays are commonly used in identifying and finding projectiles in ballistic investigations, other foreign objects lodged within the body and to identify bone fractures in forensic medicine (Bolton, 2010; Kučerová *et al*., 2014; Thali *et al*.,2003). X-rays are also used in victim identification (Kučerová *et al*., 2014), where it is used to compare ante-mortem data and post-mortem radiographs such as dental X-rays (Guglielmi *et al*., 2015). During mass fatalities, portable intraoral X-rays are considered valuable to capture dental records, which are used in victim identification (Pittayapat *et al*., 2010). Dental X-rays, display anatomical dental features, such as; the shape and roots of teeth, the presence of supernumerary teeth, implants, dental prostheses and bone pathology, to name a few (Chandrasekhar & Vennila, 2011). Numerous forensic anthropology studies have explored the use of X-rays. Some of these include the use of X-rays to estimate age-at-death using various long bone lengths in children (Carneiro *et al*., 2013; Maresh, 1955), analysing the trabeculae patterns of bones in older individuals (Anburajan *et al*., 2001) and assessing the ossification of rib cartilage in the elderly (Garamendi *et al*., 2011). Assessing the ossification of the rib cartilage has also been used in estimating sex (Rejtarová *et al*., 2009) as well as studies from the distal and

proximal radii (Kranioti, 2016), proximal epiphysis of the adult femur (Mostafa *et al.*, 2012) and length of adult metacarpals (Morsi & Hawary, 2013). X-rays images of long bones have also been used to estimate stature (Wang *et al.*, 2012). X-rays are likewise the recommended imaging modality when identifying trauma in paediatric and adult cases (Arthurs *et al.*, 2017; Garvin & Stock, 2016; van Rijn & Sieswerda-Hoogendoorn, 2012).

X-rays make use of ionizing radiation and thus emit high doses of electromagnetic radiation, which is harmful to both patients and operators (Franklin *et al.*, 2016). The use of X-rays within the forensic field is also hampered by the need for multiple scans to obtain a full-body image, which makes it time-consuming and labour intensive (Bolton, 2010; Obertová *et al.*, 2019). Regrettably, due to the superimposition of scans, subtle injuries in these structures can be missed (Burke, 2012). It also displays difficulties in truly representing the dimensions of bone as the images obtained are often distorted (Maresh, 1955).

2.3.5 Low-dose X-rays (Lodox)

Low-dose X-rays commonly known as Lodox (Lodox® Systems Pty., Sandton, South Africa) was designed and manufactured by a South African company, Lodox® Systems, where it was commercially known as the Scannex (Beningfield *et al.*, 1999; Bolton, 2010) and primarily used in diamond-mines as a security scanner to prevent theft within the workplace (Boffard *et al.*, 2006). Its initial design was a vertical machine, which produced high-quality X-ray images at a fast rate without exposing the workers to detrimentally high X-ray dosages (Knobel *et al.*, 2006). Radiation doses are often measured in millisieverts (mSv) (Lin, 2010). A detrimentally high radiation dose is considered to be within 10-100 mSv (Lin, 2010).

In 1995, the diagnostic potential of Lodox was recognized and a modified horizontal version was built to adapt it for clinical use (Beningfield *et al.*, 1999; Beningfield *et al.*, 2003). To test its clinical use, a study was conducted at the Groote Schuur Hospital in Cape Town,

South Africa, where the radiation dose, diagnostic capability, clinical utility and image quality of the modified Scannex was compared to conventional X-rays (Beningfield *et al.*, 1999). It was this study that highlighted Lodox as a useful tool to triage trauma patients with multiple injuries and following this study, a redesigned Lodox scan was placed in Groote Schuur Hospital for day-to-day evaluations (Beningfield *et al.*, 1999). Subsequently, in 2002 and 2004 Lodox was approved as a diagnostic tool by the United States Food and Drug Administration as well as the European Union, respectively (Pitcher *et al*., 2009).

Currently, there are 101 active Lodox installations in Europe, Asia, North and South America as well as Africa, in trauma departments of hospitals and forensic pathology / medico-legallaboratories (Lodox® Systems, 2012). Currently, 46 of these installations are in medico-legal settings, with the first installation at the Salt River medico-legal laboratory, South Africa (du Plessis *et al.*, 2020). There are currently three different types of Lodox systems; the Lodox Statscan, Xmplar-DR and the exero-DR, each of which caters for the use of Lodox in different fields. The Statscan, which is predominantly found and in use in hospitals and medico-legal laboratories is the older version with the newer Xmplar-DR, specifically designed for trauma units and the exero-DR intended for the mortuary setting (Lodox® Systems, 2012).

The Lodox Statscan produces a full-body image of both osseous and soft tissues in anterior-posterior (< 1 min) and lateral views, with no need to move the body to obtain either view (Amirlak *et al.*, 2009; Bernitz & Verster, 2017; Boffard *et al.*, 2006; Muligan & Flye, 2006). To produce an image, the machine consists of a C-arm which contains an X-ray tube and detector on opposite ends. During scanning, the C-arm runs parallel to the object, while the X-ray tube emits a low-dosage collimated fan-beam of X-rays (Boffard *et al.*, 2006) and typically produces less radiation than conventional radiological technology, which uses cone beam scanning (Stull *et al*., 2013). The Lodox also has a low scatter dose which means that the radiation-free zone is 1 meter away from the machine (Lodox® systems, 2012). In a study

conducted by Beningfield *et al.* (2003), which aimed to compare the diagnostic performance, radiation dose and clinical utility of Lodox to conventional x-ray in the trauma unit of Groot Schuur Hospital, it was found that Lodox required 72% and 1.6% of the radiation required in conventional X-rays, to capture the chest and pelvis, respectively. The image quality produced by Lodox showed to be similar to conventional X-rays, however, it differs in that no image stitching is required for Lodox (Beningfield *et al.*, 2003; Lodox® systems, 2012). A further advantage of Lodox compared to conventional X-ray is that it can produce a single full-body image which can be further manipulated by zooming, allowing for radiologists to increase the size of and localize a certain area of interest (Amirlak *et al.*, 2009). Other studies have also found that Lodox produces less image distortion than conventional X-rays as a result of it being a linear slot scanning device (Stull *et al.*, 2014b). The material and running costs associated with the use ofthe Lodox are also lower than conventional X-rays, CT and MRI as it makes use of conventional computer hardware (Evangelopoulos *et al.*, 2009).

The clinical benefits of the use of Lodox in the trauma units in hospitals (Evangelopoulos *et al.*, 2011; Lodox® systems, 2012; Swift & Rutty, 2006) besides triage management, include reducing radiography time and eliminating the need to transfer patients for resuscitation (Amirlak *et al.*, 2009; Whiley *et al.*, 2012). In trauma case studies, Lodox proved to be effective in various scenarios such as motor vehicle accidents and gunshot injuries. Its use in these trauma cases was to identify fractures and projectiles (Amirlak *et al.*, 2009). However, research has shown that subtle fractures viewed on Lodox scans can be missed as a result of the imaging modality providing a full-body image with no directional markers (Muligan & Flye, 2006), as is with conventional X-ray (Cattaneo *et al.*, 2006). In a study by Deyle *et al.* (2010), Lodox showed to detect upper and lower skeletal injuries with 73% sensitivity and 100% specificity (Deyle *et al.*, 2010; Spies *et al.*, 2020). In non-emergency medicine, it has shown to be useful in arteriography (Exadaktylos, 2013; Loots & du Toit- Prinsloo, 2011) and was suitable as an

alternative means of imaging ventriculoperitoneal (VP)shunts (Fathi *et al.,* 2011). In assessing the VP shunts, Lodox provided the same information as conventional X-ray in a shorter time, releasing low doses of radiation and giving a larger field of view (Fathi *et al.,* 2011).

In the medico-legal environment, the Lodox scanner was custom designed to be more durable and to suite wet laboratory conditions (Bateman, 2008). In order to further cater for the forensic pathology setup, adjustments in the density and exposure timing were made by University of Cape Town's Biomedical Engineering Department in collaboration with Lodox Systems South Africa to optimally capture bone and soft tissue of deceased individuals (Bateman, 2008). Lodox systems installed within South Africa's medico-legal laboratories include; Forensic Pathology Services in Cape Town (Alblas *et al.,* 2018), Pretoria (Beningfield *et al.,* 1999) KwaZulu Natal and Johannesburg where it is mainly used to locate foreign objects such as firearm projectiles (Fu *et al.,* 2011) and metal artefacts, such as screws, nails and wire (Loots & du Toit-Prinsloo, 2011), as well as detecting peripheral skeletal injuries (Knobel *et al.,* 2006). Lodox's ability to detect foreign objects within the body has also been found useful in determining fatalities possibly caused by pica (Loots & du Toit-Prinsloo, 2016). Pica is an eating disorder, characterised by the compulsive consumption of non-nutritional substances, such as; ice, gravel, clay, hair, laundry and metal, to name but a few (Loots & du Toit-Prinsloo, 2016). It is more efficient and sensitive in identifying foreign objects within the bodies of deceased individuals than conventional X-ray and CT, especially in the abdominal region of the body (Mantokoudis*et al.,* 2012). Its effectiveness is a result of the ability of Lodox to produce a full-body image, in comparison to X-rays; which require multiple scans of the body to be taken, followed by image stitching to view the entire body (Mantokoudis *et al.,* 2012). The identification of the location of sharp foreign objects through post-mortem imaging, prior to the post-mortem examination, also reduces health and safety risks to medico-legal personal (Loots & du Toit- Prinsloo, 2016). Furthermore, Lodox has also been useful in the identification

of air embolisms and surgical swabs that may have been left behind during surgical procedures (Bateman, 2008). In identifying an individual demonstrating fibrotic lungs, consistent with TB, Lodox has shown to be an occupational health and safety hazard benefit (du Plessis *et al.*, 2020). Allowing forensic pathologists to continue to identify possible cause of death, without placing medico-legal laboratory staff in harm's way. Radiological images are also important to rule out non- accidental injuries and to detect rib fractures associated with resuscitation in sudden unexpected death in infants (SUDI) (Weber & Sebire, 2011). A study by Douglas *et al.* (2010), showed that the pathology found in the images produced by Lodox were consistent with the cause of death in the majority of the SUDI cases. Lodox can also radiographically screen for unique dental features, which are used in victim identification (Bernitz & Verster, 2017). The overall benefits of Lodox in forensic pathology services, especially those with high case volumes, include but are not limited to, accelerating investigations and victim identification (Bateman, 2008; Bernitz & Verster, 2017).

The use of Lodox in forensic anthropology is still in its infancy and is yet to be fully explored, however, an earlier study has demonstrated the usefulness of Lodox in examining skeletal and mummified remains from an archaeological site in Limpopo, South Africa (Esterhuysen *et al.,* 2009). A study conducted by Stull *et al.* (2013) illustrated that the Lodox Statscan produced images with minimal to no distortion in the scan axis (y-axis) and as such osteometric measurements could reliably be taken from Lodox Statscan images. The scan axis refers to the direction in which the remains are scanned by Lodox Statscan as opposed to the slot axis (x-axis), which refers to the direction perpendicular to the scan axis (Stull *et al.,* 2013). To date, long bone osteometric measurements collected from the Lodox Statscan images have been assessed for estimating age and sex from South African sub-adults aged between 0-12 years of age (Stull, 2014b; Stull *et al.*, 2017). Lakha (2015) also developed standards for the age of fusion of the epiphyseal plates of the major joints in South African sub-adults.

The increased use of virtual imaging modalities in forensic science, as part of the post-mortem examination process (Grabherr *et al.,* 2017), prompts forensic anthropologists to become familiar with these modalities in forensic anthropology. This would include identifying how these imaging modalities can be helpful in collecting information used to aid in estimating biological profiles (by means of morphological and metric assessments) and in the identification of various types of trauma inflicted on bone. Metric methods are often more accurate in estimating the biological profile as the potential for intra-observer and inter-observer error is less than what is experienced using morphological methods (Spradley, 2016). The use of Lodox in medico-legal laboratories further support the need for explorations in forensic anthropology. Therefore, the aim of this study was to assess the use of Lodox in forensic anthropology by comparing the accuracy and repeatability of 2D Lodox Statscan measurements to 3D dry bone measurements.

Table 1: Table summarising the advantages and disadvantages of reflective and transmissive virtual imaging modalities

Type of virtual imaging modality	**Virtual imaging modality**	**Advantages**	**Disadvantages**
Reflective imaging modality	Three-dimensional surface scanning	• Has a higher resolution than CT (Garvin & Stock, 2016) • Provides information on the taphonomy and surface modification of bone (Errickson *et al.*, 2017; Sansoni *et al.*, 2009) • Records fractures and ballistic trauma • Inexpensive (Carew & Errickson, 2017; Garvin & Stock, 2016) • Accessible (Carew & Errickson, 2017; Garvin & Stock, 2016) • Portable (Carew & Errickson, 2017; Garvin & Stock, 2016)	• Cannot document bones with grooves and crevices (Ebert *et al.*, 2016; Errickson *et al.*, 2017; Garvin & Stock, 2016) • Cannot document sharp force trauma over a small surface area (Garvin & Stock, 2016) • Images can only be captured in controlled environment, with no external light (Carew & Errickson, 2019) • Advanced training is required (Obertová *et al.*, 2019) • Not often used in medico-legal procedure (Ebert *et al.*, 2016; Urbanová *et al.*, 2019)

Table 1: *Continued*

Type of virtual imaging modality	Virtual imaging modality	Advantages	Disadvantages
Reflective imaging modality	Photogrammetry	• Accurately and repeatably identifies cranial landmarks (Aaldridge *et al.*, 2005; Michienzi *et al.*, 2018) • Documents bone trauma (Brüschweiler *et al.*, 2003)	• Image produced is subject to the operator (Carew & Errickson, 2019; Errickson *et al.*, 2017; Sansoni *et al.*, 2009) • Unable to capture areas covered by hair (Carew & Errickson, 2019) • Loss of details with thin bones and bones with translucent concavities (Carew & Errickson, 2019) • Not often used in medico-legal procedures (Ebert *et al.*, 2016;
Transmissive imaging modality	Sonography	• Does not emit electromagnetic radiation (Franklin *et al.*, 2016) • Inexpensive (van Rijn & Sieswerda Hoogendoorn, 2012) • Easy to use (van Rijn & Sieswerda Hoogendoorn, 2012)	• Limited penetration power (Lento & Primack, 2008)

Table 1: *Continued*

Type of virtual imaging modality	Virtual imaging modality	Advantages	Disadvantages
Transmissive imaging modality	Computed Tomography (CT)	• Has a higher resolution than X-rays (Stull *et al*., 2014) • Rapid processing time (Stull *et al*., 2014) • Dimensions of bone from CT scan images are similar to dry bones' (Lorkiewicz-Muszynska *et al*, 2015) • Used to estimate biological profile (Torimitsu *et al*., 2016)	• Emits electromagnetic radiation (Franklin et al., 2016) • Not easily accessible and used in South African Forensic Pathology Services Medico-legal Laboratories
	Magnetic Resonance Imaging (MRI)	• Does not emit electromagnetic radiations (Franklin *et al*., 2016) • Dimensions of bone from MRI's scans are accurate and precise to the dry bone measurements (Rathnayaka *et al*., 2012) • Used to estimate biological profiles (Brits *et al*., 2017)	• Expensive • Not easily accessible and used in South African Forensic Pathology Services Medico-legal Laboratories

Table 1: *Continued*

Type of virtual imaging modality	Virtual imaging modality	Advantages	Disadvantages
Transmissive imaging modality	X-rays	• Helps to find projectiles in ballistic investigations • Identifies bone fractures (Kučerová *et al.,* 2014)	• Emits electromagnetic radiation (Franklin *et al*., 2016) • Multiple scans are required to obtain a full body image (Bolton, 2011) • Images of bone are often distorted (Maresh, 1955) • Time-consuming (Deyle *et al.,* 2009) • Labour-intensive
	Low-dose X-rays (Lodox)	• Produces high quality, 2-dimensional images in 10-13 seconds (Stull *et al.,* 2013) • It is custom designed for wet laboratory conditions (Bateman, 2008) • Available and in use at 9 mortuaries in 9 South African mortuaries. • Used in identifying Foreign objects within the body of deceased individuals (Fu *et al.,* 2011)	• Distortion of images along the x-axis (Stull *et al.,* 2013)

CHAPTER 3: MATERIAL & METHODS

3.1 Materials

3.1.1 Ethical clearance

Ethical approval for the current study was obtained from the Human Research and Ethics Committee (Medical) at the University of the Witwatersrand (Clearance certificate no. M190765 – Appendix A) and the Health Research Ethics Committee at Stellenbosch University (HREC no. N19/05/068 – Appendix B).

3.1.2 Sample

Fifty pre-existing Lodox Statscan images of complete skeletons and the corresponding dry bones, from the Kirsten Skeletal Collection (KSC), housed in the Department of Biomedical Sciences, Division of Clinical Anatomy, Stellenbosch University, were used in thecurrent study.

The KSC is curated from a combination of consented donations and unclaimed bodies in the Western Cape region, from the 1957 onwards. The death of these individuals was due to natural causes. Upon the intake of these bodies, they were embalmed and since 2016, full-body X-rays were taken using the Lodox Statscan. The cadavers were then dissected by undergraduate and post-graduate students at Stellenbosch University. Following dissection, the remains were macerated and the skeletons were accessioned in the KSC. As part of a previous study, the skeletal elements for each skeleton were placed in anatomical position and scanned using the Lodox Statscan (Figure 1).

Regrettably, the full-body Lodox scan images of the cadavers were not available for this study and only the Lodox scan images of the skeletal remains were available and thus used.

The specimens used in the current study were not selected based on demographic information such as age, ancestry or sex, as the focus was on the repeatability and accuracy of osteometric measurements collected from the 2D Lodox images. However, of the 50 skeletons used in the study, demographic information was available for 48 skeletons. These remains represented adult individuals aged between 23-49 years. The sample was equally distributed by sex (24 females and 24 males).

Skeletons were excluded if any skeletal remains were fused, had severe osteophytes or showed signs of trauma or pathology. Some skeletal elements were missing at the time data from the dry bones were collected. This was because a number of skeletal remains had been taken to the South African Nuclear Energy Corporation (NECSA) for scanning, as part of a larger research project. The exclusion of these bones reduced the sample sizes for some measurements. The sample sizes pertaining to each measurement is noted in Chapter 4.

Figure 1: An example of a full body Lodox image, illustrating the anatomically positioned bones of askeleton selected from the KSC**.**

3.2 Methods

3.2.1 Lodox measurements

Measurements were first collected from Lodox images. The 50 Lodox images selected, were each sieved through to establish which standard anthropometric measurements as defined in the Data Collection Procedures for Forensic Skeletal Material 2.0 (DCP manual) (Langley *et al*., 2016) could be repeatedly collected. This process, included, going through each of the 95 osteological measurements from the manual and establishing which of these measurements could potentially be collected from all of the Lodox images. Thus, all measurements, which required the bone to be 3D were excluded, except for the midshaft measurements of the long bones. The manual includes 95 osteometric measurements, of which 46 could be collected (Langley *et al*., 2016).All the measurements collected from the Lodox images were collected as prescribed by the DCP manual (Langley *et al*., 2016), except for minimum and maximum midshaft measurements, as these exact areas could not be assessed circumferentially. However, it was necessary to include these measurements to establish the margin of error, if any. The measurements collected were grouped into different data sets, which included: the skull (n=7), pectoral girdle and upper limb (n=18), as well as, pelvic girdle and lower limb (n=21) that are described in Tables 1-6.

Only a few skull measurements could be collected, as the skull was imaged with its base in view, whereas most of the skull measurements defined in the DCP, were from the anterior view. The pectoral girdle, upper limb, pelvic girdle and lower limb bones were placed in anatomical position. As a result of the images being 2D, measurements with landmarks that were not in view and circumferential measurements (except, the above mentioned midshaft measurements) were not collected. Where applicable, measurements from both the left and

right side of the bone (mandible) and body (pectoral girdle, upper limb, pelvic girdle and lower limb datasets) were collected. As a result, a total of 84 measurements were collected.

To view and collect measurements from Lodox images, Digital Viewing Station (DVS) was used as the Lodox images were stored in a Digital Imaging and Communications in Medicine (DICOM) format. The measuring unit employed in DVS is centimetres (cm). Thus, the measuring unit employed throughout the current study was cm, instead of millimetres (mm) which is commonly used in forensic anthropology. The DVS allowed for the creation of straight-lines which were used to mimic the stationary and mobile/movable parts of an osteometric board or sliding caliper. To obtain the measurements, a third line perpendicularly joining the first two lines was created. The DVS not only allows for measurements to be collected, but also allows for the image to be moved and magnified (scaled) on certain parts of the image therefore focusing on each bone being measured.

The definitions of the measurements collected from the Lodox images (Table 2-7) are accompanied by visual representations of how the measurements were collected from DVS (Figure 2-11).

3.2.2 Dry skeletal measurements

Dry bone measurements were collected using an osteometric board, sliding caliper, spreading caliper and mandibulometer, depending on the bone and measurement being collected. All osteometric instruments used, except the osteometric board were manufactured by Paleo-Tech. The accuracy of each of the instruments used were as follows; sliding caliper (0.03 mm), spreading caliper (0.5 mm), mandibulometer (0.01 mm). A traditional wooden osteometric board, with an unknown manufacture was used in the study. The instruments were calibrated prior to their use. Measurements which were recorded in mm were converted into cm.

All dry bone measurements were collected on skeletal elements. A total of 46

measurements were collected, which corresponded to the measurements collected from the Lodox images, following descriptions by Langley *et al*. (2016). The measurements collected were grouped into data sets, which included; skull (n=7), pectoral girdle and upper limb (n=18), as well as, pelvic girdle and lower limb (n=21).

The definitions of each of the measurements collected for both the Lodox images and dry bone are summarised in Table 2-7.

Table 2: Definitions of the cranial measurements collected from the dry bone, along with the corresponding definitions for Lodox measurements (Adapted from Langley *et al*., 2016) (Figure 2)

Measurement	**Dry bone measurement**	**Equipment**	**Lodox scan definition**
a. Bizygomatic breadth (ZYGB)	The maximum distance between the two zygoma, where the breadth is perpendicular to the mid- sagittal plane. Measured while the skull lays on its occiput, base facing the observer.	Spreading caliper	A straight-line running perpendicular to the midsagittal plane was reconstructed between the two zygoma to establish maximum distance.
b. Foramen magnum length (FOL)	The distance from the anteriorpoint of the foramen magnum margin to the opisthion, whilethe skull base faces upwards.	Sliding caliper	A straight-line from the anteriorpoint of the foramen magnum margin to the opisthion.
c. Foramen magnum breadth (FOB)	The distance between the margins of the greatest lateral curvature of the foramen magnum, while the skull base faces upwards.	Sliding caliper	A straight line between the widest aspects of the right and left margins of the foramen magnum.

Figure 2: Lodox image illustrating the measurements collected from the base of the skull, a) bizygomatic breadth; b) foramen magnum length; c) foramen magnum breadth.

Table 3: Definitions of the mandibular measurements collected from the dry bone, along with the corresponding definitions for Lodox measurements (Adapted from Langley *et al*., 2016) (Figure 3)

Measurement	**Dry bone measurement**	**Equipment**	**Lodox scan definition**
d. Height of mandibular body (HMB)	At the level of the mental foramen, the distance from the alveolar process to the inferior border of the mandible.	Sliding caliper	A straight-line at the level of the mental foramen, from the alveolar process to the inferior border of the mandible. The mental foramen was not always easily found on the scans.
e. Minimum ramus breadth (mRB)	The minimum breadth of the mandibular ramus, at an angle perpendicular to the height of the ramus.	Sliding caliper	A straight-line at the minimum breadth of the mandibular ramus.

Table 3: *Continued*

Measurement	Dry bone measurement	Equipment	Lodox scan definition
f. Maximum ramus height (MRh)	The length from the gonion to the superior point of the mandibular condyle. Measured using a mandibulometer, with the mandibular body resting on the base board, the movable vertical board resting on the posterior boardof the ramus and the short vertical board of the mandibulometer touching the mental eminence of the mandible.	Mandibulometer	A straight-line from the gonion to the reconstructed line horizontally resting on the superior point of the mandibular condyle.
g. Mandibular length (ML)	Measurement from the most anterior point of the mandible tothe midpoint of the mandibular angle.	Mandibulometer	A straight-line from the most anterior point of the mandible to the inferior pointof the line of the maximum ramus height.

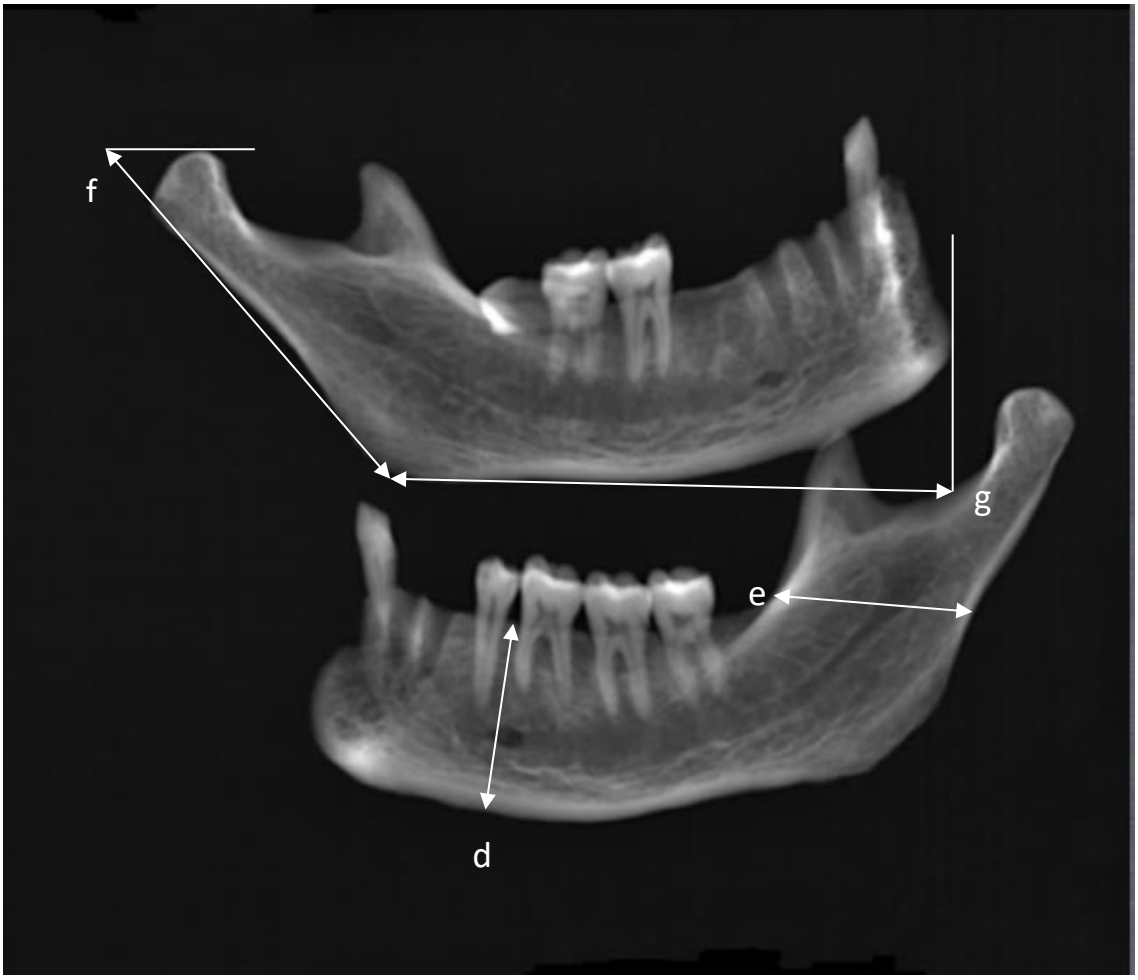

Figure 3: Lodox image illustrating the measurements collected from the left and right side of a mandible, d) height of the mandibular body; e) minimum ramus breadth; f) maximum ramus height; g) mandibular length.

Table 4: Definitions of the pectoral girdle measurements collected from the dry bone, along with their corresponding definitions for Lodox measurements *(*Adapted from Langley *et al.,* 2016*)* (Figure 4)

Measurement	**Dry bone measurement**	**Equipment**	**Lodox scan definition**
h. Maximum length of clavicle (MLC)	The maximum length between the acromial and sternal ends. Measured using an osteometric board, with the sternal end against the stationary board and the acromial end against the movable board.	Osteometric board	A straight-line extending between the most extreme ends of the clavicle.
i. Maximum diameter of clavicleat midshaft (MDC)	The bone was rotated, while in between the two arms of the sliding caliper until the maximum measurement was obtained.	Sliding caliper	A straight-line at the midpoint of the clavicle midshaft with the greatest width size.
j. Minimum diameter of clavicle at midshaft (mDC)	The bone was rotated, while in between the two arms of the sliding caliper until minimum measurement was obtained.	Sliding caliper	A straight-line at the midpoint of the clavicle midshaft with the narrowest width size.

Table 4: *Continued*

Measurement	Dry bone measurement	Equipment	Lodox scan definition
k. Height of scapula (HS)	The length from the most superior point of the scapula to the most inferior point of the inferior angle. The superior point of the scapula against the stationary board and the inferior angle against the movable board.	Osteometric board	A straight-line from the most superior point of the scapula to the most inferior point of the inferior angle. *(Refer to Figure 4)*
l. Breadth of scapula (BS)	The length from the dorsal border of the glenoid fossa, at the midpoint to the vertebral border, at the region in the middle of the two ridges of the scapula's spine. The one tip of the caliper is on the midpoint of the dorsal border of the glenoid fossa and the other at the midpoint of the two ridges of the spine along the vertebral border.	Spreading caliper	A straight-line from the midpoint of the dorsal border of the glenoid fossa to the midpoint of the two ridges of the spine along the vertebral border.

Figure 4: Lodox image of the measurements collected from the skeletal elements of the pectoral girdle (the right clavicle and scapula), h) maximum length of clavicle; i) maximum diameter of clavicle at midshaft; j) minimum diameter of clavicle at midshaft; k) height of scapula; l) breadth of scapula.

Table 5: Definitions of the upper limb measurements collected from the dry bone, along with their corresponding definitions for Lodox measurements (Adapted from Langley *et al*., 2016) (Figure 5)

Measurement	**Dry bone measurement**	**Equipment**	**Lodox scan definition**
m. Maximum length of humerus (MLH)	The length from the superior point of the humeral head to the inferior point of the trochlear region. Measured using an osteometric board, with the anterior aspect of the humerus facing down on the osteometric board and the shaft of the humerus parallel to it. The head of the humerus is placed against the stationary board and the trochlear against the movable board.	Osteometric board	A straight-line, extending from the most extreme point of the humeral head to the trochlear notch, while the anterior aspect of the humerus is in view.
n. Epicondylar breadth of humerus (EBH)	The breadth from the most protruding part of the lateral epicondyle to the most protruding part of the medial condyle.	Sliding caliper	A straight-line, extending from the most protruding part of the lateral epicondyle to the most protruding part of the medial condyle.

Table 5: *Continued*

Measurement	Dry bone measurement	Equipment	Lodox scan definition
o. Maximum vertical diameter ofthe head of humerus (MVDhH)	The length extending from the superior to the inferior point of the articular surface.	Sliding caliper	A straight-line extending from the superior to the inferior points of the articular surface.
p. Maximum diameter of humerus at midshaft (MDH)	Measured using a sliding caliper, where the bone is rotated, while being between the two arms of the caliper, until the maximum diameter at the midshaft was measured.	Sliding caliper	A straight-line at the midpoint of the humeral midshaft with the greatest width size.
q. Minimum diameter of humerus at midshaft (mDH)	Measured using a sliding caliper, where the bone is rotated, while being between the two arms of the caliper, until the minimum diameter at the midshaft was measured.	Sliding caliper	A straight-line at the midpoint of the humeral midshaft with the narrowest width size.

Table 5: *Continued*

Measurement	**Dry bone measurement**	**Equipment**	**Lodox scan definition**
r. Maximum length of radius(MLR)	The length from the most proximal end of the radius to the distal end of the styloid process. Measured using an osteometric board. The head of the radius placed against the stationary end of the osteometric board, while the styloid process is against the movable board.	Osteometric board	A straight-line, perpendicular to the reconstructed stationary and movable boards, extending from the head of the radius to the styloid process.
s. Maximum diameter of radius at the midshaft (MDR)	Measured using a sliding caliper,where the bone is rotated, between the two arms of the caliper, until the maximum diameter at the midshaft is measured.	Sliding caliper	A straight-line at the midpoint of the radial midshaft with the greatest width size.
t. Minimum diameter of the radius at midshaft (mDR)	Measured using a sliding caliper,where the bone is rotated, between the two arms of the caliper, until the minimum diameter at the midshaft ismeasured.	Sliding caliper	A straight-line at the midpoint of the radial midshaft with the narrowest width size.

Table 5: *Continued*

Measurement	Dry bone measurement	Equipment	Lodox scan definition
u. Maximum diameter of radial head (MDRh)	The maximum radial head of the radius. The part which articulates with the ulna. Measured using a sliding caliper, which is rotated around the margin of the radial head, to obtain the maximum diameter.	Sliding caliper	A straight-line between the most extreme parts along the margin of the radial head, while the anterior aspect of the radius is viewed.
v. Maximum length of ulna (MLU)	The length of the ulna from the most superior point of the olecranon to the most inferior point of the styloid process. Measured using an osteometric board. The most superior point of the olecranon was placed on the stationary board and the most inferior point of the styloid process.	Osteometric board	A straight-line perpendicular tothe reconstructed stationary and moveable boards extending from the superior point of the olecranon to the most inferior point of the styloid process.
w. Maximum diameter of ulnaat midshaft (MDU)	Measured using a sliding caliper, where the bone was rotated until the maximum diameter of the midshaft of the ulna was obtained.	Sliding caliper	A straight-line at the midpoint of the ulna midshaft with the greatest width size.

Table 5: *Continued*

Measurement	**Dry bone measurement**	**Equipment**	**Lodox scan definition**
x. Minimum diameter of ulna at midshaft (mDU)	Measured using a sliding caliper, where the bone was rotated until the minimum diameter of the midshaft of the ulna was obtained.	Sliding caliper	A straight-line at the midpoint of the ulna midshaft with the greatest width size.
a. Physiological length of ulna(PLU)	The length of the ulna from the deepest point of the articular surface of the coronoid process to the inferior point on the distal articular process.	Spreading caliper	A straight-line perpendicular to the reconstructed stationary and movable boards extends from the articular surface of the coronoid process to the inferior point on the distal articular process.

Figure 5: Lodox images illustrating the measurements collected from the upper limb skeletal elements (left to right; right humerus, right radius, right ulna), m) maximum length of humerus; n) epicondylar breadth of the humerus; o) maximum vertical diameter of the head of humerus; p) maximum diameter of humerus at midshaft; q) minimum diameter of humerus at midshaft; r) maximum length of radius; s) maximum diameter of the radius at midshaft; t) minimum diameter of the radius at midshaft; u) maximum diameter of the radial head; v) maximum length of ulna; w) maximum diameter of the ulna at midshaft; x) minimum diameter of the ulna at midshaft; y) physiological length of ulna.

Table 6: Definitions of the pelvic girdle measurements collected from the dry bone, along with their corresponding definitions for Lodox measurements (Adapted from Langley *et al.*, 2016) (Figure 6-8)

Measurement	**Dry bone measurement**	**Equipment**	**Lodox scan definition**
z. Anterior height of sacrum (AHS)	The measurement taken from the protruding point along the midsagittal plane of the anterior aspect of the sacrum to the distal tip.	Sliding caliper	A straight-line from the lowest point along the midsagittal plan of the anterior aspect of the sacrum to the distal tip, visible on the scan.
aa. Anterior breadth of sacrum (ABS)	The maximum breadth of the sacrum from the most protruding points of the auricular surfaces.	Sliding caliper	A straight-line from the most protruding points of the auricular surfaces.
bb. Transverse diameter of sacral segment 1 (TDSS1)	The distance between the most lateral points on the superior auricular surface, which are perpendicular the midsagittal plane of S1.	Sliding caliper	A straight-line perpendicular to the midsagittal plane between the most lateral points on the superior auricular surface of S1.
cc. Maximum innominate height (MInh)	The length from the superior point of the iliac crest, to the inferior point on the ischial tuberosity.	Spreading caliper	A straight-line extending from the superior point of the iliac crest to the inferior point on the ischial tuberosity.

Table 6: *Continued*

Measurement	Dry bone measurement	Equipment	Lodox scan definition
dd. Maximum iliac breadth (MIB)	The length along the superior iliac spines, from the anterior to the posterior end.	Spreading caliper	A straight-line extending from the anterior superior iliac spine to the posterior superior iliac spine.
ee. Minimum iliac breadth (WIB)	The minimum length from the inward curvature of the greater sciatic notch to the anterior inferior iliac spine.	Spreading caliper	A straight-line from the inward curvature of the greater sciatic notch to the anterior inferior iliac spine.
ff. Anterior superior iliac spine to the symphysion (ASISS)	The length taken from the symphysion to the anterior superior iliac spine.	Spreading caliper	A straight-line from the symphysion to the anterior superior iliac spine.

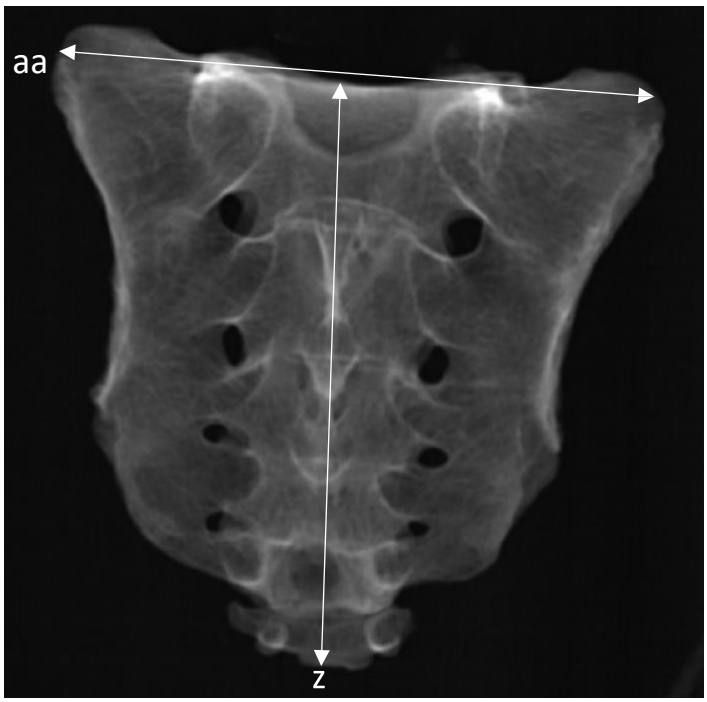

Figure 6: Lodox image illustrating the measurements collected from the anterior aspect of thesacrum, z) anterior height of sacrum; aa) anterior breadth of sacrum.

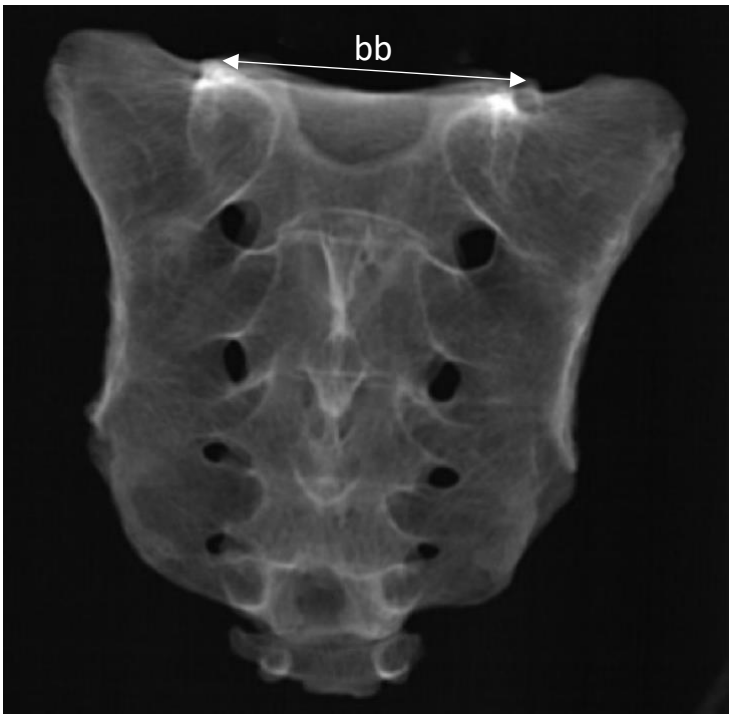

Figure 7: Lodox image illustrating the measurement collected from the anterior aspect of the sacrum, bb) transverse diameter of sacral segment 1.

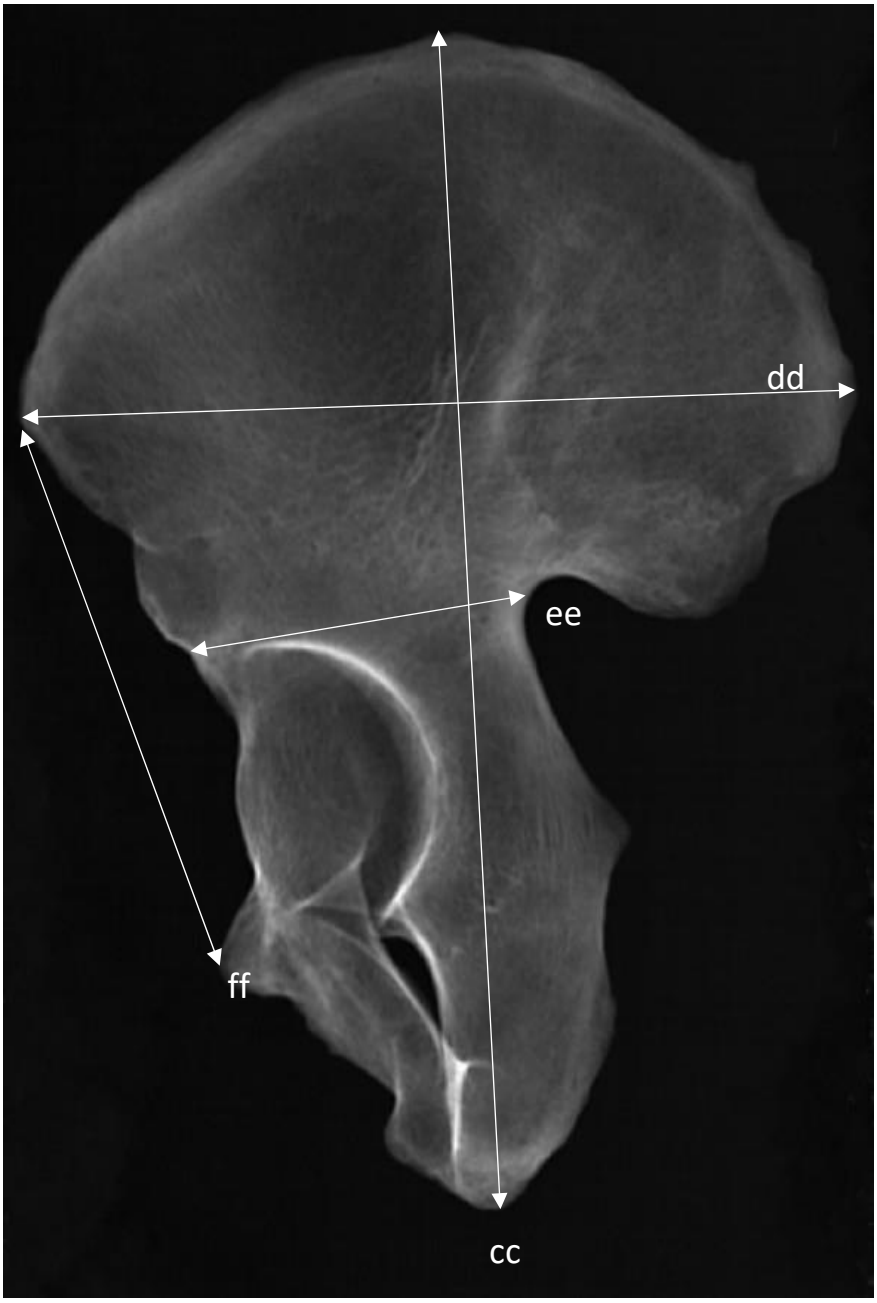

Figure 8: Lodox image illustrating the measurements collected from the right anterio-lateral aspect of the os coxae, cc) maximum innominate height; dd) maximum iliac breadth; ee) minimum iliac breadth; ff) anterior superior iliac spine to symphysion.

Table 7: Definitions of the lower limb measurements collected from the dry bone along with their corresponding definitions for Lodox measurements (Adapted from Langley *et al*., 2016) (Figure 9-11)

Measurement	**Dry bone measurement**	**Equipment**	**Lodox scan definition**
gg. Maximum length of femur (MLF)	The length from the most proximal point on the head of the femur to the most distal point of the femur, while the posterior aspect of the femur faces the osteometric board. (The most distal part may lie on either, the medial or lateral condyle). Measured using an osteometric board where the proximal point on the head of the femur was against the stationary board and the most distal point of the femur was on the movable board.	Osteometric board	A straight-line, extending from the proximal point on the head of the femur to the most distal point of the femur.

Table 7 *Continued*

Measurement	Dry bone measurement	Equipment	Lodox scan definition
hh. Bicondylar length of femur (BLF)	The length from the most proximal point of the femur to the plane which touches both distal medial and lateral condyles, while the femur is rested on its posterior surface. (The most distal part maylie on either the medial or lateral condyle). Measured using an osteometric board, where the medial and lateral condyle are both touching the stationary board and the head of the femur against the movable board.	Osteometric board	A straight- line perpendicular to the reconstructed stationary and movable boards (boards are reconstructed parallel to one another) extending from the most proximal point of the femur to the plane which touches both distal medial and lateral condyles.

Table 7: *Continued*

Measurement	Dry bone measurement	Equipment	Lodox scan definition
ii. Epicondylar breadth of femur (EBF)	From the most projecting end ofthe medial condyle, to the most projecting end of the lateral condyle. Measured using an osteometric board, while the femur was rested on its posterioraspect. One condyle against the stationary board and the otheragainst the moveable board.	Osteometric board	Lines parallel to one another were reconstructed to touch the most protruding parts of the medial andlateral condyles. A straight-line, touching these two lines represented the epicondylar breathof the femur.
jj. Maximum midshaft diameter of femur (MDF)	The maximum diameter of thediaphysis of the femur at the midshaft. The sliding caliper was rotated along the midshaft to obtain the maximum diameter.	Sliding caliper	A straight-line at the midpoint of the femoral shaft with the greatestwidth size.
kk. Minimum midshaft diameter of femur (mDF)	The minimum diameter of thediaphysis of the femur at the midshaft. The sliding caliper was rotated along the midshaft to obtain the minimum diameter.	Sliding caliper	A straight-line at the midpoint ofthe femoral shaft with the narrowest width size.

Table 7: *Continued*

Measurement	Dry bone measurement	Equipment	Lodox scan definition
ll. Length of tibia (LT)	The length from the articular surface of the lateral condyle tothe distal end of the medial malleolus. Measured using an osteometric board. The auricular surface ofthe lateral condyle was placed against the stationary board, while the moveable board was placed against the distal end ofthe medial malleolus.	Osteometric board	Lines representing the stationary and movable boards (lines were parallel to one another) were reconstructed. One touching the articular surface of the lateral condyle and the other, the distal end of the medial malleolus. A straight-line perpendicular to these boards was constructed.

Table 7: *Continued*

Measurement	Dry bone measurement	Equipment	Lodox scan definition
mm. Maximum diameter of. femur head (MDFh)	The maximum diameter of the femoral head on the border of its articular surface. The arms of the caliper are rotated around the femoral head, on the border of the articular surface.	Sliding caliper	A straight-line was reconstructed from the superior to the inferior points on the border of the articular surface.
nn. Transverse subtrochanteric diameter of femur (TSDF)	The transverse diameter of the proximal part of the diaphysis at the point of its greatest lateral expansion. Measured using a sliding caliper, with the anterior aspect of thefemur facing the observer.	Sliding caliper	A straight-line was constructed which runs along the transverseon the greatest lateral expansion of the proximal part of the diaphysis.
oo. Maximum proximal epiphyseal breadth of tibia (MPeBT)	The measurement from the most laterally projecting ends of the medial and lateral condyles of the tibia.	Osteometric board	The stationary and moveable boards of the osteometric board were reconstructed, parallel to each other. One board touching the medial condyle and the other the lateral condyle. A straight-line perpendicular to these boards was constructed.

Table 7: *Continued*

Measurement	Dry bone measurement	Equipment	Lodox scan definition
pp. Distal epiphyseal breadth of tibia (DeBT)	The distance between the most medially projecting point of the medial malleolus to the most laterally projecting point ofthe lateral surface of the distal epiphysis.	Osteometric board	The stationary and moveable boards of an osteometric board were reconstructed and placed on the most protruding point of the lateral surface and the most medially projecting point of the medial malleolus. These boards were reconstructed parallel to one another. A straight-line was reconstructed perpendicular to the two boards.
qq. Maximum midshaft diameter of tibia (MT)	The maximum diameter ofthe diaphysis at the midshaft. The sliding caliper was rotated along the midshaft to obtain the maximum diameter.	Sliding caliper	A straight-line at the midpoint ofthe tibial shaft with the greatest width size.

Table 7: *Continued*

Measurement	Dry bone measurement	Equipment	Lodox scan definition
rr. Minimum midshaft diameter of tibia (mT)	The minimum diameter ofthe diaphysis at the midshaft. The sliding caliper was rotated along the midshaft toobtain the minimum diameter.	Sliding caliper	A straight-line at the midpoint ofthe tibial shaft with the narrowest width size.
ss. Maximum length of the fibula (MLFib)	The distance from the most superior point on the fibular head and the tip of the lateral malleolus.	Osteometric board	The stationary and moveable boards of an osteometric board were reconstructed and placed on the most superior point of the fibular head and the tip of the lateral malleolus. These boards were reconstructed parallel to one another. A straight-line perpendicular to the two reconstructed boards represented the maximum length of the fibula.

Table 7: *Continued*

Measurement	Dry bone measurement	Equipment	Lodox scan definition
tt. Maximum diameter of the fibula at midshaft (MDFib)	The maximum diameter of the diaphysis at the midshaft.	Sliding caliper	A single straight-line at the midpoint of the fibula shaft, along the x-axis.

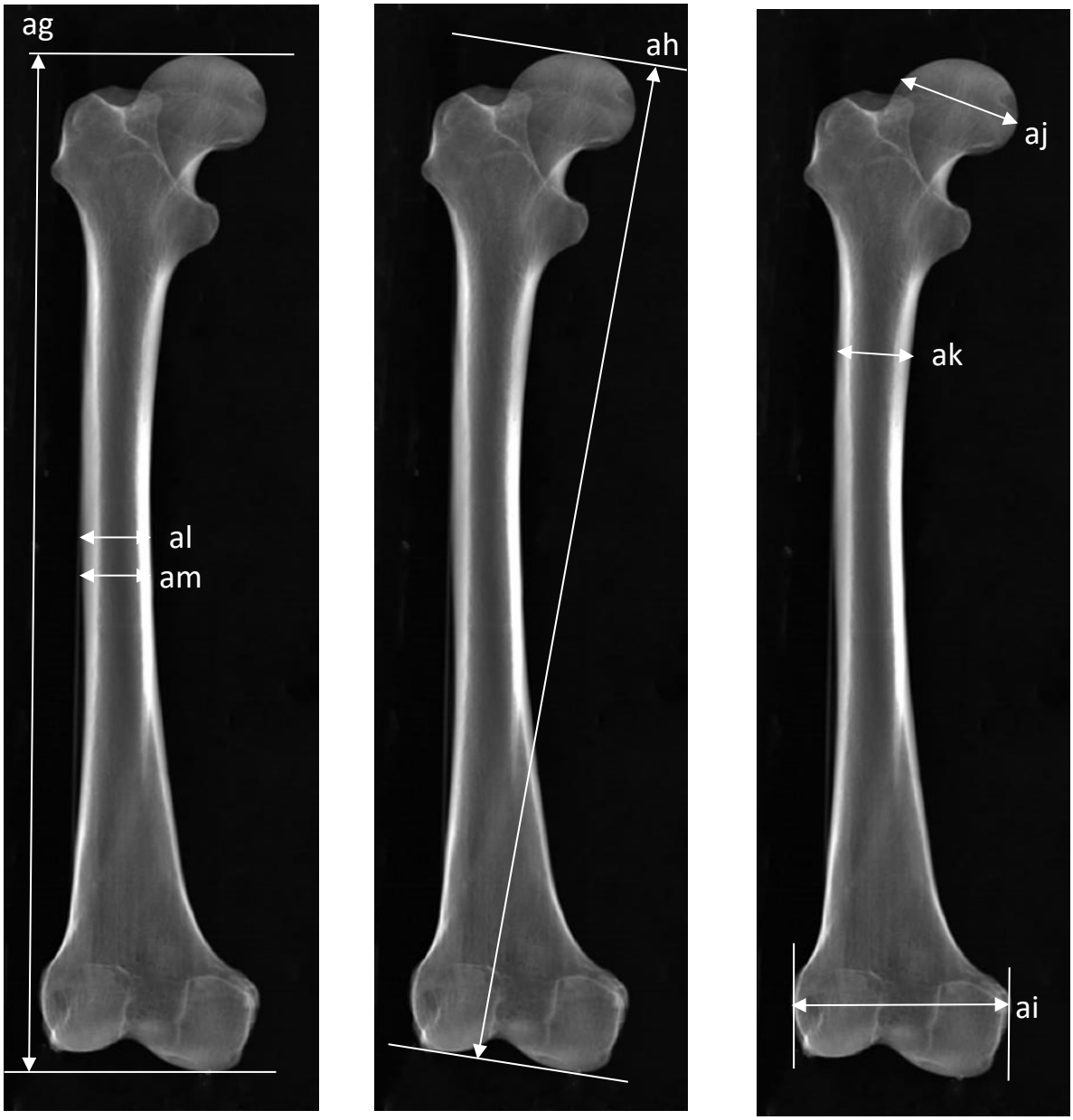

Figure 9: Lodox images illustrating the measurements collected from the anterior aspect of the right femur, gg) maximum length of femur; hh) bicondylar length of femur; ii) epicondylar breadth of femur; jj) maximum diameter of femur head; kk) transverse subtrochanteric diameter of femur; ll) maximum midshaft diameter of femur; mm) minimum midshaft diameter of femur.

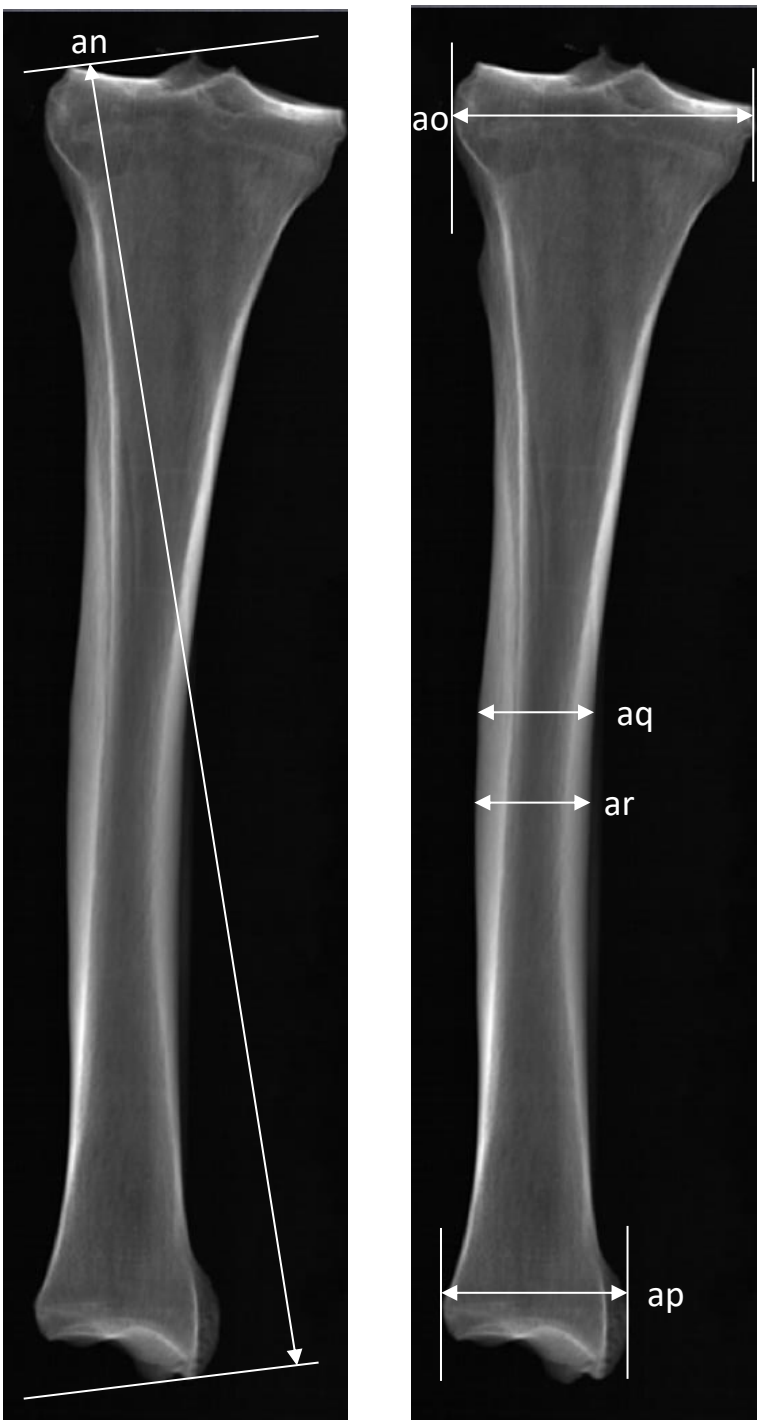

Figure 10: Lodox images illustrating the measurements collected from the anterior aspect of the right tibia, nn) length of tibia; oo) maximum proximal epiphyseal breadth of tibia; pp) distal epiphyseal breadth of tibia; qq) maximum midshaft diameter of tibia; rr) minimum midshaft diameter of tibia.

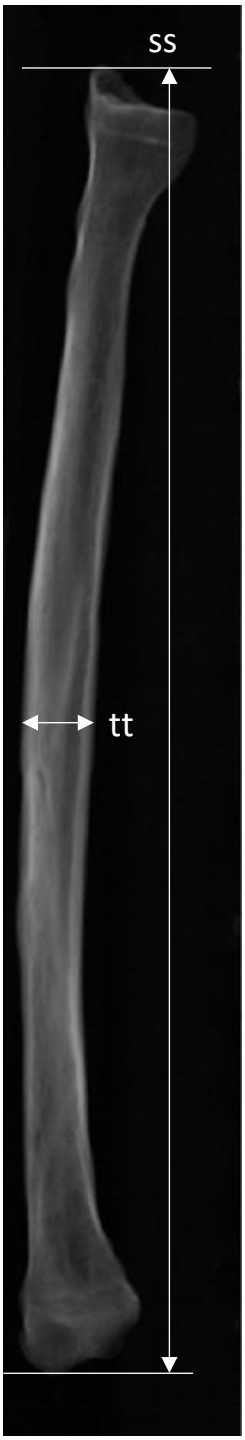

Figure 11: Lodox image of the measurements collected from the anterior aspect of the right fibula in anatomical position, ss) maximum length of fibula; tt) maximum midshaft diameterof fibula.

3.3 Data Analysis

3.3.1 Descriptive statistics

All statistical analyses were conducted using SPSS version 25.0.0.0. Normality was assessed on each data set, for both Lodox images and dry bone measurements, using a Shapiro-Wilk test. Measurements were considered normally distributed when the Shapiro-Wilk test results had a p-value >0.05 and the histogram generated had a bell-shaped curve (Kim, 2014).

Descriptive statistics, for the measurements collected from the Lodox images and the corresponding dry bones were calculated and recorded to provide an initial comparison of the osteometric measurements collected from the two methods. The descriptive statistics include; minimum (min), maximum (max), mean and standard deviation (SD).

3.3.2 Repeatability

Intra-observer and inter-observer errors were calculated to assess the reproducibility of the measurements collected in the study. Intra-observer error, measured the reproducibility of the data by the primary investigator on different days, using the same instruments. While inter-observer error, measured the reproducibility of the data between the primary investigator and a second investigator, on different days, using the same instruments for dry bone measurements and the same software program (DVS) for Lodox images. Ten sets were used in assessing the intra- and inter-observer repeatability for Lodox images and dry bones.

Technical error of measurement (TEM) was used to establish the reproducibility of both the Lodox and dry bone measurements (Jamaiya *et al.*, 2010). Particularly, the absolute TEM (TEM), measured in cm and relative TEM (rTEM), measured as a percentage. According to Stull *et al.*(2014a), the acceptable TEM range in forensic anthropometry is <2 mm (0.2 cm).

The accepted TEM range for intra- and inter-observer error are <1.5% and <2.0%, respectively (Goto & Mascie-Taylor, 2007; Perini *et al.*, 2005; Ulijaszek and Kerr, 1999). To obtain rTEM, absolute TEM is required. The equations used to calculate the TEM (equation 1) and rTEM (equation 2) were as follows (Ulijaszek and Kerr, 1999):

Equation 1:

$$\text{TEM} = \sqrt{((\sum D^2)/2N)}$$

D = the difference between the two measurements

N = the number of individuals measured

Equation 2:

$$\text{TEM} = \frac{TEM}{mean} \times 100$$

3.3.3 Accuracy

To assess the accuracy of measurements collected from Lodox images to the corresponding dry bone measurements, three methods were employed. These methods were the percentage difference (%), paired t-test/Wilcoxon signed-rank test (p-values) and the Bland-Altman plot.

3.3.3.1 Mean and Percentage difference

The mean difference between the measurements (dry bone – Lodox) was calculated to compare how different each measurement collected from Lodox images was from the corresponding dry bones.

Percentage difference was employed to assess how different the same measurements collected from Lodox images were from the corresponding dry bone, for each measurement.

The equation used to calculate percentage difference is shown in equation 3 (Stull *et al*., 2014a).

Equation 3:

$$\% \text{ Difference} = \frac{X_1 - X_2}{(\frac{X_1 + X_2}{2})}$$

X_1= The measurements taken from the Lodox image

X_2= The measurements from the dry bone.

3.3.3.2 Paired t-test / Wilcoxon signed-rank test

The paired t-test was used to assess differences between the data sets when the normality test results were considered normally distributed (Kim, 2014). Paired t-test compared the mean values generated from the measurements collected from the Lodox images and dry bones. The hypotheses for the test were as follows:

Null hypothesis (H_0): $\mu_1 = \mu_2$ (The means of the two measurement methods are the same).

Alternative hypothesis (H_1): $\mu_1 \neq \mu_2$ (The means of the two measurement methods are different).

Where;

μ_1= Mean of measurements taken from the Lodox image

μ_2 = Mean of measurements from the dry bones

The Wilcoxon signed-rank test was used for measurements where the data sets were not normally distributed (the Shapiro-Wilk test results showed p-values <0.05 and the histograms generated were skewed, either to the left or right of the graph). This test compared the median

values generated from the measurements collected from the Lodox images and dry bones. The hypotheses for the test were as follows:

Null hypothesis (H_0): $\mu_1 = \mu_2$ (The medians of the test methods are the same/no significant difference)

Alternative (H_1): $\mu_1 \neq \mu_2$ (The medians of the two measurement methods are different/significant difference)

Where;

μ_1 = Median of measurements taken from the Lodox image

μ_2 = Median of measurements from the dry bones

For both the paired t-test and Wilcoxon signed-rank test, a p-value was generated. For measurements where the p-value generated was greater than 0.05 ($p>0.05$), the null hypothesis was accepted and the alternative hypotheses were rejected, therefore suggesting that no significant difference existed between the same measurements collected from Lodox images compared to the corresponding dry bones (Elliot & Woodward, 2011).

3.3.4 Bland-Altman Plot

Bland-Altman plots provided a graphical representation (in the form of a scatter plot), showing the agreement between two quantitative measurements (Altman & Bland, 1983; Bland & Altman, 1999; Giavarina, 2013).

The x-axis represented the mean of the measurements (Lodox images and the dry bones), while the y-axis represented the difference between the two measurements. The graph was generated by calculating the mean and the standard deviation as well as by constructing limits

of agreement (Altman & Bland, 1983; Bland & Altman, 1999). The agreed limitation employed, requires 95% of the data to fall within ±2SD of the mean difference for anthropometricmeasurements (Altman & Bland, 1983; Bland & Altman, 1999; Giavarina, 2013).

CHAPTER 4: RESULTS

4.1 Introduction

The sample size (n), minimum (min), maximum (max), mean and standard deviations (SD), for each measurement collected from Lodox images and dry bone, were assessed and are summarised in Tables 12-14.

Although data was collected from 50 Lodox images and 50 skeletons, not all measurements could be collected. The difference in the sample sizes for each measurement was the result of the exclusion of skeletal elements which showed signs of pathology, remodelling or damage. In addition, some dry skeletal elements were missing or absent at the time of data collection. This resulted in the alteration of the sample size for some measurements. The measurement, bizygomatic breadth had the biggest reduction in sample size. This substantial reduction was largely due to the broken zygomatic arches of the dry bone, which occurred after the skeletal elements were captured using Lodox Statscan. However, the decrease in sample size of the bizygomatic breadth, to n=36, had no significant effect on the results obtained. Particularly with the results of the significant difference (Kim & Park, 2019).

Most of the dry bone measurements for the skull were greater than those of their corresponding Lodox measurements, ranging from 0.05 – 0.37 cm (Table 12). This was the opposite for the pectoral and upper limb (Table 13), as well as the pelvic girdle and lower limb (Table 14) datasets, as the measurements collected from the Lodox images for these sections were overall greater than the measurements collected from their corresponding dry bone, ranging from 0.01-0.59 cm and 0.07-0.76 cm, respectively.

A normality test was conducted for each of the dry bone and Lodox image measurements. The histogram and the Shapiro-Wilk test (p-values) displaying the normality results of each

measurement from the dry bone and Lodox images are shown in appendix C. Most of the measurements for both dry bone and Lodox were normally distributed with a few exceptions. Table 8 summarises the measurements which were not normally distributed ($p<0.05$/skewed graph).

Table 8: Table summarising the measurements which were not normally distributed ($p<0.05$/skewed graph)

Data set	**Lodox**	**Dry bone**
Skull	- ZYGB	- FOL - FOB
Pectoral girdle and upper limb	- BS (L and R)	- MDC (L and R) - mDC (L and R) - BS (L) - mDU (L) - PLU (R)
Pelvic girdle and lower limb	- WIB (L) - ASISS (L and R) - AHS - ABS - EBF (L) - LT (R)	- MInH - AHS - MDFh (L)

4.2 Repeatability

Technical error of measurement (TEM) was used to assess the repeatability of the measurements collected from the Lodox images and the corresponding dry bones (Ulijaszek and Kerr, 1999). The results of the intra- and inter-observer TEM for dry bone and Lodox scan images are summarised in Tables 9-11.

The repeatability results are represented as absolute TEM (TEM (cm)) and relative TEM (rTEM (%)). Measurements in the study were collected in cm's as the measurements were first collected from the Lodox images, using the DICOM software program. For the rTEM the acceptable ranges for bone intra- and inter-observer measurements are rTEM<1.5% and rTEM<2.0%, respectively (Ulijaszek and Kerr, 1999; Goto & Mascie-Taylor, 2007).

The results (Table 9-11) illustrate that most of the intra- and inter-observer results for dry bone and Lodox measurements, were repeatable as the results for the measurements collected, had rTEM values within the acceptable ranges (<1.5% for intra-observer and <2.0% for inter-observer).

All dry bone intra-observer repeatability results were, within the acceptable range (<1.5%) and were deemed repeatable. However, for dry bone inter-observer repeatability, some measurements from the skull, pelvic girdle and lower limb data set, were deemed unrepeatable. These included; MRH (L) (3.94%) (Table 9), TSDF (R) (2.02%), MDF (R) (3.38%) and (L) (4.20%), mDF (R) (2.94%) and (L) (3.00%) (Table 11).

Most of the intra- and inter-observer repeatability results for the Lodox measurements were deemed repeatable with a few measurements which were not. Lodox intra-observer repeatability results which were deemed unrepeatable (rTEM>1.5%) were from all three data sets. These included the skull: MRH (L) (1.60%) (Table 9); pectoral girdle/upper limb: MDC (L) (1.85%), MVDhH (L) (1.53%) and (R) (1.51%) (Table 10) and the pelvic girdle/lower limb:

MDFh (R) (1.51%) and mDF (R) (1.51%) (Table 11). Inter-observer repeatability results for Lodox measurements which were deemed unrepeatable were from all three data sets, skull: mRB (L) (8.53%) (Table 9): pectoral girdle/upper limb: MLC (R) (2.04%), MDC (L) (2.39%) and (R) (3.40%), mDC (L) (3.99%) and (R) (2.86%), MVDhH (R) (2.61%), MDH (L) (2.51%), mDH (L) (2.04%), MDR (L) (2.05%), mDR (L) (2.01%), MDU (R) (2.42%), mDU (L) (4.24%), PLU (L) (2.81%) and (R) (2.95%) (Table 10) and pelvic girdle/lower limb: MDF (L) (3.58%), mDF (L) (8.57%) and MDFib (L) (2.60%) (Table 11).

Table 9: Table summarising the absolute TEM and relative TEM (%) for intra-observer and inter-observer repeatability results of the dry bone and Lodox skull dataset

Measurements	**Dry bone**				**Lodox**			
	Intra-observer		**Inter-observer**		**Intra-observer**		**Inter-observer**	
	TEM	**rTEM (%)**	**TEM**	**rTEM (%)**	**TEM**	**rTEM (%)**	**TEM**	**rTEM (%)**
ZYGB[x]	0.09	0.71	0.03	0.20	0.02	0.17	0.07	0.03
FOL[y]	0.04	1.07	0.05	1.59	0.01	0.34	0.04	1.16
FOB[x]	0.04	1.35	0.02	0.83	0.01	0.49	0.02	0.02
mRB[y] (R)	0.05	1.43	0.05	1.61	0.02	0.63	0.05	1.82
HMB[x] (R)	0.03	1.18	0.12	0.41	0.03	0.91	0.06	1.99
mRB[y] (L)	0.04	1.09	0.05	1.33	0.03	0.98	0.25	8.53
HMB[x] (L)	0.03	0.92	0.05	1.69	0.03	0.90	0.06	1.95
MRH[x] (L)	0.08	1.49	0.22	3.94	0.05	1.60	0.10	1.62
ML[y] (L)	0.10	1.27	0.28	0.34	0.06	0.63	0.10	0.99

[x] *Measurements taken along the x-axis on the Lodox scan.*

[y] *Measurements taken along the y-axis on the Lodox scan.*

R- Right; L- Left; ZYGB- Bizygomatic breath; FOL- Length of foramen magnum; FOB- Breadth of foramen magnum; HMB- Height of mandibular body; mRB- Minimum ramus breadth; MRh- Maximum ramus height; ML- Mandibular length.

Measurements which were unrepeatable are highlighted.

Table 10: Table summarising the absolute TEM and relative TEM (%) for intra-observer and inter-observer repeatability results of the dry bone and Lodox pectoral girdle and upper limb dataset.

Measurements	**Dry bone**				**Lodox**			
	Intra-observer		**Inter-observer**		**Intra-observer**		**Inter-observer**	
	TEM	**rTEM (%)**	**TEM**	**rTEM (%)**	**TEM**	**rTEM (%)**	**TEM**	**rTEM (%)**
MLC[x] (R)	0.16	1.11	0.20	1.44	0.16	1.11	0.30	2.04
MDC[x] (R)	0.16	1.40	0.02	1.89	0.01	0.29	0.30	2.39
mDC[x] (R)	0.12	1.32	0.03	1.92	0.00	0.40	0.30	2.86
HS[y] (R)	0.07	0.48	0.12	0.82	0.01	0.08	0.03	0.20
BS[x] (R)	0.08	0.85	0.13	1.33	0.12	1.18	0.14	1.41
MLC[x] (L)	0.10	0.69	0.30	1.99	0.09	0.60	0.22	1.47
MDC[x] (L)	0.16	1.43	0.02	1.98	0.02	1.85	0.04	3.40
mDC[x] (L)	0.10	1.00	0.01	1.04	0.02	1.40	0.04	3.99
HS[y] (L)	0.10	0.68	0.10	0.69	0.01	0.05	0.05	0.33
BS[x] (L)	0.07	0.75	0.07	0.70	0.07	0.75	0.06	0.56

[x] *Measurements taken along the x-axis on the Lodox scan.*

[y] *Measurements taken along the y-axis on the Lodox scan.*

R- Right; L- Left; MLC- Maximum length of clavicle; MDC-Maximum diameter of clavicle; mDC-Minimum diameter of clavicle; HS- Height of scapula; BS- Breadth of scapula.

Measurements which were unrepeatable are highlighted.

Table 10: *Continued*

Measurements	Dry bone				Lodox			
	Intra-observer		Inter-observer		Intra-observer		Inter-observer	
	TEM	rTEM (%)	TEM	rTEM (%)	TEM	rTEM (%)	TEM	rTEM (%)
MLH[y] (R)	0.01	0.35	0.16	0.52	0.08	0.27	0.15	0.49
EBH[x] (R)	0.00	0.06	0.02	0.41	0.07	1.12	0.07	1.17
MVDhH[d] (R)	0.01	0.29	0.03	0.68	0.07	1.51	0.11	2.61
MDH[x] (R)	0.02	0.93	0.04	1.66	0.01	0.67	0.03	1.48
mDH[x] (R)	0.93	1.27	0.03	1.47	0.01	0.47	0.03	1.63
MLR[y] (R)	0.92	0.2	0.44	1.80	0.04	0.16	0.26	1.08
MDR[x] (R)	0.23	0.94	0.03	1.91	0.01	0.76	0.03	1.72
mDR[x] (R)	0.01	0.83	0.02	1.39	0.02	1.34	0.03	1.95
MDRh[x] (R)	0.02	1.15	0.19	0.76	0.01	0.78	0.02	1.06

[x] Measurements taken along the x-axis on the Lodox scan.

[y] Measurements taken along the y-axis on the Lodox scan.

[d] Measurements taken diagonally on the Lodox scan.

R- Right; L- Left; MLH- Maximum length of humerus; EBH- Epicondylar breadth of humerus; MVDhH- Maximum vertical diameter of the head of humerus; MDH- Maximum diameter of humerus at midshaft; mDH- Minimum diameter of humerus at midshaft; MLR- Maximum length of radius; MDR- Maximum diameter of radius at midshaft; mDR- Minimum diameter of radius at midshaft; MDRh- Maximum diameter of radial head.

Measurements which were unrepeatable are highlighted.

Table 10: *Continued*

Measurements	Dry bone				Lodox			
	Intra-observer		Inter-observer		Intra-observer		Inter-observer	
	TEM	rTEM (%)	TEM	rTEM (%)	TEM	rTEM (%)	TEM	rTEM (%)
MLU[y] (R)	0.12	0.47	0.19	0.76	0.14	0.53	0.07	0.28
MDU[x] (R)	0.01	0.96	0.03	1.86	0.01	0.62	0.03	2.42
mDU[x] (R)	0.01	0.62	0.01	1.07	0.02	1.36	0.00	0.28
PLU[y] (R)	0.17	0.69	0.26	1.14	0.04	0.15	0.68	2.95
MLH[y] (L)	0.21	0.68	0.12	0.40	0.17	0.53	0.26	0.84
EBH[x] (L)	0.01	0.23	0.90	0.66	0.07	1.19	0.26	0.84
MVDhH[d] (L)	0.01	0.23	0.02	0.59	0.07	1.53	0.10	1.56
MDH[x] (L)	0.01	0.38	0.04	1.91	0.03	1.32	0.11	2.51
mDH[x] (L)	0.02	1.26	0.03	1.57	0.01	0.35	0.04	2.04

[x] *Measurements taken along the x-axis on the Lodox scan.*

[y] *Measurements taken along the y-axis on the Lodox scan.*

[d] *Measurements taken diagonally on the Lodox scan.*

R- Right; L- Left; MLU- Maximum length of ulna; MDU-Maximum diameter of ulna at midshaft; mDU-Minimum midshaft diameter of ulna at midshaft; PLU-Physiological length of ulna; MLH- Maximum length of humerus; EBH- Epicondylar breadth of humerus; MVDhH- Maximum vertical diameter of the head of humerus; MDH- Maximum diameter of humerus at midshaft; mDH- Minimum diameter of humerus at midshaft.

Measurements which were unrepeatable are highlighted.

Table 10: *Continued*

Measurements	Dry bone				Lodox			
	Intra-observer		Inter-observer		Intra-observer		Inter-observer	
	TEM	rTEM (%)	TEM	rTEM (%)	TEM	rTEM (%)	TEM	rTEM (%)
MLR[y] (L)	0.16	0.69	0.10	0.40	0.03	0.11	0.22	0.91
MDR[x] (L)	0.01	0.41	0.03	1.67	0.01	0.93	0.03	2.05
mDR[x] (L)	0.02	1.47	0.01	1.23	0.02	1.46	0.03	2.01
MDRh[x] (L)	0.02	1.18	0.03	1.07	0.03	1.43	0.03	1.95
MLU[y] (L)	0.13	0.49	0.20	0.78	0.07	0.29	0.09	0.34
MDU[x] (L)	0.02	1.03	0.03	1.89	0.01	0.91	0.02	1.61
mDU[x] (L)	0.01	0.79	0.02	1.56	0.01	0.93	0.06	4.24
PLU[y] (L)	0.24	0.99	0.19	0.83	0.09	0.37	0.65	2.81

[x] *Measurements taken along the x-axis on the Lodox scan.*

[y] *Measurements taken along the y-axis on the Lodox scan.*

[d] *Measurements taken diagonally on the Lodox scan.*

R- Right; L- Left; MLR- Maximum length of radius; MDR- Maximum diameter of radius at midshaft; mDR- Minimum diameter of radius at midshaft; MDRh- Maximum diameter of radial head; MLU- Maximum length of ulna; MDU-Maximum diameter of ulna at midshaft; mDU-Minimum diameter of ulna at midshaft; PLU-Physiological length of ulna.

Measurements which were unrepeatable are highlighted.

Table 11: Table summarising the absolute TEM and relative TEM (%) for intra-observer and inter-observer repeatability results of the dry bone and Lodox pelvic girdle and lower limb dataset

Measurements	**Dry bone**				**Lodox**			
	Intra-observer		**Inter-observer**		**Intra-observer**		**Inter-observer**	
	TEM	**rTEM (%)**	**TEM**	**rTEM (%)**	**TEM**	**rTEM (%)**	**TEM**	**rTEM (%)**
AHS[y]	0.16	1.48	0.18	1.77	0.01	0.07	0.21	1.89
ABS[x]	0.15	1.48	0.11	1.05	0.01	0.10	0.09	0.83
TDSS1[x]	0.15	0.42	0.10	1.83	0.05	1.13	0.04	0.80
Minh[y] (R)	0.17	0.88	0.28	0.87	0.03	0.15	0.03	0.15
MIB[x] (R)	0.10	0.68	0.05	0.37	0.02	0.12	0.02	0.12
WIB[x] (R)	0.05	0.82	0.10	1.63	0.08	1.27	0.08	1.27
ASISS[y] (R)	0.14	1.33	0.22	1.95	0.03	0.29	0.03	0.29
MInh[y] (L)	0.18	0.95	0.24	1.27	0.02	0.13	0.02	0.13
MIB[x] (L)	0.15	1.02	0.20	1.37	0.01	0.09	0.01	0.09

[x] *Measurements taken along the x-axis on the Lodox scan.*

[y] *Measurements taken along the y-axis on the Lodox scan.*

R- Right; L- Left; AHS- Anterior height of sacrum; mDU-Minimum midshaft diameter of ulna; ABS- Anterior breadth of sacrum; TDSS1- Transverse diameter of the first sacral segment; Minh- Maximum innominate height; MIB- Maximum innominate breadth; WIB- Minimum innominate breadth; ASISS- Anterior superior iliac spine to symphysion.

Table 11: *Continued*

Measurements	Dry bone				Lodox			
	Intra-observer		Inter-observer		Intra-observer		Inter-observer	
	TEM	rTEM (%)	TEM	rTEM (%)	TEM	rTEM (%)	TEM	rTEM (%)
WIB[x] (L)	0.03	0.53	0.11	1.91	0.01	0.18	0.01	0.18
ASISS[y] (L)	0.07	0.71	0.13	1.10	0.04	0.48	0.04	0.48
MLF[y] (R)	0.25	0.51	0.80	1.83	0.19	0.44	0.19	0.44
BLF[y] (R)	0.06	0.13	0.07	0.17	0.05	0.12	0.05	0.12
EBF[x] (R)	0.10	1.23	0.08	1.02	0.03	0.34	0.02	0.34
MDFh[d] (R)	0.06	1.38	0.04	0.88	0.07	1.51	0.07	1.51
TSDF[x] (R)	0.02	0.72	0.06	2.02	0.04	1.37	0.04	1.37
MDF[x] (R)	0.04	1.34	0.01	3.38	0.04	1.32	0.04	1.32
mDF[x] (R)	0.02	0.89	0.07	2.94	0.04	1.51	0.04	1.50
LT[y] (R)	0.23	0.64	0.23	0.65	0.42	1.18	0.42	1.18

[x] Measurements taken along the x-axis on the Lodox scan.[y]
Measurements taken along the y-axis on the Lodox scan.[d]
Measurements taken diagonally on the Lodox scan.
R- Right; L- Left; WIB- Minimum innominate breadth; ASISS- Anterior Superior Iliac Spine to Symphysion; MLF- Maximum length of the femur; BLF- Bicondylar length of femur; EBF- Epicondylar breadth of femur; MDFh- Maximum diameter of the femur head; TSDF- Transverse subtrochanteric diameter of femur; MDF- Maximum midshaft diameter of femur; mDF- Minimum midshaft diameter of femur; LT- Length of tibia.
Measurements which were unrepeatable are highlighted

Table 11: *Continued*

Measurements	Dry bone				Lodox			
	Intra-observer		Inter-observer		Intra-observer		Inter-observer	
	TEM	rTEM (%)	TEM	rTEM (%)	TEM	rTEM (%)	TEM	rTEM (%)
MPeBT[x] (R)	0.09	1.29	0.10	1.32	0.03	0.35	0.03	0.35
DeBT[x] (R)	0.06	1.33	0.09	1.83	0.03	0.51	0.03	0.51
MT[x] (R)	0.03	1.21	0.05	1.71	0.01	0.38	0.01	0.38
mT[x] (R)	0.02	0.69	0.04	1.85	0.02	0.98	0.02	0.98
MLFib[y] (R)	0.11	0.32	0.10	0.27	0.06	0.16	0.06	0.16
MDFib[x] (R)	0.02	1.43	0.03	1.99	0.02	1.13	0.02	1.13
MLF[y] (L)	0.15	0.35	0.59	1.33	0.11	0.24	0.11	0.24
BLF[y] (L)	0.24	0.55	0.83	1.89	0.03	0.08	0.03	0.08
EBF[x] (L)	0.11	1.45	0.05	1.42	0.02	0.21	0.02	0.21
MDFh[d] (L)	0.04	0.83	0.06	1.43	0.06	1.48	0.06	1.48
TSDF[x] (L)	0.04	1.42	0.04	1.44	0.02	0.61	0.02	0.61

[x] Measurements taken along the x-axis on the Lodox scan.[y]
Measurements taken along the y-axis on the Lodox scan.[d]
Measurements taken diagonally on the Lodox scan.
R- Right; L- Left; MPeBT- Maximum proximal epiphyseal breadth of tibia; DeBT- Distal epiphyseal breadth of tibia; MT- Maximum midshaft diameter of tibia; mT- Minimum midshaft diameter of tibia; MLFib- Maximum length of fibula; MDFib-Maximum diameter of fibula at midshaft; MLF- Maximum length of femur; BLF- Bicondylar length of femur; EBF- Epicondylar breadth of femur; MDFh- Maximum diameter of the femur head; TSDF- Transverse subtrochanteric diameter of femur.

Table 11: *Continued*

Measurements	Dry bone				Lodox			
	Intra-observer		Inter-observer		Intra-observer		Inter-observer	
	TEM	rTEM (%)	TEM	rTEM (%)	TEM	rTEM (%)	TEM	rTEM (%)
MDF[x] (L)	0.02	0.73	0.12	4.20	0.04	1.36	0.10	3.58
mDF[x] (L)	0.03	1.28	0.07	3.00	0.04	1.44	0.23	8.57
LT[y] (L)	0.07	0.19	0.30	0.84	0.10	0.27	0.41	1.14
MPeBT[x] (L)	0.1	1.42	0.12	1.66	0.03	0.34	0.05	0.69
DeBT[x] (L)	0.06	1.20	0.08	1.70	0.04	0.70	0.05	0.98
MT[x] (L)	0.04	1.39	0.04	1.42	0.01	0.58	0.03	1.03
mT[x] (L)	0.02	1.03	0.03	1.71	0.02	0.69	0.03	1.20
MLFib[y] (L)	0.13	0.36	0.12	0.35	0.02	0.06	0.13	0.36
MDFib[x] (L)	0.02	1.46	0.03	1.87	0.01	0.75	0.03	2.60

[x] *Measurements taken along the x-axis on the Lodox scan.*

[y] *Measurements taken along the y-axis on the Lodox scan.*

R- Right; L- Left; MDF- Maximum midshaft diameter of femur; mDF- Minimum midshaft diameter of femur; LT- Length of tibia; MPeBT- Maximum proximal epiphyseal breadth of tibia; DeBT- Distal epiphyseal breadth of tibia; MT- Maximum midshaft diameter of tibia; mT- Minimum midshaft diameter of tibia; MLFib- Maximum length of fibula; MDFib-Maximum diameter of the fibula at midshaft.

Measurements which were unrepeatable are highlighted

4.3 Differences between Lodox and dry bone measurements

Generally, skeletal measurements which differ with no more than 2 mm (0.2 cm) are acceptable in forensic anthropology (Stull *et al.,* 2013). Most of the measurements collected had average differences greater than 0.2 cm (Table 12 to 14). For the skull dataset, this was all, except for the FOB (0.14 cm), HMB (L) (0.05 cm) and (R) (0.05 cm) and the MRH (L) (0.00 cm) (Table 12).

For the pectoral girdle and upper limb dataset, most mean differences were less than 0.2 cm, with the exceptions of the measurements; MLC (R) (0.45 cm), HS (R) (0.32 cm), BS (R) (0.59 cm), MLC (L) (0.46 cm), BS (L) (0.31 cm), EBH (R) (0.33 cm) and PLU ((R) (1.97 cm) and (L) (2.32 cm)) (Table 13).

For the pelvic and lower limb dataset, overall mean differences were greater than 0.2 cm, with exceptions of the measurements; MInH (L) (0.15 cm), WIB (R) (0.08 cm), TSDF (L) (0.03 cm) and (R) (0.04 cm), MDF (L) (0.16 cm) and (R) (0.13 cm), mDF (L) (0.19 cm) and (R) (0.18 cm), MT (L) (0.13 cm) and (R) (0.07 cm) and MLFib (L) (0.2 cm), MDFib (L) (0.04 cm) and (R) (0.03 cm) (Table 14). Measurements in this section which were noticeably high were the ASISS (L) (1.28 cm) and (R) (1.33 cm) (Table 12).

4.3.1 Percentage difference- Lodox vs. dry bone

The calculated percentage difference between Lodox and dry bone measurements showed how much the dry bone and Lodox measurements differed from each other (Stull *et al*., 2014). The minimum, maximum and average percentage difference for each measurement were summarised in Table 12 to14. The average percentage differences ranged from 0.82%-17.48%, with most of the measurement's averages being below 10%.

For the skull, the FOB (5.29%) showed the lowest average percentage difference and the MRH (L) (17.48%) the greatest (Table 12). For the pectoral girdle and upper limb measurements, the lowest and highest average percentage difference were the MLU (R) (0.82%) and the MDC (L) (13.88%), respectively (Table 13). The lowest average percentage difference from the pelvic girdle and lower limb measurements was the left BLF (0.82%) and the highest was the left ASISS (15.74%) (Table 14).

4.3.2 Paired t-test-/Wilcoxon signed-rank test Lodox vs. dry bone

A normality test was conducted for each of the dry bone and Lodox measurements. The results of the Shapiro-Wilk test (p-values) for the dry bone and Lodox scan measurements are shown in Appendix C.

Based on the results of the normality test (Appendix C) conducted on the dry bone and Lodox measurements, either a paired t-test or the Wilcoxon signed-rank test was used to compare the dry bone measurements with the Lodox measurements. The comparison was to determine whether a significant difference existed between the dry bone and Lodox measurements. Where the measurements for both the dry bone and Lodox were normally distributed, the paired t-test was used. The paired t-test compared the mean values between the measurements collected from the dry bone and those collected from the Lodox images (Kim, 2015). The Wilcoxon signed-rank test is a nonparametric test used when the data of either the dry bone or Lodox measurements, or both were not normally distributed (Kim, 2015). The Wilcoxon signed-rank test compared the median values between the measurements collected from the dry bone and Lodox measurements (Kim, 2015). Out of the 84 measurements collected, paired t-test was conducted on 67 measurements and the Wilcoxon signed-rank test was conducted on the remaining, 17 measurements.

These results are summarised in Tables 12 to 14. From the 84 measurements, 21

measurements showed that no significant difference existed between the dry bone and Lodox measurements ($p>0.05$). For the skull, only the HMB (L) and (R), showed no significant difference between the dry bone and Lodox measurements (Table 12). For the pectoral and upper limb measurements, no significant difference was found between the dry bone and Lodox measurements of the MDC (L) and (R), MLH (L) and (R), mDR (L) and (R), mDU (L) and (R) and the HS (L) (Table 13). No significant difference was noted between the dry bone and Lodox measurements of pelvic girdle and lower limb measurements; ABS, BLF (R), TSDF (L) and (R), LT (L), MT (R), MLFib (L) and (R) and MDFib (L) and (R) (Table 14).

Table 12: Summary of the descriptive statistics including the minimum (min), maximum (max), mean and standard deviation (SD) as well as the differences between dry bone and Lodox skull dataset

Measurements		**Dry bone (cm)**				**Lodox (cm)**				**Mean difference (cm)**	**Percentage difference (%)**			**Paired t-test /Wilcoxon signed-rank test**
	n	**Min**	**Max**	**Mean**	**SD**	**Min**	**Max**	**Mean**	**SD**	**(Dry bone-Lodox)**	**Min**	**Max**	**Mean**	**p-value**
ZYGB	36	10.00	13.90	12.49	0.79	10.56	14.50	13.25	0.81	-0.76	2.36	14.61	6.05	0.000[w]
FOL	49	1.46	4.19	3.66	0.43	2.49	4.02	3.45	0.30	0.21	0.00	86.82	9.58	0.000 [w]
FOB	49	2.41	3.75	2.85	0.24	2.55	3.47	2.99	0.23	-0.14	0.38	18.34	5.29	0.000 [w]
HMB (R)	43	2.18	3.67	2.81	0.32	1.72	3.85	2.76	0.42	0.05	0.00	26.91	7.74	0.291*
mRB (R)	44	2.23	4.12	3.17	0.44	2.06	3.65	2.85	0.42	0.32	0.00	33.02	11.26	0.000
HMB (L)	47	2.03	3.57	2.75	0.39	2.10	3.57	2.80	0.34	-0.05	0.38	18.34	6.37	0.178*
mRB (L)	47	2.19	4.13	3.20	0.42	1.70	3.76	2.83	0.46	0.37	0.00	30.04	12.99	0.000
MRh (L)	49	3.10	6.90	5.03	0.65	3.10	6.90	5.03	0.62	0.00	0.92	34.55	17.48	0.000
ML (L)	47	7.54	10.05	8.59	0.62	5.90	11.70	8.23	1.21	0.36	1.07	48.48	9.54	0.006

*R- Right; L- Left; w- Wilcoxon signed-rank test; *p>0.05 (Highlighted)*

ZYGB- Bizygomatic breath; FOL- Length of foramen magnum; FOB- Breadth of foramen magnum; HMB- Height of mandibular body; mRB- Minimum ramus breadth;MRh- Maximum ramus height; ML- Mandibular length.

Table 13: Summary of the descriptive statistics including the minimum (min), maximum (max), mean and standard deviation (SD) as well as the differences between dry bone and Lodox pectoral girdle and upper limb dataset

Measurements		**Dry bone (cm)**				**Lodox (cm)**				**Mean difference (cm)**	**Percentage difference (%)**			**Paired t-test /Wilcoxon signed-rank test**
	n	**Min**	**Max**	**Mean**	**SD**	**Min**	**Max**	**Mean**	**SD**	**(Dry bone-Lodox)**	**Min**	**Max**	**Mean**	**p-value**
MLC (R)	50	11.70	16.50	14.21	1.21	11.44	17.16	14.66	1.35	-0.45	0.27	15.40	4.24	0.000
MDC (R)	49	0.86	1.63	1.13	0.17	0.78	1.72	1.11	0.20	0.02	0.00	34.20	11.93	0.331 w*
mDC (R)	50	0.75	1.50	1.03	0.18	0.75	1.52	1.08	0.16	-0.05	0.00	33.66	13.53	0.033
HS (R)	49	11.90	17.30	14.42	1.33	9.48	17.16	14.10	1.39	0.32	0.00	42.52	2.60	0.004
BS (R)	49	7.80	11.10	9.47	0.88	8.02	14.46	10.06	1.12	-0.59	0.09	43.43	5.47	0.000 w
MLC (L)	49	11.90	16.50	14.32	1.16	12.04	17.70	14.78	1.31	-0.46	0.23	13.27	3.53	0.000
MDC (L)	49	0.78	1.69	1.10	0.21	0.82	1.52	1.12	0.16	-0.02	0.00	32.32	13.88	0.573 w*
mDC (L)	49	0.74	1.50	1.01	0.18	0.75	1.45	1.07	0.16	-0.06	1.77	42.55	12.37	0.019 w
HS (L)	48	11.50	17.00	14.31	1.30	11.37	16.82	14.21	1.27	0.10	0.00	7.00	2.07	0.093*

*R- Right; L- Left; w- Wilcoxon signed-rank test; *p>0.05 (Highlighted)*

MLC- Maximum length of clavicle; MDC-Maximum diameter of clavicle at midshaft; mDC-Minimum diameter of clavicle at midshaft; HS- Height of scapula; BS-Breadth of scapula.

Table 13: *Continued*

Measurements		Dry bone (cm)				Lodox (cm)				Mean difference (cm)	Percentage difference(%)			Paired t-test /Wilcoxon signed-rank test
	n	Min	Max	Mean	SD	Min	Max	Mean	SD	(Dry bone-Lodox)	Min	Max	Mean	p-value
BS (L)	49	7.70	11.00	9.51	0.93	8.00	11.24	9.82	0.90	-0.31	0.00	14.43	3.65	0.000 [w]
MLH (R)	50	25.05	35.90	30.24	2.14	22.74	35.83	30.26	2.34	-0.02	0.03	19.31	0.93	0.850*
EBH (R)	50	4.74	6.75	5.72	0.53	4.87	7.48	6.05	0.58	-0.33	1.92	14.25	5.55	0.000
MVDhH (R)	50	3.22	5.05	4.13	0.41	3.39	5.25	4.29	0.41	-0.16	0.25	13.64	4.11	0.000
MDH (R)	50	1.52	2.71	2.03	0.25	1.60	2.88	2.11	0.30	-0.08	0.53	20.96	4.97	0.000
mDH (R)	50	1.45	2.41	1.90	0.25	1.49	2.54	1.97	0.27	-0.07	0.00	28.31	6.84	0.001
MLR (R)	47	18.90	27.40	22.91	1.74	19.20	27.33	22.80	1.67	0.11	0.00	2.89	1.03	0.005
MDR (R)	47	1.12	1.99	1.44	0.18	0.94	1.91	1.39	0.22	0.05	0.00	29.39	8.62	0.036
mDR (R)	47	1.00	1.76	1.32	0.20	0.90	1.89	1.33	0.22	-0.01	0.00	24.39	9.00	0.836*

*R- Right; L- Left; w- Wilcoxon signed-rank test; *p>0.05 (Highlighted)*

BS- Breadth of scapula; MLH- Maximum length of humerus; EBH- Epicondylar breadth of humerus; MVDhH- Maximum vertical diameter of the head of humerus; MDH- Maximum diameter of humerus at midshaft; mDH- Minimum diameter of humerus at midshaft; MLR- Maximum length of radius; MDR- Maximum diameter ofradius at midshaft; mDR- Minimum diameter of radius at midshaft.

Table 13: *Continued*

Measurements		Dry bone (cm)				Lodox (cm)				Mean difference (cm)	Percentage difference(%)			Paired t-test /Wilcoxonsigned-rank test
	n	Min	Max	Mean	SD	Min	Max	Mean	SD	(Dry bone-Lodox)	Min	Max	Mean	p-value
MDRh (R)	48	1.60	2.47	2.05	0.23	1.43	2.57	1.95	0.22	0.10	0.50	22.46	8.00	0.000
MLU (R)	44	21.70	28.40	24.88	1.64	21.97	28.41	25.03	1.61	-0.15	0.04	3.63	0.82	0.000
MDU (R)	46	1.15	2.00	1.49	0.20	0.97	1.98	1.37	0.25	0.12	0.00	42.28	13.63	0.000
mDU (R)	46	0.96	1.88	1.34	0.20	0.89	1.94	1.31	0.24	0.03	0.00	38.63	12.82	0.524*
PLU (R)	45	12.20	28.30	23.74	2.43	19.14	25.45	21.77	1.47	1.97	0.18	17.46	10.62	0.000 [w]
MLH (L)	50	22.90	35.70	29.86	2.30	25.27	35.75	30.22	2.11	-0.36	0.00	36.4	1.37	0.084*
EBH (L)	49	4.67	6.81	5.73	0.54	4.94	7.62	6.05	0.58	-0.32	1.70	17	5.53	0.000
MVDhH (L)	50	3.20	4.98	4.10	0.40	3.37	5.18	4.25	0.39	-0.15	0.00	11.17	3.77	0.000
MDH (L)	50	1.41	2.58	1.99	0.25	1.59	2.63	2.07	0.26	-0.08	0.00	23.20	4.97	0.000

*R- Right; L- Left; w- Wilcoxon signed-rank test; *p>0.05 (Highlighted)*

MDRh- Maximum diameter of radial head; MLU-Maximum length of ulna; MDU- Maximum diameter of ulna at midshaft; mDU- Minimum diameter of ulna at midshaft; PLU- Physiological length of ulna. EBH- Epicondylar breadth of humerus; MVDhH- Maximum vertical diameter of the head of humerus; MDH- Maximumdiameter of humerus at midshaft.

Table 13: *Continued*

Measurements		Dry bone (cm)				Lodox (cm)				Mean difference (cm)	Percentage difference (%)			Paired t-test /Wilcoxonsigned-rank test
	n	Min	Max	Mean	SD	Min	Max	Mean	SD	(Dry bone-Lodox)	Min	Max	Mean	p-value
mDH (L)	50	1.04	2.40	1.86	0.27	1.46	2.46	1.94	0.24	-0.08	0.00	26.53	6.47	0.004
MLR (L)	48	19.40	27.60	22.83	1.72	18.97	27.26	22.65	1.69	0.18	0.08	4.17	0.94	0.000
MDR (L)	48	1.10	1.82	1.43	0.16	1.02	1.68	1.33	0.18	0.10	0.00	30.53	9.17	0.000
mDR (L)	48	0.89	1.79	1.32	0.19	0.95	1.66	1.31	0.19	0.01	0.00	32.47	9.3	0.753*
MDRh (L)	48	1.69	2.49	2.04	0.21	1.57	2.33	1.96	0.19	0.08	0.00	22.73	6.08	0.000
MLU (L)	42	21.60	28.50	24.82	1.66	21.82	28.58	24.93	1.64	-0.11	0.05	5.11	0.90	0.018
MDU (L)	43	1.08	1.89	1.48	0.18	1.01	2.02	1.42	0.22	0.06	0.62	30.49	8.41	0.009
mDU (L)	43	0.99	1.84	1.35	0.18	0.97	1.79	1.34	0.20	0.01	0.00	43.41	1.41	0.448 w*
PLU (L)	44	20.40	28.40	23.95	1.93	18.13	26.44	21.72	1.67	2.23	0.19	16.02	9.73	0.000

*R- Right; L- Left; w- Wilcoxon signed-rank test; *p>0.05 (Highlighted)*
mDH- Minimum diameter of humerus at midshaft; MLR- Maximum length of radius; MDR- Maximum diameter of radius at midshaft; mDR- Minimum diameter of radius at midshaft; MDRh- Maximum diameter of radial head; MLU-Maximum length of ulna; MDU- Maximum diameter of ulna at midshaft; mDU- Minimum of ulna at midshaft; PLU- Physiological length of ulna.

Table 14: Summary of the descriptive statistics, minimum and maximum percentage difference and paired t-test results between the dry bone and Lodox pelvic and lower limb dataset

Measurements		**Dry bone (cm)**				**Lodox (cm)**				**Mean difference(cm)**	**Percentage difference(%)**			**Paired t-test /Wilcoxonsigned-rank test**
	n	**Min**	**Max**	**Mean**	**SD**	**Min**	**Max**	**Mean**	**SD**	**(Dry bone-Lodox)**	**Min**	**Max**	**Mean**	**p-value**
AHS	46	5.26	11.97	10.40	1.20	8.57	14.50	10.86	1.02	-0.47	0.50	56.87	4.56	0.000
ABS	46	9.26	12.05	10.41	0.63	3.87	12.93	10.67	1.30	-0.26	0.03	9.46	1.46	0.146*
TDSS1	42	3.77	6.01	4.91	0.57	2.89	5.17	4.25	0.60	0.66	0.62	37.36	15.17	0.000
MInh (R)	48	17.00	21.60	19.07	1.15	17.05	21.66	19.22	1.26	-0.15	0.05	4.06	1.45	0.003
MIB (R)	46	12.65	16.10	14.33	0.88	13.14	17.19	15.01	1.01	-0.68	1.78	12.40	14.67	0.000
WIB (R)	49	4.57	7.08	5.88	0.54	4.70	7.49	5.96	0.581	-0.08	0.16	12.90	3.54	0.044
ASISS (R)	46	9.18	12.13	10.57	0.72	7.19	12.68	9.29	0.94	1.28	0.38	32.79	14.48	0.000 ^{w}
MInh (L)	48	16.90	21.60	19.10	1.28	16.85	21.86	19.31	1.35	-0.21	0.00	4.50	1.71	0.000 ^{w}
MIB (L)	44	12.80	16.40	14.26	0.85	12.97	16.97	15.02	1.00	-0.76	1.31	19.93	14.64	0.000
WIB (L)	48	4.63	7.54	5.89	0.55	4.70	9.11	6.10	0.68	-0.23	0.33	41.32	5.16	0.001 ^{w}
ASISS (L)	41	8.90	12.53	10.52	0.77	7.50	12.40	9.19	1.00	1.33	0.09	29.21	15.74	0.000 ^{w}

*R- Right; L- Left; w- Wilcoxon signed-rank test; *p>0.05 (Highlighted)*

AHS- Anterior height of sacrum; ABS- Anterior breadth of sacrum; TDSS1- Transverse diameter of the first sacral segment; Minh- Maximum innominate height; MIB- Maximum innominate breadth; WIB- Minimum innominate breadth; ASISS- Anterior superior iliac spine to symphysion.

Table 14: *Continued*

Measurements		Dry bone (cm)				Lodox (cm)				Mean difference (cm)	Percentage difference (%)			Paired t-test /Wilcoxonsigned-rank test
	n	Min	Max	Mean	SD	Min	Max	Mean	SD	(Dry bone-Lodox)	Min	Max	Mean	p-value
MLF (R)	49	32.20	49.70	42.39	3.03	37.79	50.00	42.96	2.67	-0.57	0.14	19.51	1.85	0.021
BLF (R)	49	36.10	49.30	42.12	2.82	37.46	49.52	42.45	2.65	-0.33	0.00	15.41	1.40	0.124*
EBF (R)	48	5.55	8.40	7.25	0.63	6.07	9.31	7.94	0.68	-0.69	0.50	24.21	9.23	0.000
MDFh (R)	49	2.36	5.11	4.14	0.49	3.51	5.22	4.45	0.42	-0.31	0.97	27.05	8.10	0.000
TSDF (R)	49	2.28	3.73	2.84	0.34	2.16	3.99	2.80	0.34	0.04	0.00	33.28	4.96	0.286*
MDF (R)	48	2.00	3.53	2.57	0.303	1.98	3.23	2.70	0.28	-0.13	1.19	34.20	8.42	0.001
mDF (R)	48	1.91	3.04	2.46	0.27	1.94	3.17	2.64	0.27	-0.18	0.36	36.64	8.28	0.000
LT (R)	47	31.85	42.00	35.48	2.33	25.46	42.62	35.69	2.76	-0.21	0.03	31.84	2.09	0.000 w
MPeBT (R)	46	5.30	8.40	6.90	0.60	5.99	8.97	7.61	0.63	-0.71	0.66	26.45	10.19	0.000
DeBT (R)	47	3.90	5.80	4.55	0.40	4.29	5.96	5.03	0.39	-0.48	0.59	29.88	10.50	0.000

*R- Right; L-Left; w- Wilcoxon signed-rank test; *p>0.05 (Highlighted)*

MLF- Maximum length of femur; BLF- Bicondylar length of femur; EBF- Epicondylar breadth of femur; MDFh- Maximum diameter of the femur head; TSDF- Transverse subtrochanteric diameter of femur; MDF- Maximum midshaft diameter of femur; mDF- Minimum midshaft diameter of the femur; LT- Length of tibia; MPeBT- Maximum proximal epiphyseal breadth of tibia; DeBT- Distal epiphyseal breadth of tibia.

Table 14: *Continued*

Measurements		Dry bone (cm)				Lodox (cm)				Mean difference (cm)	Percentage difference (%)			Paired t-test /Wilcoxon signed-rank test
	n	Min	Max	Mean	SD	Min	Max	Mean	SD	(Dry bone-Lodox)	Min	Max	Mean	p-value
MT (R)	48	1.68	3.37	2.40	0.38	1.88	3.16	2.47	0.31	-0.07	0.00	34.93	8.77	0.128*
mT (R)	48	1.60	2.78	2.15	0.28	1.86	3.09	2.41	0.30	-0.26	0.00	38.39	13.43	0.000
MLFib (R)	44	31.00	40.90	34.89	2.21	31.51	41.52	35.11	2.19	-0.22	0.00	9.29	1.40	0.080*
MDFib (R)	45	1.02	1.85	1.40	0.20	0.97	1.91	1.37	0.22	0.03	0.00	35.57	7.75	0.160*
MLF (L)	47	37.80	49.90	42.89	2.74	37.99	49.99	43.16	2.80	-0.27	0.08	6.58	0.90	0.007
BLF (L)	47	37.30	49.30	42.45	2.73	37.82	49.76	42.68	2.70	-0.23	0.07	3.05	0.82	0.000
EBF (L)	48	5.60	8.90	7.27	0.66	4.92	9.14	7.79	0.77	-0.52	0.7	45.28	8.74	0.000 [w]
MDFh (L)	48	2.41	4.95	4.19	0.49	3.35	5.35	4.41	0.43	-0.22	0.21	47.47	6.40	0.000 [w]
TSDF (L)	48	1.78	4.05	2.84	0.44	2.22	3.85	2.81	0.31	0.03	0.00	47.54	7.78	0.491*

*R- Right; L- Left; w- Wilcoxon signed-rank test; *p>0.05 (Highlighted)*

MT- Maximum midshaft diameter of the tibia; mT- Minimum midshaft diameter of the tibia; MLFib- Maximum length of the fibula; MDFib-Maximum diameter of thefibula at midshaft; MLF- Maximum length of the femur; BLF- Bicondylar length of the femur; EBF- Epicondylar breadth of femur; MDFh- Maximum diameter of thefemur head; TSDF- Transverse subtrochanteric diameter of femur.

Table 14: *Continued*

Measurements		Dry bone (cm)				Lodox (cm)				Mean difference (cm)	Percentage difference(%)			Paired t-test /Wilcoxonsigned-rank test
	n	Min	Max	Mean	SD	Min	Max	Mean	SD	(Dry bone-Lodox)	Min	Max	Mean	p-value
MDF (L)	48	1.79	3.55	2.55	0.31	2.12	3.29	2.71	0.26	-0.16	0.00	53.58	8.02	0.000
mDF (L)	48	2.03	2.96	2.49	0.26	2.08	3.76	2.68	0.30	-0.19	0.87	35.74	7.92	0.000
LT (L)	47	31.00	42.10	35.37	2.30	32.07	42.42	35.71	2.29	-0.34	0.03	21.22	2.22	0.161*
MPeBT (L)	47	5.35	7.90	6.85	0.60	5.97	8.87	7.60	0.60	-0.75	0.13	34.88	10.82	0.000
DeBT (L)	48	3.90	5.60	4.57	0.42	4.26	5.83	5.04	0.40	-0.47	1.22	27.21	10.63	0.000
MT (L)	49	1.70	3.12	2.35	0.36	1.86	3.09	2.48	0.31	-0.13	0.50	40.99	10.30	0.005
mT (L)	49	1.61	2.64	2.08	0.24	1.81	3.02	2.43	0.30	-0.35	0.79	44.07	15.09	0.000
MLFib (L)	44	29.10	41.30	34.63	2.43	30.38	40.82	34.83	2.25	-0.20	0.03	13.99	1.56	0.184*
MDFib (L)	47	0.97	1.74	1.37	0.18	0.94	1.98	1.33	0.24	0.04	0.00	39.66	11.75	0.234*

*R- Right; L- Left; w- Wilcoxon signed-rank test; *p>0.05 (Highlighted)*

MDF- Maximum midshaft diameter of femur; mDF- Minimum midshaft diameter of femur; LT- Length of tibia MPeBT- Maximum proximal epiphyseal breadth of the tibia; DeBT- Distal epiphyseal breadth of the tibia; MT- Maximum midshaft diameter of the tibia; mT- Minimum midshaft diameter of the tibia; MLFib- Maximum length of fibula; MDFib-Maximum diameter of fibula at midshaft.

4.4 Bland-Altman Plot

Band-Altman plots were included, as it graphically represents the difference between the Lodox and dry bone measurements. The graphs represented below, include the measurements which showed no statistically significant difference between the Lodox and dry bone measurements, according to the paired t-tests and the Wilcoxon signed-rank test (Figures12-18). The Bland-Altman plots for measurements, which showed statistical difference between the dry bone and Lodox images, are illustrated in appendix D.

The mean (represented as the red line) provides an estimate of the value that each of the measurement differences should tend to. While the limits of agreement provide the acceptable range which the measurements should fall under. In all the graphs, majority of the measurements exist within the limits of agreement (mean ± (1.96×SD) (Bland & Altman, 1999).

Most of the differences between the dry bone and Lodox measurements were randomly scattered around zero, with a large number of these measurements falling within the limits of agreement. In some instances, the limits of agreement were greater (upper limit of agreement) or smaller (lower limit of agreement) than the values shown in the graph and couldnot be shown, as a result of the scale set by the software program used (SPSS). Although the differences were within the limits of agreement, most were not within the acceptable 0.2 cm measurement error. Measurements whose differences were not within the acceptable 0.2 cm measurement error were the, HMB (L) and (R), HS (L), mDU (R), MT (L) and MDFib (L).

A

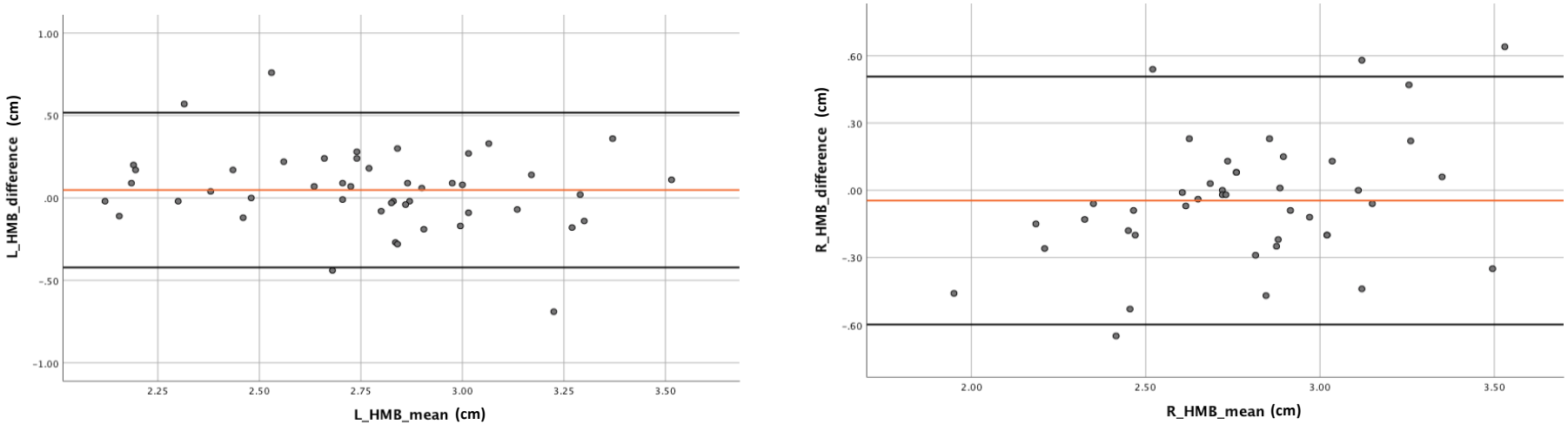

Figure 12 Bland-Altman plots representing the agreement of the skull measurements for the A) height of the mandibular body on the left and B) right side, taken from the dry bone and Lodox images. The graph shows the mean (red line) and the limits of agreement (with a 95% confidence interval, represented by the solid black lines).

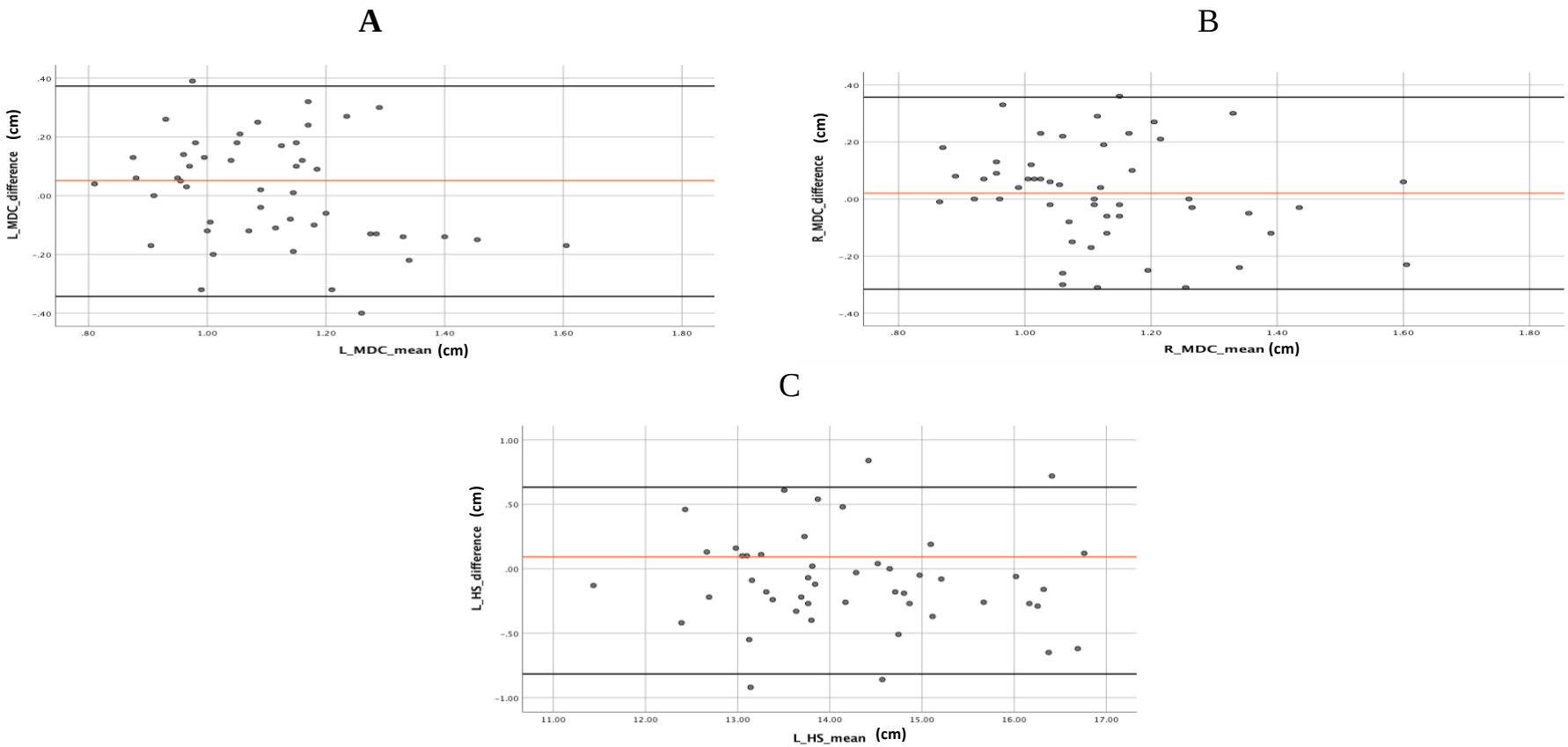

Figure 13 Bland-Altman plots representing the agreement of pectoral girdle measurements for the A) maximum diameter of clavicle at midshaft on the left and B) right side and C) the height of scapula, taken from the dry bone and Lodox images. The graph shows the mean (red line) and the limits of agreement (with a 95% confidence interval, represented by the solid black lines).

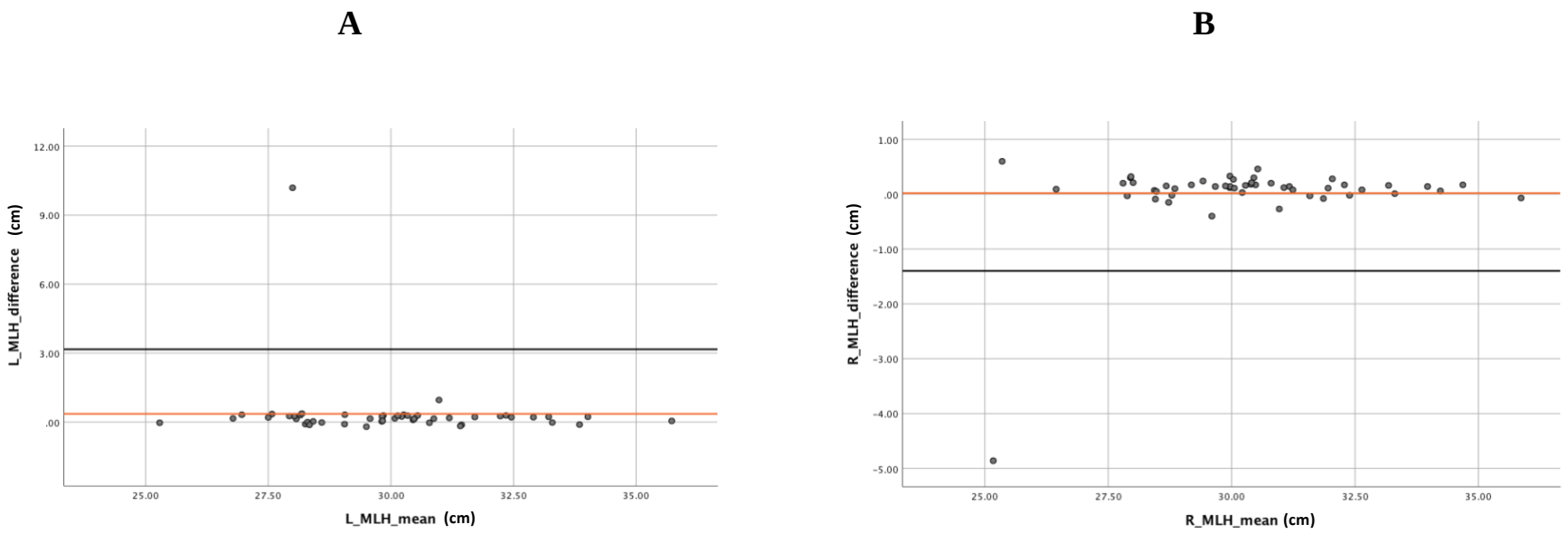

Figure 14 Bland-Altman plots representing the agreement of upper limb measurements for the A) maximum length of humerus on the left and B) right side, taken from the dry bone and Lodox images. The graph shows the mean (red line) and the limits of agreement (with a 95% confidence interval, represented by the solid black lines). In the case of F) and G) the lower limits of agreement and upper limits of agreement, respectively, could not fit into the scale of the graph.

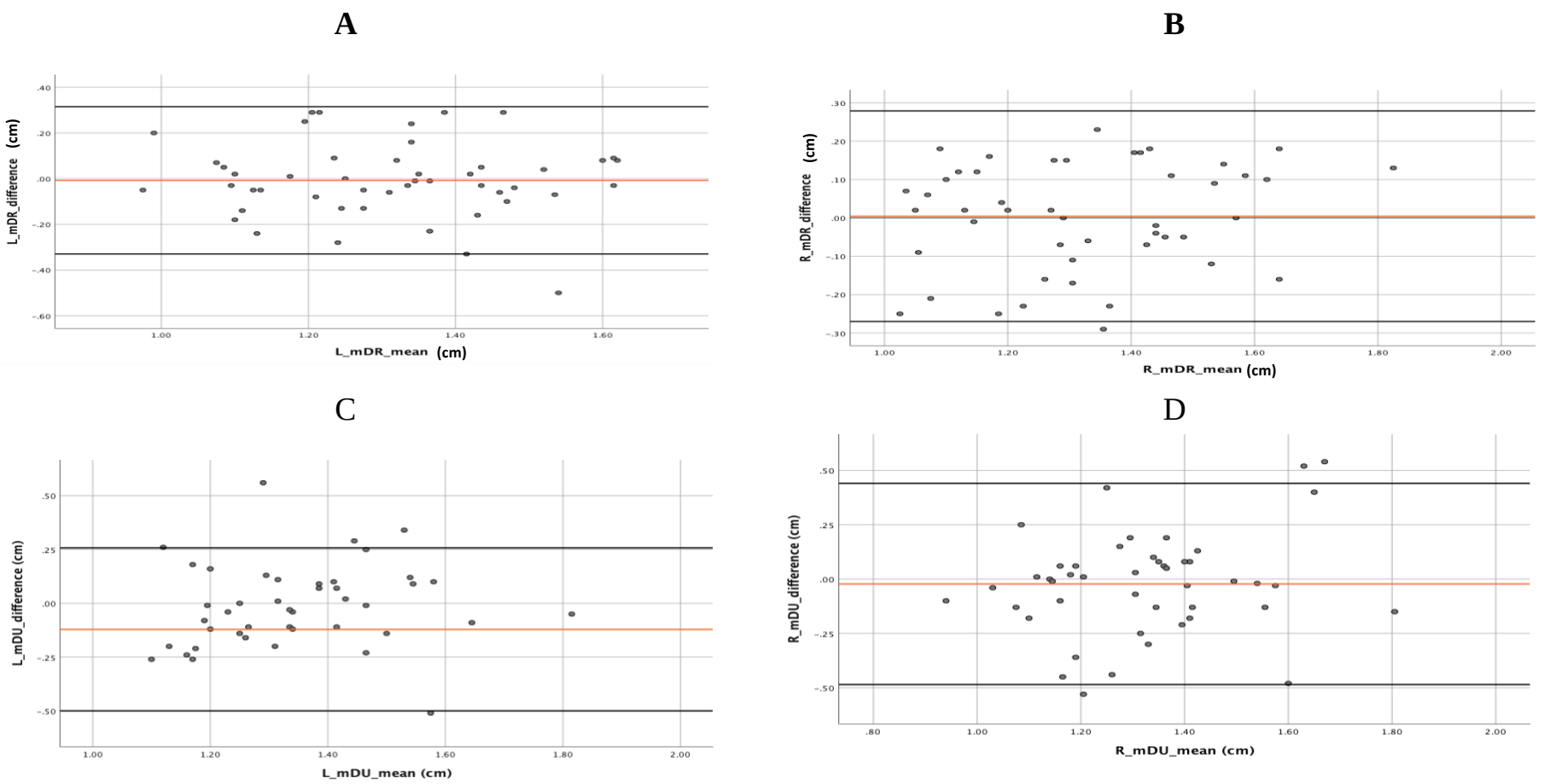

Figure 15 Bland-Altman plots representing the agreement of upper limb measurements for the A) minimum diameter of radius at midshaft on the left and B) right side and the C) minimum diameter of ulna at midshaft on the left and D) right side, taken from the dry bone and Lodox images. The graph shows the mean (red line) and the limits of agreement (with a 95% confidence interval, represented by the solid black lines).

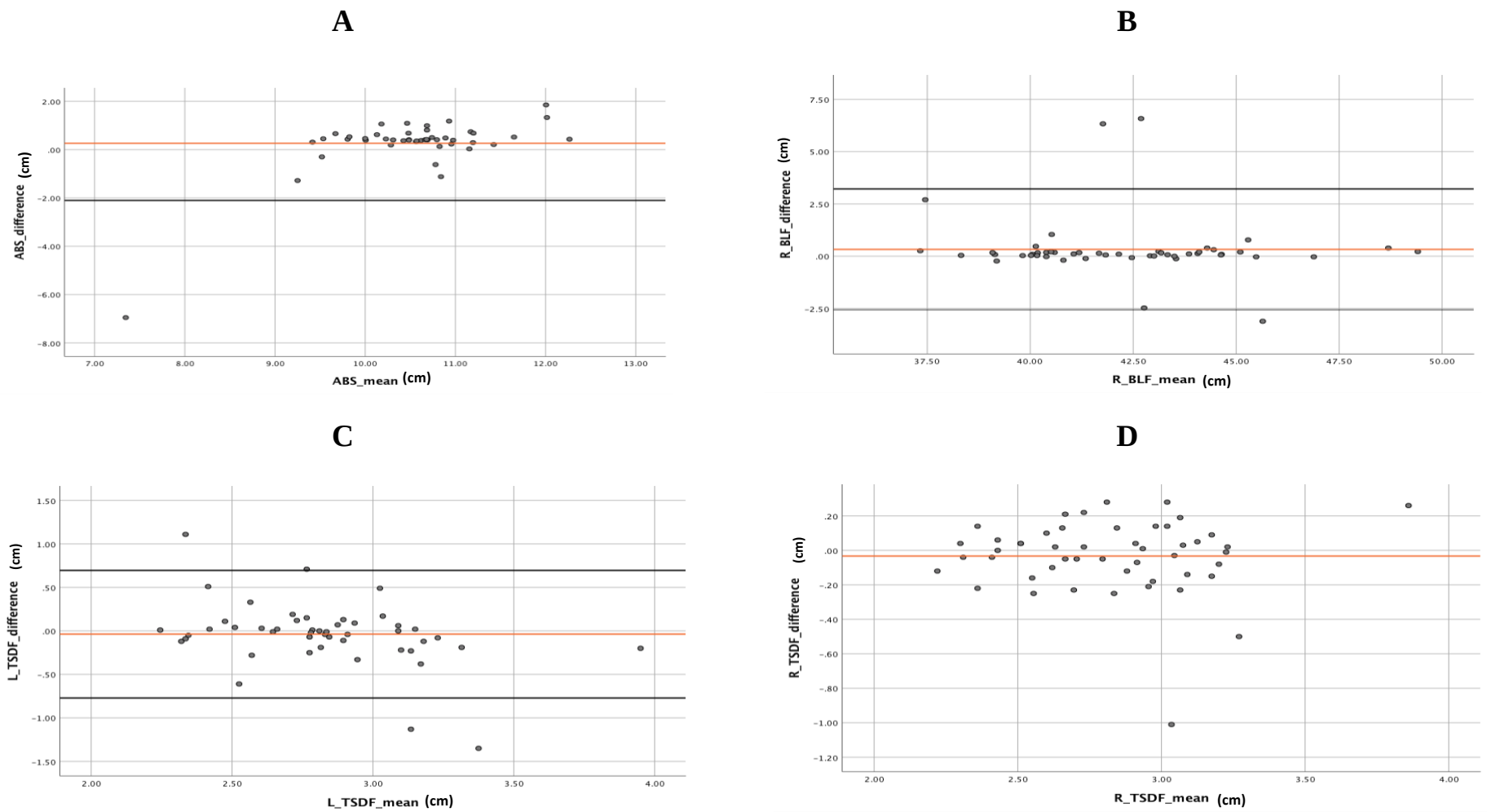

Figure 16 Bland-Altman plots representing the agreement of the pelvic girdle and lower limb measurements for the A) anterior breadth of scapula, B) bicondylar breadth of femur on the right side and the C) transverse diameter of femur on the left and D) right side taken from the dry bone and Lodox images. The graph shows the mean (red line) and the limits of agreement (with a 95% confidence interval, represented by the solid black lines).

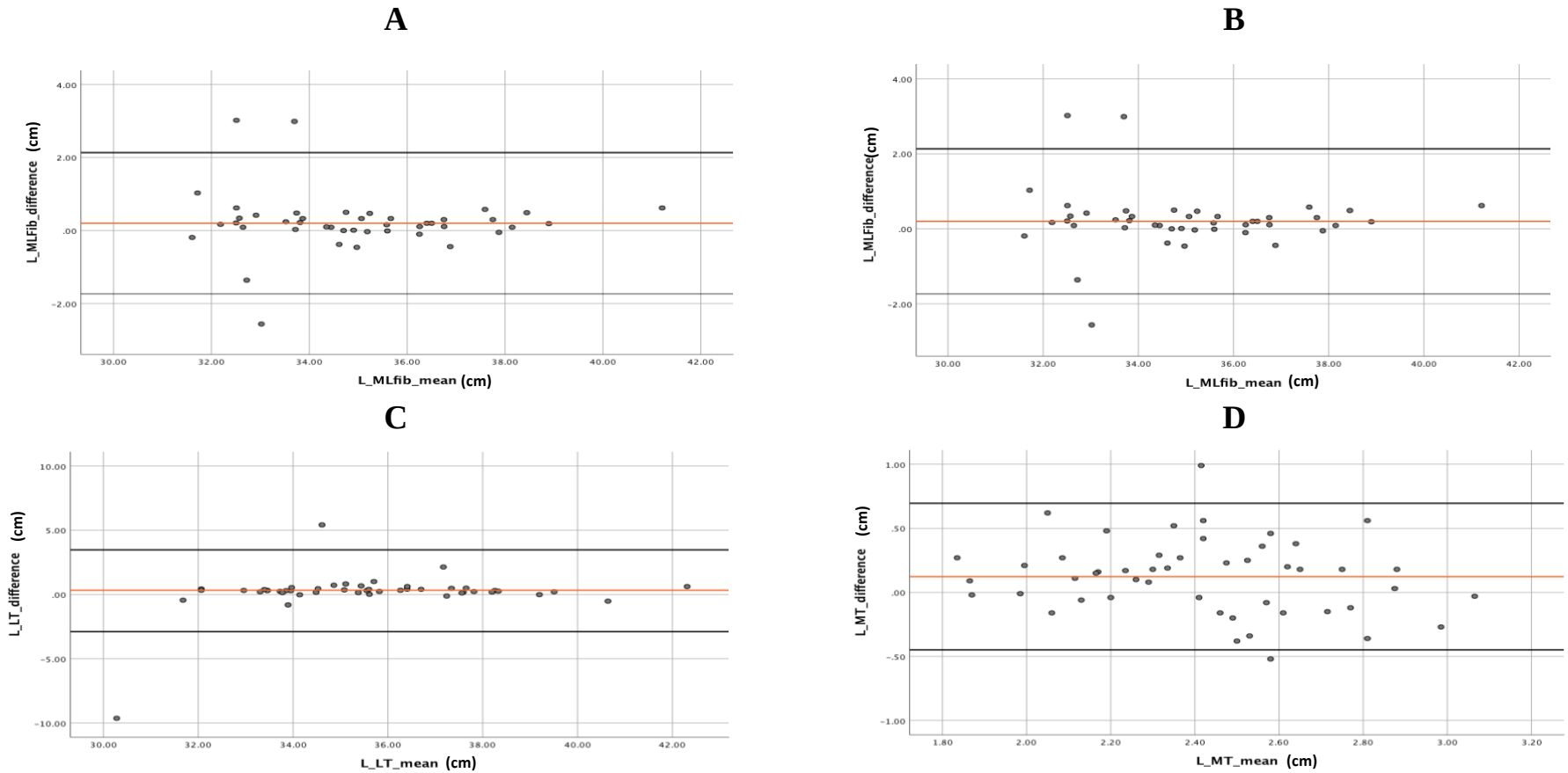

Figure 17 Bland-Altman plots representing the agreement of the pelvic girdle and lower limb measurements for the A) length of tibia on the left side, B) maximum midshaft diameter of tibia on the right side and the C) maximum length of fibula on the left and D) right side, taken from the dry bone and Lodox images. The graph shows the mean (red line) and the limits of agreement (with a 95% confidence interval represented by the solid black lines).

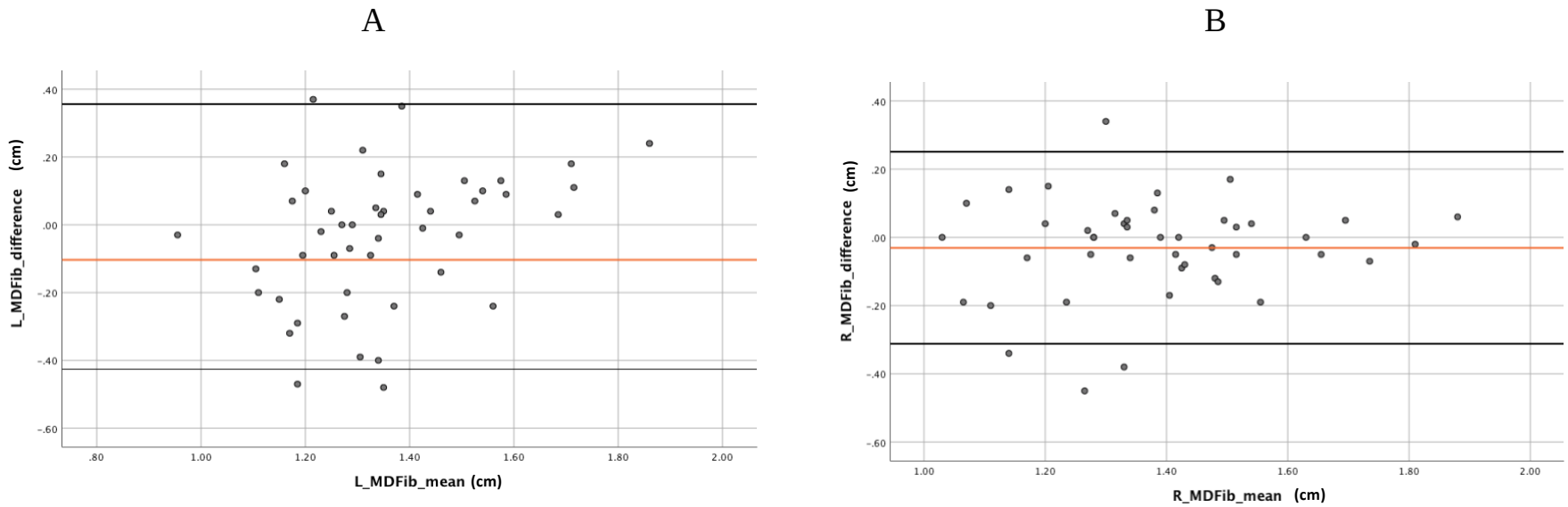

Figure 18 Bland-Altman plots representing the agreement of the lower limb measurements for the A) maximum midshaft diameter of fibula on the left and B) right side, taken from the dry bone and Lodox images. The graph shows the mean (red line) and the limits of agreement (with a 95% confidence interval, represented by the solid black lines).

The results display that most of the measurements were repeatable, except for the eight measurements collected from dry bone and the eight measurements collected from Lodox images.

Most of the measurements collected showed a significant difference ($p<0.05$) exist between Lodox images and dry bone. From these measurements was, the ABS, whose measurement was found not to be repeatable from Lodox images. The remaining measurements, showing no significant difference ($p>0.05$), were a combination of midshaft measurements with percentage differences greater than 10% and length measurements with percentage differences less than 10%. The results in the current study were found to have similarities and differences to what was found in other studies using other virtual imaging modalities (CT and MRI) and in Lodox images. The similarities, differences and reasons for the results obtained in this study are explained in the following discussion chapter (Chapter 5).

CHAPTER 5: DISCUSSION

Virtual imaging modalities are demonstrating to be of great importance in forensic science. In forensic science, virtual imaging modalities are used to document information on taphonomy (Fahrni *et al.,* 2017; Sansoni *et al.,* 2009), to locate foreign objects lodged in the bodies of deceased individuals (Bolton, 2010; Kučerová *et al.,* 2014; Thali *et al.,* 2003) and are used in mass fatalities (Rutty *et al.,* 2007), to name but a few applications.

The use of virtual imaging modalities in forensic anthropology is no longer only limited to aiding in the identification of deceased individuals, by means of comparing ante-mortem data to post-mortem data (Aalders *et al.,* 2017; Kahana & Hiss, 2005; Kučerová *et al.,* 2014; Thali *et al.,* 2009). The use extends to helping alleviate issues pertaining to cultural and religious beliefs of deceased individuals such as, in the Islamic and Indian population and the effects of secular trends on skeletal collections (Golmakani *et al.,* 2005; Goodman *et al.,* 2011; Gurley *et al.,* 2011; O'Sullivan *et al.,* 2018). Secular trends result in the lack of skeletal collections which can be considered as reference samples, as they are often no longer a representation of the demographics of given populations of a current time period. This makes forensic anthropological research on biological profiles, difficult (Dirkmaat *et al.,* 2009). In addition to these issues, is the lack of physical storage space for such collections and the time required to macerate the remains in order to have a physical skeletal collection. With the use of virtual imaging modalities to aid in post-mortem examinations and the rise of the virtual autopsy project (Thali *et al.,* 2009), forensic anthropologists have acknowledged the virtual shift and have begun to explore the uses of virtual imaging modalities in identifying trauma and pathology and in establishing biological profiles, using morphological and metric assessmentsof skeletal remains (Franklin *et al.,* 2016, Garvin & Stock, 2016; Obertová *et al.*,

2019).

Low-dose X-rays (Lodox) is a virtual imaging modality which is frequently used in medico-legal laboratories in various parts of the world, including South Africa (Lodox systems, 2012). The current study aimed to establish the repeatability and accuracy of standard osteometric measurements, collected from the 2D Lodox images. This was achieved by comparing the measurements collected from the 2D Lodox images to the measurements collected from the 3D corresponding dry bones. The repeatability and accuracy of the osteological measurements are discussed in the sections below.

5.1 Repeatability

Repeatability in the current study was assessed to test the variation between repeated measurements on the same skeletal elements at different times, by the principal investigator (intra-observer repeatability) and by a second investigator (inter-observer repeatability). This was done for measurements collected from Lodox images and dry bones. Results in the current study showed that most of the collected measurements could be repeated as they had rTEM values which were within the acceptable ranges, as suggested by Goto and Mascie-Taylor (2007). These ranges are <1.5% for intra-observer and <2% for inter-observer repeatability (Ulijaszek and Kerr, 1999; Perini *et al*., 2005; Goto and Mascie-Taylor, 2007).

5.1.1 Dry bone

In line with results by the DCP manual (Langley *et al*., 2016), most measurements collected from dry bone were found to be repeatable for intra- (<1.5%) and inter-observer (<2%), except for the inter-observer results for the measurements from the skull: MRH (L) (3.94%) and pelvic girdle/lower limb: TSDF (R) (2.02%), MDF (R) (3.38%) and (L) (4.20%),

mDF (R) (2.94%) and (L) (3.00%).

The difference in inter-observer results between the current study and that of Langley *et al.* (2016) is that it made use of four different observers, each with a different level of osteometric experience, while the current study only made use of two observers, with minimal experience. The collection of dry bone measurements for inter-observer data during the current study, were collected by the primary investigator and a second investigator, respectively. Both investigators are students with little experience in collecting osteometric measurements. The primary investigator had an honours level experience in collecting osteological measurements, while the secondary investigator had no experience in collecting post-cranial osteological measurements. The level of experience would have an effect on the ability to accurately collect osteological measurements, subsequently affecting the repeatability results (Byrnes *et al.,* 2016; Langley *etal.,* 2016). The more experienced the observers, the more repeatable the results (Decker *et al.,*2011; Langley *et al.,* 2016).

Similar to the current study, Langley and colleagues (2016) showed that the measurements, from the skull, pectoral girdle and upper limb were repeatable, with the exception of the MRH which was also found to be unrepeatable in the study conducted by Langley and colleagues (2016). The mandibular measurements collected in the study were collected from severed mandibles. The mandibles were severed in the middle, along the mental protuberance and symphysis menti, during dissection. In order to collect measurements from the mandible, particularly the measurements; MRH and ML, (using a mandibulometer), the mandible was re-articulated. This could have had an effect, on the results of the inter-observer repeatability.

The repeatability results for the data set, pelvic girdle and lower limb; TSDF (R), MDF (R) and (L) and mDF (R) and (L), in the current study, differed to what was found by Langley and colleagues (2016),as these measurements, which were deemed unrepeatable in the current

study, were found to be repeatable by Langley and colleagues (2016).

The measurements, MDF and mDF, are midshaft measurements collected from a robust bone, the femur. Due to its robustness, collection of the midshaft measurements proved to be difficult as this bone, proved difficult to handle (particularly when collecting these midshaft measurements). According to the DCP manual, to collect the midshaft measurements, the bone needs to be rotated using one hand, while the second-hand places the arms of the sliding caliper on the midpoint of the midshaft (Langley *et al.*, 2016). As a result of this bones robustness, the arms of the sliding caliper tended to slip along the midshaft, which likely contributed to this measurement being unrepeatable between the primary and secondary examiner.

5.1.2 Lodox images

Most measurements collected from the Lodox images were deemed repeatable for both intra- (<1.5%) and inter-observer (<2%).

From the skull, most of measurements collected were deemed repeatable for both the intra-observer and inter-observer repeatability, with the exception of the intra-observer result for MRH (L) (1.60%) and the inter-observer result for mRB (L) (8.53%). The reason for the measurement MRH (L) being deemed unrepeatable, was likely due to the difficulties experienced in collecting this measurement from the Lodox scan images. These difficulties were in the reconstruction of the boards of the mandibulometer, from which measurements are collected from when measuring dry bone. The measurement, mRB being deemed unrepeatable, was likely due to the fact that this measurement does not make use of identifiable landmarks. Thus, difficulties in identifying the narrowest point of the ramus were experienced by both the principal and secondary investigator. The results for both MRH and mRB differed to the repeatability results of the skull measurements collected from 3D CT scans, which found all skull measurements (inclusive of the MRH and mRB) to be repeatable (Verhoff *et al.*, 2008).

This is likely due to the fact that 3D CT scans more accurately reflect the dry bone (Richtsmeier *et al.,* 1995). This is largely through its ability to capture the actual size and shape of the bone in its entirety, at all angles (Colman *et al.,* 2019; Lopes *et al.,* 2008).

Skull measurements collected in the current study, although repeatable, were slightly difficult to collect from Lodox images as landmarks pertaining to each measurement were not easily identifiable. This differed to what was found for the imaging modalities such as 3D surface scanners and photogrammetry (Katz & Friess, 2014), as cranial landmarks were easily identifiable in these studies. A study by Franklin *et al.* (2013), noted that landmarks used to collect the measurements, FOL and FOB are type III landmarks. These landmarks consist of measurements with tips and bumps from which points of maximum curvature, for example, need to be identified (O'Higgins, 2000; Simonis *et al.,* 2009). As a result of the base of the skull being captured by Lodox, overlapping of bone landmarks was noted within the Lodox images. This contributed to the difficulties in identifying landmarks required for measurements.

Most pectoral girdle and upper limb measurements collected from Lodox images in the current study were found to be repeatable. The intra-observer results which were unrepeatable were; MDC (L) (1.85%), MVDhH (L) (1.53%) and (R) (1.51%), while the inter-observer results which were deemed unrepeatable were the MLC (R) (2.04%), MDC (L) (3.40%) and (R) (2.39%), mDC (L) (3.99%) and (R) (2.86%), MVDhH (R) (2.61%), MDH (L) (2.51%), mDH (L) (2.04%), MDR (L) (2.05%), mDR (L) (2.01%), MDU (R) (2.42%), mDU (L) (4.24%), PLU (L) (2.81%) and (R) (2.95%).

All the definitions for midshaft measurements collected from Lodox images were modified. As the definitions for the midshafts measurements, as prescribed by the manual, require the bone to be rotated along its midshaft for the minimum and maximum midshaft measurements to be obtained (Langley *et al.,* 2016). This cannot be done from the 2D images produced by the Lodox Statscan. To obtain the maximum and minimum midshaft

measurements from the 2D Lodox images of the bones, the diameters along the midshaft of the bone which were the widest and narrowest were collected respectively. In addition to the modification of these measurements, no osteological landmarks are used in collecting midshaft measurements. The unrepeatability of this modified definition indicates that the modified definition requires more specificity. Most studies which collected osteological measurements from imaging modalities did not collect midshaft measurements and as such no comparisons can be made.

The definition for the measurement, MVDhH, according to Langley and colleagues (2016), is the distance between the most inferior and superior points on the border of the articular process. In some of the Lodox images, the borders of the articular process, were not visibly clear. This made it difficult to collect this measurement from the Lodox images.

Although, the measurement PLU makes use of identifiable landmarks, ton of these landmarks cannot be seen on 2D Lodox images. Particularly, the deepest point of the articular surface of the coronoid process of the ulna, which is classified as a Type III landmark (O'Higgins, 2000; Simonis *et al.*, 2009). As above-mentioned in the skull section, these landmarks consist of bumps and grooves, which can only be identified in 3D images (O'Higgins, 2000; Simonis *et al.*, 2009).

Similar to the repeatability results for the data sets, skull and pectoral girdle and upper limb, most of the pelvic girdle and lower limb were deemed repeatable, with exceptions of the intra-observer results for, MDFh (R) (1.51%) and mDF (R) (1.51%) and the inter-observer results for MDF (L) (3.58%), mDF (L) (8.57%) and MDFib (L) (2.60%). Reasons pertaining to these measurements being deemed unrepeatable were similar to those found within the pectoral girdle and upper limb. The measurements MVDhH and the pectoral girdle and upper limb midshaft measurements share similar reasons for unrepeatability with the MDFh and lower limb midshaft measurements, respectively. According to the DCP manual, the MDFh, is

measured along the articular border of the femoral head (Langley *et al.,* 2016). Similar to the MVDhH, the articular border of the femoral head was not visibly clear. The measurement, MDFh, like the midshaft measurements, requires the rotation of the arms of the sliding caliper along the articular border, until the maximum diameter of the femoral head is obtained. As a result of the femur being placed in anatomical position and the image being 2D, the measurement was taken from the inferior to the superior point, along the articular border of the femoral head, which is captured in the Lodox Statscan image.

5.2 Accuracy

Accuracy in the current study was used to assess how close Lodox measurements were to the corresponding dry bone measurements. Measurements collected from dry bone are often considered the current gold standard in forensic anthropology (Brough *et al.,* 2013, Garvin & Stock, 2016). In order for forensic anthropologists to continue to be able to make use of existing formulae to estimate parameters of the biological profile, such as ancestry, sex, age and stature, from Lodox images, the accuracy of Lodox measurements must first be assessed.

In the current study, the measurements which were collected from Lodox Statscan images, were those that could be collected despite the limitation of the images being 2D and the fact that skeletal remains were scanned in the anatomical position. This was with the exception of the midshaft measurements. The definitions for the minimum and maximum midshaft measurement were redefined in order to collect these measurements from Lodox images.

Not all measurements collected from Lodox images represented similar dimensions to the corresponding dry bone elements. Reasons for this were the result of the distortion of the images produced by Lodox Statscan (Stull *et al.,* 2014b), the orientation of the bone which

caused difficulties in identifying landmarks associated with measurements and landmarks which couldn't be identified because of the characteristics of these landmarks. Literature reporting the accuracy and repeatability of the collection of osteometric measurements from virtual images is mostly limited to cranial and long bone (femur and humerus) measurements, but efforts have been made to compare results from the current study, where possible.

Majority of the Lodox measurements were on average greater than their corresponding dry bone measurements, with the exception of the skull measurements. The overestimation of measurements collected from Lodox images is likely due to the distortion of images caused by this imaging modality (Stull *et al.,* 2014b). The magnitude of this distortion is often not taken into consideration at hospitals and medico-legal laboratories (Stull *et al.,* 2014b). Similar to the current study, overestimation as a result of distortion were also identified from osteometric measurements collected from X-rays (Maresh, 1955) caused by object image distance (OID) and subject image distance (SID). Similarly, clinical CT scans and 3D virtual bone models derived from CT scans were also found to be greater than their corresponding dry bone (Rathnayaka *et al.,* 2012; Colman *et al.,* 2019). In clinical CT scans, this was a result of the presence of soft tissue, which caused image noise (Rathnayaka *et al.,* 2012, Colman *et al.,* 2019). Dissimilar to the current study, measurements collected from MRI derived 3D models underestimated the dry bone measurements (Rathnayaka *et al.,* 2012). This was a result of the reconstruction software used in the study conducted by Rathnayaka *et al.* (2012). In addition to this, MRI is not conventionally used to view bones. In order for bone to be documented using MRI, the imaging modality utilises its ability to visualise the soft tissue, surrounding thebone (Rathnayaka *et al.,* 2012; Carew & Errickson, 2019), which in turn, could contribute tothe underestimation of dry bone, by this imaging modality.

In the current study, majority of the mean differences between dry bone and Lodox Statscan images were all within the acceptable anthropological range of <0.2 cm (Stull *et al.,*

2013).

5.2.1 Measurements with no statistically significant difference

Overall, the measurements that were collected in the current study, showed a statistically significant difference ($p<0.05$) between dry bone and Lodox images. This was with exceptions which included measurements from the skull: HMB (R) (0.291) and (L) (0.178); from the pectoral girdle/upper limb: MDC (R) (0.331) and (L) (0.573), HS (L) (0.093), MLH (R) (0.850) and (L) (0.084), mDR (R) (0.836) and (L) (0.753), mDU (R) (0.524) and (L) (0.448); from the pelvic girdle/lower limb: ABS (0.146), BLF (R) (0.124),TSDF (R) (0.286) and (L) (0.491), MT (R) (0.128), LT (L) (0.161), MLFib (R) (0.080) and (L) (0.184) and MDFib (R) (0.160) and (L) (0.234)

The placement of the two halves of the mandible in the Lodox images, resulted in easily identifying the mental foramina, which is the landmark required for collecting the measurement, HMB. Similar to the HMB measurement, the midshaft measurements from the upper limb (mDR and mDU) as well as the pelvic girdle and lower limb (MT, MDFib and TSDF) were also collected along the x-axis. All these x-axis measurements, with exception of the ABS, are small measurements, in comparison to the larger measurements collected along this axis (EBH, EBF, MPeBT, DeBT, TDSS1, MIB, WIB). Despite these measurements showing no statistically significant difference between dry bone and Lodox images, the differences were large, as noted from the mean percentage differences of these measurements. Thus, although, Lodox Statscan distorts images produced, along the x-axis, resulting in a high difference between Lodox images and dry bone is, the difference between them is seen as not significant. (Stull *et al.*, 2013).

Similarly, high percentage differences were found in other studies which collected midshaft measurements from images produced using CT (Bookstein, 1991, Sholts *et al.*, 2011,

Stull *et al.,* 2014a). The reasons for the high percentage difference of midshaft measurements in those studies, was that midshaft measurements are not defined by anatomic landmarks (Bookstein, 1991, Sholts *et al.,* 2011, Stull *et al.,* 2014a). A similar reason could be employed in the current study for the high mean percentage difference for midshaft measurements and for the TSDF. In addition to this reason and that previously mentioned, modification of the definition for midshaft measurements, for Lodox images in the current study could also have contributed to the high mean percentage difference. The definitions for the minimum and maximum midshaft measurements for Lodox images in the current study, were slightly modified due to the placement of bones in anatomical position and Lodox Statscan producing 2D images, therefore, the measurements were not collected as prescribed by the DCP manual (Langley *et al*., 2016).According to the DCP manual, in order to obtain the minimum and maximum diameter of the midshaft of long bones, the bone being measured should be rotated along its midshaft, until the minimum or maximum value is found, perpendicular to one another (Langley *et al*., 2016). Although the midshaft, could be identified on the 2D Lodox images, the bones could not be rotated to obtain the minimum and maximum diameters of the midshaft and as such narrower and wider widths along the midshaft of the long bones were used as the minimum and maximum diameter of the midshafts, respectively. These measurements thus clearly do not correspond to the minimum and maximum diameters of the bone.

As indicated above, the measurement, ABS showed no statistically significant difference ($p>0.05$) between dry bone and Lodox images, despite the measurement being a larger measurement collected along the x-axis. The landmarks required to collect this measurement were easily identifiable on the Lodox images, contributing to the small mean percentage differences and no significant difference. These landmarks were the most anterior projections of the auricular surface (Langley *et al.,*2016). Unlike the midshaft measurements, the small mean percentage difference could be accounted for by Lodox Statscan producing a full-body

image, which is known to reduce the distortion produced by the x-ray (Knobel *et al.*,2006, Evangelopoulos *et al.*, 2009, Deyle *et al.*, 2010, Douglas *et al.*, 2010; Stull *et al.*, 2013).

The midshaft measurement, MDC (R) and (L), was the only midshaft measurement that was measured along the y-axis. However, the results of this midshaft measurement were similar to the above-mentioned midshaft measurements. Thus, the reasons which affected the above-mentioned midshaft measurements, likely also affected the MDC. Other length measurements which were collected along the y-axis and showed no statistically significant difference ($p>0.05$) between dry bone and Lodox images (HS (L), MLH (R), BLF (R), LT (L) and MLFib (R) and (L)) had low percentage differences. Measurements collected along the y-axis of Lodox images according to Stull *et al.* (2013), experience minimal distortion and are thus more accurate. Similarly, the measurements, HS and MLH, collected from CT (Stull *et al.*, 2014b) and the measurement, MLH, collected from Lodox images of sub-adults' skeletal elements (Stull *et al.*, 2013), also showed low percentage differences between the measurements collected from dry bone and CT (Stull *et al.*, 2014b), as well as Lodox images (Stull *et al.*, 2013).

Similar to the current study, the measurement, LT, showed no significant difference ($p>0.05$) between dry bone and CT scans (Robinson *et al.*, 2008) and between dry bone and MRI scanograms (Doyle & Winsor *et al.*, 2011). All post-cranial length measurements collected along the y-axis, presented with low mean percentage differences, with exceptions of the PLU (R) and (L), AHS, ASISS (R) and (L). The low percentage difference is due to the minimal distortion experienced using Lodox Statscan along this axis (Stull *et al.*, 2013). However as seen with the above-mentioned measurements, not all measurements collected along the y-axis showed no significant difference.

5.2.2 *Measurements with statistically significant difference*

From the 46 osteological measurements selected from the DCP manual, 33 showed a significant difference, between Lodox images and dry bone. As mentioned above, most of the measurements collected from Lodox images were statistically significantly different ($p<0.05$) to the corresponding dry bone measurements. The significant differences of these measurements collected from Lodox images to the corresponding dry bone were a result of three main issues.

The first was the inability to identify landmarks such as for the measurements, FOL and FOB of the skull and PLU of the upper limb. Similarly, measurements FOL and FOB, collected from CT scan images were considerably different from their corresponding dry bone measurements (Franklin *et al.,* 2013). As mentioned in the repeatability section, the use of Type III landmarks to collect these measurements is difficult, as these landmarks are not noticed on 2D images. The measurement, MLF, was difficult to collect from the Lodox images as the DCP manual definition requires the bone to the moved (similar to the MLC, as explained in the repeatability section) once correctly placed on the osteometric board, which cannot be achieved on a 2D fixed image (Langley *et al*., 2016). The MLF also showed a difference between dry bone and CT measurements and although the difference was small, it was significant (Zech *et al.,* 2016). The study by Zech *et al.* (2016), indicated that CT, underestimated the MLF collected from dry bone. Similarly, reasons for the difference, was due to the identification of landmarks and possibly the image quality used in their study (Zech *et al.,* 2016). The accuracy results of the MLF in the study conducted by Leitzes *et al.*, (2005), differed from the results of this current study as MLF collected from MRI, CT and X-ray scanograms, were accurate. As mentioned in the repeatability section, the mandible was not in situ and was severed in half. This meant that measurements in the prescribed manual that required a full mandible could not be collected. This contributed to all mandibular measurements showing statistically significant

differences, with exception of the previously mentioned HMB.

The second reason was the orientation of the bone when documented into a 2D image, which in turn hampered the ability to identify landmarks required for certain measurements. These included those from the upper limb; MLR, MLU and PLU and the pelvic girdle; WIB and ASISS. The upper limb measurements as prescribed by Langley *et al.*, (2016), require the most distal, proximal and or inferior points, of the bone measured, to be located. As a result of the bones being placed in anatomical position and the images being 2D,the true most distal, proximal or inferior points on the bone are not the same as those seen on the Lodox images. Similarly, the orientation of the os coxae, when documented by Lodox Statscan into a 2D image, resulted in the collection of inaccurate measurements. When collecting the ASISS and MIB measurements from dry bone, the lateral aspect of the os coxae faces the observer (Langley *et al.,* 2016). This orientation of the os coxae differs from the orientation it was placed in when captured by the Lodox Statscan. The os coxae was scanned with most of the posterolateral aspects of the bone being visible. The landmarks required to collect the measurement, ASISS, are the apices of the superior anterior iliac spine and the symphysion. Despite these landmarks being visible on the Lodox images, they are facing away from the observer and towards the mat the os coxae was placed on and not towards the observer as is, when collecting the measurement from dry bone. The orientation of the os coxae also affects the measurements; MInh and the MIB. Similar os coxae measurements (MInh, MIB andASSIS), have been collected from 3D CT scans (Bor *et al.,* 2016) with no significant difference($p>0.05$) to corresponding dry bone measurements (Bor *et al.,* 2016). Computed Tomography produces 3D images or models of bone which are geometrically more accurate (Rathnayaka *etal.*, 2012).

As a result of the bones, in the Lodox images, being placed in anatomical position, the diameters of the radial and femoral heads, noted on the Lodox images did not represent the true maximum diameters of the radial and femoral head. Similar to the midshaft measurements,

to obtain these measurements, as prescribed by the DCP manual (Langley *et al.,* 2016), the bones need to be rotated until the maximum measurement is obtained. Which cannot be performed on 2D images.

In addition to the above-mentioned reasons, statistically significant differences were also the result of the distortion of images produced by Lodox Statscan, along the x-axis (Stull *et al.*, 2013), as previously mentioned. Other measurement affected by distortion, were the ZYGB of the skull, MLC,BS, EBH, MDH and mDH of the pectoral girdle and upper limb, the EBF, MDF, mDF, MPeBT, DeBT, TDSS1 of the lower limb. Some of these measurements including, MLC (Brough *et al.,* 2013), EBF (Ismail *et al.,* 2019) and the DeBT (Robinson *et al.,* 2008), collectedfrom CT scans, showed no difference compared to dry bone and are likely due to the 3D nature of these scans (Rathnayaka *et al.,* 2012). The lower limb measurement, MVDhH, was a measurement that was collected diagonally and like the above-mentioned measurements, showed a statistically significant difference between Lodox images and dry bone. The results for this measurement, also differed to CT scans (Ismail *et al.,* 2019).

5.3 Limitations and Future directions

With the rise of virtual autopsy, forensic anthropologists are likely to receive images of remains which have not been macerated, in the near future. Thus, it is of great importance to fully explore the potential of virtual imaging modalities, such as Lodox, in forensic anthropology.

One of the major limitations of the current study included the use of a small sample size. This was due to the lack of Lodox images of skeletal remains, with corresponding dry bone elements and it is highly suggested that future studies explore larger samples.

The effects of soft tissue on the visibility of bone landmarks and whether the presence

of soft tissue affect the distortion of the Lodox images should also be explored. The current study only had access to Lodox images of skeletal remains and not remains in situ.

Future studies, pertaining to the collection of osteometric measurements from Lodox images, should include defining landmarks which can be easily identified from Lodox images. These landmarks which can be easily identified should be used to redefine osteometric measurements suitable for Lodox images, which subsequently allow for a biological profile to be estimated from it.

For the measurements collected, which showed a statistically significant difference, as a result of the distortion produced by x-rays, distortion correction formulae should be formulated. These could be used to aid obtaining the correct measurements, needed to estimate biological profiles.

CHAPTER 6: CONCLUSION

Virtual imaging modalities, mainly CT and MRI, have been used in forensic settings. However, the cost associated, and the availability of these imaging modalities in general forensicpathology services/medicolegal laboratories, limit its use in forensic anthropology. Lodox imaging is available and in use in forensic medico-legal laboratories across the world, especially in South Africa. The current use of Lodox images in forensic medico-legal laboratories include, locating foreign objects (Mantokoudis *et al.*, 2012, Loots & du Toit-Prinsloo, 2016), aiding in victim identification (Bateman, 2008, Bernitz & Verster, 2017) and in post-mortem examinations (Douglas *et al.*, 2010, Weber & Sebire, 2011, du Plessis *et al*, 2020); however, its full potential in forensic anthropology is yet to be explored.

The aim of this study was to assess the accuracy and repeatability of osteometric measurements as prescribed by Langley *et al. (*2016), collected from 2D Lodox images. The results from the study suggest that although most of the measurements collected from the DCP manual (Langley *et al*., 2016) were repeatable, they were not accurate. Reasons for the lack of repeatability or inaccuracy of these measurements related mainly to the fact that 3D measurements were collected from 2D images, which resulted in the inability to identify landmarks from Lodox images. In addition to this, 3D dependant measurements prescribed by the DCP manual (Langley *et al*., 2016) could not be collected due to the challenges faced with the orientation of the scans. Distortion produced by Lodox Statscan along the x-axis overestimated the measurements collected from Lodox images. Lastly, the study was limited by the inability to collect the standard osteological measurements from the virtual imaging modality. This prompts the need for further research before measurements can reliably and accurately collected from Lodox images.

REFERENCES

Aalders, M.C., Adolphi, N.L., Daly, B., Davis, G.G., de Boer, H.H., Decker, S.J. *et al*. (2017). Research in forensic radiology and imaging; Identifying the most important issues. *Journal of Forensic Radiology and Imaging*, 8, 1-8.

Abu-Zidan, F.M., Hefny A.F., Corr P. Clinical ultrasound physics. (2011). *Journal of Emergencies, Trauma, and Shock*, 4(4), 501-503.

Albanese, J. (2010). A critical review of the methodology for the study of secular change using skeletal data. In: Ellis C., Ferris N., Timmins P., White C. (eds). *Papers in Honour of Michael Spence*. Ontario Archaeological Society Occasional Publication, London, Ontario. 9, 139-155.

Alblas, A., Greyling, L.M., Geldenhuys, E. (2018). Composition of the Kirsten Skeletal Collection at Stellenbosch University. *South African Journal of Science*, 114, 1-6.

Aldridge, K., Boyadjiev, S.A., Capone, G.T., DeLeon, V.B., Richtsmeir, J.T. (2005). Precision and error of three-dimensional phenotypic measures acquired from 3dMD photogrammetric images. *American Journal of Medical Genetics Part A*, 138, 247–253.

Altman, D.G., Bland, J.M. (1983). Measurement in medicine: the analysis of method comparison studies. *Statistician*, 32, 307-17.

Amirlak, B., Zakharay, B., Weichman, K., Ahluwalia, H., Forse, A.R., Gaines, R.D. (2009). Novel use of Lodox Statscan in a level one trauma centre. *Turkish Journal of Trauma and Emergency Surgery*, 15(6), 521-528.

Anburajan, M., Rethinasabapathi, C., Korath, M.P., Ponnappa, B.G., Govindan, A., Jagadeesan, K. (2001). Age related proximal femur bone mineral loss in south Indian women: A dual-energy x-ray absorptiometry (DXA) study. *Journal of the Association of Physicians of India*, 49, 442-445.

Arthurs, O.J., Hutchinson, J.C., Sebire, N.J. (2017). Current issues in postmortem imaging of perinatal and forensic childhood deaths. *Forensic Science, Medicine and Pathology*, 13, 58-66.

Arthurs, O.J., van Rijn, R.R., Whitby, E.H., Johnson, K., Miller, E., Stenzel, M. *et al.* (2016). ESPR. Postmortem imaging task force: where we begin. *Pediatric Radiology*, 46, 1363-1369.

Austin, D., King, R.E. (2016). The biological profile of unidentified human remains in a forensic context. *Academic Forensic Pathology*, 6(3), 370-390.

Bateman, C. (2008). New local scanners transform forensic pathology. *South African Medical Journal*, 98(2), 75-76.

Beningfield, S.J., Potgieter, J.H., Bautz, P. (1999). Evaluation of a new type of direct digital radiography machine. *South African Medical Journal*, 89, 1182–1188.

Beningfield, S.J., Potgieter, J.H., Nicol, A. (2003). Report on a new type of trauma full-body digital X-ray machine. *Emergency Radiology*, 10, 23–29.

Bernitz, H., Verster, J. (2017). Lodox® digital imaging – a tool for dental identification in single and mass fatality situations. *South African Dental Journal*, 72 (3), 118 – 121.

Birdseye, C.H. (1940). Stereoscopic photographic mapping. *Annals of the Association of American Geographers*, 30(1), 1-24.

Biwasaka, H., Aoki, Y., Sato, K., Tanijiri, T., Fujita, S., Dewa, K. *et al.* (2012). Analyses of sexual dimorphism of reconstructed pelvic computed tomography images of contemporary Japanese using curvature of the greater sciatic notch, pubic arch and greater pelvis. *Forensic Science International*, 10, 219(1-3), 288.e1-8.

Bland, J.M., Altman, D.G. (1999). Measuring agreement in method comparison studies. *Statical Methods in Medical Research*, 8, 135-60.

Boffard, K.D., Goosen, J., Plani, F., Degiannis, E., Potgieter, H. (2006). The use of Low

Dosage X-Ray (Lodox/Statscan) in major trauma: comparison between low dose X-ray and conventional X-Ray techniques. *Journal of Trauma and Acute Care Surgery*, 60(6), 1175-1183.

Bolton, F. (2010). Automated 3D reconstruction of lodox statscan images for forensic application. Unpublished thesis: University of Cape Town.

Bookstein, S. (1991). *Morphometric Tools for Landmark Data: Geometry and Biology*. Cambridge University Press, Cambridge.

Bor, P., Colman, K., Dobbe, J.G.G., Stull, K., Streekstra, G., Oostra, R.J. (2016). Towards "virtual" forensic anthropology: the accuracy of 3D skeletal reconstructions from full-body CT-scans. [Poster]. *International Society for Forensic Radiology and Imaing*. Amsterdam, Netherlands.

Bornik, A., Urschler, A., Schmalstieg, D., Bischof, H., Krauskopf, A., Schwark, T. *et al.* (2018). Integrated computer-aided forensic case analysis, presentation, and documentation based on multimodal 3D data. *Forensic Science International*, 287, 12-24.

Brits, D. (2016). Stature estimation in South African juveniles and adult females (Thesis). University of the Witwatersrand, Johannesburg.

Brits, D.M., Bidmos, M.A., Manger, P.R. (2017). Stature estimation from the femur and tibia in black South African sub-adults. *Forensic Science International*, 270 (277), e1–277.e10.

Brits, D., Manger, P.R., Bidmos, M.A. (2018). Assessing the use of the anatomical method for the estimation of sub-adult stature in black South Africans. *Forensic Science International*, 283, 221.e1-221.e9.

Brogdon, B.G. (2006). Forensic Aspects of Radiology. In: Spitz, W.U., Spitz, D.J., Clark, R.,

Fisher, R.S. (eds), *Spitz and Fishers Medico-Legal Investigation of Death: Guidelines for the Application of Pathology to Crime Investigation* (4th edn). Springfield, Illinois, USA, 1092-1135.

Brough, A.L., Bennett, J., Morgan, B., Black, S., Rutty, G.N. (2013) Anthropological measurement of the juvenile clavicle using multi-detector computed tomography—affirming reliability. *Journal of Forensic Science*, 58, 4, 946-951.

Brough, A.L., Morgan, B., Rutty, G.N. (2015). Postmortem computed tomography and disaster victim identification. La *radiologia medica*, 120(9), 866-873.

Brüschweiler, W., Braun, M., Dirnhofer, R., Thali, M.J. (2003). Analysis of patterned injuries and injury-causing instruments with forensic 3D/CAD supported photogrammetry (FPHG): an instruction manual for the documentation process. *Forensic Science International*, 132, 130-138.

Burke, M.P. (2012). *Forensic Pathology of Fractures and Mechanisms of Injury. Postmortem CT Scanning*. CRC Press, Boca Raton.

Byrnes, J.F., Kenyhercz, M.W., Berg, G.E. (2016). Technical note: examining interobserver reliability of metric and morphoscopic characteristics of the mandible*. *Journal of Forensic Science*, 62(4), 981-985.

Cambridge University Press. (2021). High-resolution. In Cambridge dictionary. Retrieved 22 April, 2021. From: https://dictionary.cambridge.org/dictionary/english/high-resolution

Cardoso, H.F.V. (2006). Brief communication: the collection of identified human skeletons housed the Bocage Museum (National Museum of Natural History), Lisbon, Portugal. *American Journal of Physical Anthropology*, 129(2), 173-176.

Carew, R.M., Errickson, D. (2019). Imaging in forensic science: Five years on. *Journal of Forensic Radiology and Imaging*, 16, 24-33.

Carew, R.M., Morgan, R.M., Rando, C. (2019). A preliminary investigation into the accuracy

of 3D modelling and 3D printing in forensic anthropology evidence reconstruction. *Forensic Science International,* 64, 342-352.

Carneiro, C., Curate, F., Borralho, P., Cunha, E. (2013). Radiographic fetal osteometry: Approach on age estimation for Portuguese population. *Forensic Science International,* 231 (1-3), 397.e1-397.e5.

Cattaneo, C., Marinelli, E., Di Giancamillo, A., Di Giancamillo, M., Travetti, L., Vigano, L. *et al*. (2006). Sensitivity of autopsy and radiological examination in detecting bone fractures in an animal model: implications for the assessment of fatal child physical abuse. *Forensic Science International,* 164, 131-137.

Chandrasekhar, T., Vennila, P. (2011). Role of radiology in forensic dentistry. *Journal of Indian Academy of Oral Medicine and Radiology*, 23(3), 229-231.

Clemente, M.A., La Tegola, L. Mattera, M. and Guglielmi, G. (2017). Forensic radiology: an update. *Journal of the Belgian Society of Radiology,* 101(S2):21, 1-4.

Colman, K.L., Dobbe, J.G.G., Stull, K.E., Ruijter, J.M., Oostra, R., van Rijn, R.R. *et al*. (2017). The geometrical precision of virtual bone models derived from clinical computed tomography data for forensic anthropology. *International Journal of Legal Medicine,* 131, 1155–63.

Colman, K.L., de Boer, H.H., Dobbed, J.G.G., Libertone, N.P.T.J., Stull, K.E., van Eijnattenh, M. *et al*. (2019). Virtual forensic anthropology: the accuracy of osteometric analysis of 3D bone models derived from clinical computed tomography (CT) scans. *Forensic Science International*, 304109963, 1-10.

Dayal, M.R., Kegley, A.D.T., Štrkalj, G., Bidmos, M.A. Kuykendall, K.L. (2009). The history and composition of the Raymond A. Dart Collection of human skeletons at the University of the Witwatersrand, Johannesburg, South Africa. *American Journal of Physical Anthropology*, 140, 324–335.

Deadman, W.J. (1964). The identification of human remains. *Canadian Medical Association Journal*, 91(15), 808–811.

Decker, S.J., Davy-Jow, S.L., Ford, J.M., Hilbelink, D.R. (2011). Virtual determination of dex: metric and nonmetric traits of the adult pelvis from 3D computed tomography models*. *Journal of Forensic Science*, 56(5), 1107-1114.

Dedouit, F., Auriol. J., Rousseau, H., Rougé, D., Crubézy, E., Telmon, N. (2012). Age assessment by magnetic resonance imaging of the knee: a preliminary study. *Forensic Science International*, 217, 232. e1–7.

Dedouit, F., Savall, F., Mokrane, F.Z., Rousseau, H., Crub'ezy, E., Roug'e, D. *et al.* (2013). Virtual anthropology and forensic identification using multidetector CT. *British Journal of Radiology*, 87, 1-12.

Dedouit, F., Telmon, N., Costagliola, R., Otal, P., Joffre, F., Rougé, D. (2007). Virtual anthropology and forensic identification: report of one case. *Forensic Science International*, 173(2-3), 182-87.

Deyle, S., Brehmer, T., Evangelopoulos, D.S., Krause, F., Benneker, L.M., Zimmermann, H. *et al.* (2010). Review of Lodox/Statscan in the detection of peripheral skeletal fractures in multiple injury patients. *Injury*, 41, 818-822.

Dirkmaat, D.C. (2012). Introduction to Part V. In: Dirkmaat, D.C. (eds), *A Companion to Forensic Anthropology*. Wiley-Blackwell. 415-417.

Dirkmaat, D.C., Cabo, L. (2012). Forensic Anthropology: Embracing the New Paradigm. In: Dirkmaat, D.C. (eds.) *A Companion to Forensic Anthropology*. Wiley-Blackwell. 1-40.

Dirkmaat, D.C, Cabo, L.L., Ousley, S.D., Symes, S.A. (2009). New Perspectives in Forensic Anthropology. *Yearb Phys Anthropol*, 51, 33–52.

Djorojević, M., Roldán, C., Botella, M., Alemán, I. (2019). Sex estimation from the proximal femur in Spanish population based on three-dimensional computed tomography metric

analysis. *Vojnosanitetski Pregled,* 76(12), 1245-1252.

Douglas, T., Pitcher, R., van As, A. (2010). Full-body digital radiographic imaging of the injured child. *Continuing Medical Education*, 28(3), 108–112.

Doyle, A.J., Winsor, S. (2011). Magnetic resonance imaging (MRI) lower limb length measurement. *Journal of Medical Imaging Radiation Oncology*, 55, 191–194.

du Plessis, M., Date-Chong, M., Liebenberg, M. (2020). Lodox: the invaluable radiographic solution in forensic settings. *International Journal of Legal Medicine,* 135, 655-662.

Ebert, L.C., Flach, P., Schweitzer, W., Leipner, A., Kottner, S., Gascho, D. *et al.* (2016). Forensic 3D surface documentation at the Institute of Forensic Medicine in Zurich – workflow and communication pipeline. *Journal of Forensic Radiology and Imaging*, 5, 1-7.

Elliot, A.C., Woodward, W.A. (2011). Comparing one or two means using the t-test. In: Elliot, A.C., Woodward, W.A. (eds), *Statistical Analysis Quick Reference Guidebook.* Sage Publication Inc. 47-76.

Errickson, D., Grueso, I., Griffith, S., Setchell, J., Thompson, T.J.U., Thompson, C.E.L. *et al.* (2017). Towards a best practice for the use of active non-contact surface scanning to record human skeletal remains from archaeological contexts. *International Journal of Osteoarchaeology,* 27 (4), 650–661.

Errickson, D., Thompson, T. (2017). *Human Remains: Another Dimension. The Application of Imaging to the Study of Human Remains.* Academic Press, London.

Esterhuysen, A.B., Sanders, V.M., Smith, J.M. (2009). Human skeletal and mummified remains from the AD 1854 siege of Mugombane, Limpopo South Africa. *Journal of Archaeological Science,* 36, 1038–1049.

Evangelopoulos, D., Deyle, S., Zimmermann, H., Exadaktylos, A.K. (2009). Personal experience with whole body, low dosage, digital X-ray scanning (LODOX-Statscan) in

trauma. *Scandinavian Journal of Trauma, Resuscitation and Emergency Medicine,* 17, 41.

Evangelopoulos, D.S., Deyle, S., Zimmermann, H., Exadaktylos, A.K. (2011). Full-body radiography (Lodox/Statscan) in trauma and emergency medicine: a report from the first European installation site. *Trauma,* 1, 5-15.

Exadaktylos, A.K. (2013). How reliable and safe is full-body low-dose radiography (LODOX Statscan) in detecting foreign bodies ingested by adults? *Emergency Medicine Journal,* 30, 559-564.

Fahrni, S., Campana, L. Dominguez, A., Uldin, T., Dedouit, F., Delémont, O. *et al*. (2017) CT-scan vs. 3D surface scanning of a skull: first considerations regarding reproducibility issues. *Forensic Science Research,* 2(2), 93-99.

Fathi, A.R., Mariani, L., Farkas, Z.S., Exadaktylos, A.K., Bonel, H.M. (2011). Evaluation ofthe new statscan radiography device for ventriculoperitoneal shunt assessment. *American Journal of Roentgenology*, 196(3), W285–W289.

Filiault, M. (2012). Digitization protocols for laser scanning human bone in forensic anthropology. Unpublished thesis: University of Central Florida.

Franklin, D., Cardini, A., Flavel, A., Kuliukas, A., Marks, M.K., Hart, R. (2013). Concordance of traditional osteometric and volume rendered MSCT interlandmark cranial measurements. *International Journal of Legal Medicine*, 127, 505–520.

Franklin, D., Cardini, A., Flavel, A., Marks, M.K. (2014). Morphometric analysis of pelvic sexual dimorphism in a contemporary Western Australian population. *International Journal of Legal Medicine*, 128, 861–72.

Franklin, D., Flavel, A. (2015). CT evaluation of timing for ossification of the medial clavicular epiphysis in a contemporary Western Australian population. *International Journal of Legal Medicine*, 129, 583–94.

Franklin, D., Flavel, A., Kuliukas, A., Cardini, A., Marks, M.K., Oxnard, C. (2012). Estimation of sex from sternal measurements in a Western Australian population. *Forensic Science International*, 217(230), e1–5.

Franklin, D., Swift, L., Flavel, A. (2016). 'Virtual anthropology' and radiographic imaging in the Forensic Medical Sciences. *Egyptian Journal of Forensic Science*, 6, 31-43.

Fu, C.Y., Wang, Y.C., Hsieh, C.H., Chen, R.J. (2011). Lodox/Statscan provides benefits in evaluation of gunshot injuries. *American Journal of Emergency Medicine*, 29(7), 823-827.

Garamendi, P.M., Landa, M.I., Botella, M.C., Alemán, I. (2011). Forensic age estimation on digital X-ray images: medial epiphyses of the clavicle and first rib ossification in relation to chronological age. *Journal of Forensic Science*, 56(1), S3-12.

Garvin, H.M., Stock, M.K. (2016). The utility of advanced imaging in forensic anthropology. *Academic Forensic Pathology International*, 499-516.

Giavarina, D. (2013). Understanding Bland Altman analysis. *Biochemia Medica*, 25(2), 141–151.

Golmakani, M.M., NIknam, M.H., Hedayat, K.M. (2005). Transplantation ethics from the Islamic point of view *Medical Science Monitor*, 11, 105-109.

Goodman, N.R., Goodman, J.L., Hofman, W.I. (2011). Autopsy: traditional Jewish laws and customs "Halacha". *American Journal of Forensic Medicine and Pathology*, 32(3), 300–3.

Goto R, Mascie-Taylor CGN. (2007). Precision of measurement as a component of human variation. *Journal of Physiological Anthropolology*, 26, 253-56.

Grabherr, S., Cooper, C., Ulrich-Bochsler, S., Uldin, T., Ross, S., Oesterhelweg, L. *et al.* (2009). Estimation of sex and age of "virtual skeletons"–a feasibility study. *European Journal of Radiology*, 19, 419–429.

Grabherr, S., Egger, C., Vilarino, R., Campana, L., Jotterand, M., Dedouit, F. (2017). Modern post-mortem imaging: an update on recent developments. *Forensic Science Research*, 2(2), 52-64.

Griffith, J.F., Genant, H.K. (2011). New Imaging Modalities in Bone. *Current Rheumatology Reports*, 13, 241–250.

Guglielmi, G., Nasuto, M. (2014). Forensic radiology special feature: preface. *British Journal of Radiology*, 87, 1-2.

Guglielmi, G., Nasuto, M., Pinto, A. (2015). Forensic and medico-legal radiology: challenges, issues and new perspectives. *La Radiologia Medica*, 120, 777-778.

Gurley, E.S., Parveen, S., Islam, M.S., Hossain, M.J., Nahar, N., Homaira, N. (2011). Family and community concerns about post-mortem needle biopsie in a Muslim society. *BMC Medical Ethics*, 12(10), 1-11.

Hargreaves, B., Worters, P.W., Pauly, K.B., Pauly, J.M., Koch, K.M., Garry, E.G. (2011). Metal induced artefacts. *American Journal of Roentgenology*, 197(3), 547-555.

Hatipoglu, H.G., Ozcan, H.N., Hatipoglu, U.S., Yuksel, E. (2008). Age, sex and body mass index in relation to calvarial diploe thickness and craniometric data on MRI. *Forensic Science International*, 182, 46–51.

Heike, C.L., Upson, K., Stuhaug, E., Weinberg, S.M. (2010). 3D digital stereophotogrammetry: a practical guide to facial image acquisition. *Head & Face Medicine*, 6(18), 1-11.

Hildebolt, C.F., Vannier, M.W., Knapp, R.H. (1990). Validation study of skull three-dimensional computerized tomography measurements. *American Journal of Physical Anthropology*, 82, 283-294.

Hillewig, E., De Tobel, J., Cuche, O., Vandemaele, P., Piette, M., Verstraete, K. (2011). Magnetic resonance imaging of the medial extremity of the clavicle in forensic bone age

determination: a new four-minute approach. *European Radiology*, 21, 757–67.

Hillewig, E., Degroote, J., Van der Paelt, T., Visscher, A., Vandemaele, P., Lutin, B. *et al.* (2013). Magnetic resonance imaging of the sternal extremity of the clavicle in forensic age estimation: towards more sound age estimates. *International Journal of Legal Medicine*, 127, 677–689.

Hishmat, A.M., Michiue, T., Sogawa, N., Oritani, S., Ishikawa, T., Fawzy, I.A. *et al.* (2015). Virtual CT morphometry of lower limb long bones for estimation of the sex and stature using postmortem Japanese adult data in forensic identification. *International Journal of Legal Medicine,* 129, 1173–1182.

Hunt, D.R., Albanese, J. (2005). History and demographic composition of the Robert J. Terry anatomical collection. *American Journal of Physical Anthropology*, 127, 406–417.

Interpol (2021). Disaster Victim Identification (DVI). Viewed 22 April 2021. https://www.interpol.int/en/How-we-work/Forensics/Disaster-Victim-Identification-DVI

Ismail, N.A., Abdullah, N., Noor, M.H.M., Lai, P.S., Shafie, M.S., Nor, F.M. (2019). Accuracy and reliability of virtual femur measurement from CT scan. *Journal of Forensic and Legal Medicine,* 63, 11-17.

Jacques, S., Christe, B. (2020). Chapter 2-Healthcare technology basics. In: Jacques, S., Christe, B. (eds), *Introduction to Clinical Engineering.* Academic Press. 21-50.

Jalalzadeh, H., Giannakopoulos, G.F., Berger, F.H., Fronczek, J., van de Goot, F.R.W., Reijnders, U.J. *et al.* (2015). Postmortem imaging compared with autopsy in trauma victims--A systematic review. *Forensic Science International,* 257, 29-48.

Jamaiyah, H., Geeta, A., Safiza, M.N., Khor, G.L., Wong, N.F., Kee, C.C. *et al.* (2010). Reliability, technical error of measurements and validity of length and weight measurements for children under two years old in Malaysia. *Medical Journal of*

Malaysia, 56A, 131-137.

Johnson, A., Pandey, A. (2019). Three-dimensional scanning – A futuristic technology in forensic anthropology. *Journal of Indian Academy of Forensic Medicine*, 41(2), 128-131

Kahana, T., Hiss, J. (2005). Forensic Radiology. In: M. Tsokos (eds), *Forensic Pathology Reviews*. Humana Press Inc., Totowa, NJ. 3, 443-460.

Kalender, W.A. (2011). *Computed Tomography: Fundamentals, System Technology, Image Quality, Applications* (3rd edn). John Wiley & Sons, Germany.

Katsura, M., Sato, J., Akahane, M., Kunimatsu, A., Abe, O. (2018). Current and novel techniques for metal artifact reduction at CT: practical guide for radiologists. *Radiographs,* 38(2), 450-461.

Katz, D., Friess, M. (2014). Technical Note: 3D from standard digital photography of human crania—A preliminary assessment. *American Journal of Physical Anthropology*, 154, 152-158.

Kempter, M., Ross, S., Spendlove, D., Flach, P.M., Preiss, U., Thali, M.J. *et al*. (2009). Post-mortem imaging of laryngohyoid fractures in strangulation incidents: first results. *Legal Medicine (Tokyo)*, 11, 267–271.

Kern, K.F., Wingate, T. (2006). Pioneer of modern American physical anthropology. *Kirtlandia,* 55, 1-42.

Kim, H. (2014). Statistical notes for clinical researchers: nonparametric statistical methods: 1. nonparametric methods for comparing two groups. *Restorative Dentistry and Endodontics*, 39(3), 235-239.

Kim, T.K. T-test as a parametric statistic. (2015). *Korean Journal of Anesthesiology*, 68(6), 540-546.

Kim, T.K. Park, J.H. (2019). More about the basic assumptions of t-test: normality and sample

size. *Korean Journal of Anesthesiology*, 72(4): 331-335.

Kistler, M., Pfahrer, M., Niklaus, R., Tomas, V., Buechler, P. (2013). The virtual skeleton database: an open access repository for biomedical research and collaboration. *Journal of Medical Internet Research*, 15(11), e245.

Knobel, G.J., Flash, G., Bowie, G.F. (2006). Lodox Statscan proves to be invaluable in forensic medicine. *South African Medical Journal*, 96(7), 593-596.

Komar, D.A., Grivas, C. (2008). Manufactured populations: what do contemporary reference skeletal collections represent? A comparative study using the Maxwell Museum documented collection. *American Journal of Physical Anthropology*, 137, 224-233.

Krämer, J.A., Schmidt, S., Jürgens, K., Lentschig, M., Schmeling, A., Vieth, V. (2014). Forensic age estimation in living individuals using 3.0T MRI of the distal femur. *International Journal of Legal Medicine*, 128, 509–514.

Kranioti, E.F. (2016). The value of radiometry in sex assessment of bone fragments: a study on the radius in modern Greek population. *Journal of Forensic Radiology and Imaging*, 1(4), 20-28.

Krantz, P., Holtas, S. (1983). Postmortem computed tomography in a diving fatality. *Journal of Computed Assisted Tomography*, 7, 132–134.

Kraus, K. (2007). *Photogrammetry: Geometry from Images and Laser Scans* (2nd edn). Walter de Gruyter.

Krogman, W.M. (1962). *The Human Skeleton in Forensic Medicine*. Charles C. Thomas, Springfield, Illinois, USA.

Kučerová, S., Safr, S., Ublová, M., Urbanová, P., Hejna, P. (2014). The application of X-ray imaging in forensic medicine. *Soudni Lekarstvi*, 59(3), 34-8.

L'Abbè, E.N., Loots, M., Meiring, J.H. (2005). The Pretoria bone collection: a modern South African skeletal sample. *Journal of Comparative Human Biology*, 56, 197–205.

Lakha, K. (2015). Standards for epiphyseal union in South African children between the ages of 6 to 24 years using low dose X-rays (LODOX). Unpublished thesis: University of Cape Town.

Langley, N.R., Meadows Jantz, L., Ousley, S.D., Jantz, R.L. and Milner, G. (2016). *Data Collection Procedures for Forensic Skeletal Material 2.0.* Forensic Anthropology Center Department of Anthropology the University of Tennessee Knoxville, Tennessee.

Leitzes, A.H., Potter, H.G., Amaral, T., Marx, R.G., Lyman, S., Widmann, R.F. (2005). Reliability and accuracy of MRI scanogram in the evaluation of limb length discrepancy. *Journal of Pediatric Orthopaedics,* 25, 747–749.

Lento, P.H., Primack, S. (2008). Advances and utility of diagnostic ultrasound in musculoskeletal medicine. *Current Reviews in Muscoskeletal Medicine,* 1, 24-31.

Lin, E.C. (2010). Radiation risk from medical imaging. *Mayo Clinic Proceedings,* 85(12), 1142-1146.

Lodox critical imaging technology [Internet]. Available from: [http://www.lodox.com], 2 November 2020.

Loots, D.P., du Toit-Prinsloo, L. (2011). A fatal outcome of pica. *Forensic Science, Medicine and Pathology,* 12(1), 108–112.

Lopes, P.M.L., Moreira, C.R., Perrella, A., Antunes, J.L., Cavalcanti, M.G.P. (2008). 3-D volume rendering maxillofacial analysis of angular measurements by multislice CT. *Oral Surgery, Oral Medicine, Oral Pathology, Oral Radiology and Endodontology,* 105(2), 224-230.

Mann, R.W. (2013). Our bones: the need for diverse human skeletal collections. *Anthropology,* 1(2), e103.

Mantokoudis, G., Hegner, S., Dubach, P., Bonel, H.M., Senn, P., Caversaccio, M.D. *et al.* (2012). How reliable and safe is full-body low-dose radiography (LODOX Statscan) in

detecting foreign bodies ingested by adults? *Emerg Med,* 1-6.

Maresh, M.M. (1955). Linear growth of long bones of extremities from infancy through adolescence. *The American Journal of Diseases of Children,* 89(6), 725-742.

Marks, M. (1995). William M. Bass and the development of forensic anthropology in Tennessee. *Journal of Forensic Science,* 40(5), 741-750.

McPherron, S.P., Gernat, T., Hublin, J. (2009). Structured light scanning for high-resolution documentation of in situ archaeological finds. *Journal of Archaeological Science*, 36(1), 19–24.

Mehta, B.V., Rajani, S., Sinha, G. (1997). Comparison of image processing techniques (magnetic resonance imaging, computed tomography scan and ultrasound) for 3D modeling and analysis of the human bones. *Journal of Digital Imaging*, 3(10), 203-206.

Mehta, M., Saini, V., Nath, S., Menon, S.K. (2015). CT scan sex images for sex discrimination-a preliminary study on Gujarati population. *Journal of Forensic Radiology and Imaging*, 3, 43-48.

Michienzi, R., Meier, S., Ebert, L.C., Martinez, R.M., Sieberth, T. (2018). Comparison of forensic photo-documentation to a photogrammetric solution using the multi-camera system "Botscan". *Forensic Science International*, 288, 46-52.

Morsi, D.A., Hawary, A.A. (2013). Sex determination by the length of metacarpals and phalanges: X-ray study on Egyptian population. *Journal of Forensic and Legal Medicine,* 20(1), 6-13.

Mostafa, M., Elemi, A.H., Beblawy, M.A., Dawood, A.W.A. (2012). Adult sex identification using digital radiographs of the proximal epiphysis of the femur at Suez Canal University Hospital in Ismailia Egypt. *Egyptian Journal of Forensic Science,* 2(3), 81-88.

Muligan, M.E., Flye, C.W. (2006). Initial experience with Lodox Statscan imaging system for

detecting injuries of the pelvis and appendicular skeleton. *Emergency Radiology,* 13, 129-133.

Obertová, Z., Leipner, A., Messina, C., Vanzulli, A., Fliss, B., Cattaneo, C. *et al.* (2019). Postmortem imaging of perimortem skeletal trauma. *Journal of Forensic Science,* 1-23.

O'Higgins, P. (2000). The study of morphological variation in hominid fossil record: biology, landmarks and geometry. *Journal of Anatomy,* 197 (1), 103-120.

O'Sullivan, S., Sajid, M.I., Agusto, F.B., Mwangangi, J., Manguvo, A, Wichmann, D. *et al.* (2018). Virtual autopsy and community engagement for outbreak response in Africa: traditional, religious and sociocultural perspectives. *Egyptian Journal of Forensic Science,* 8(67), 1-6.

Ousley, S.D., Jantz, R.L. (1998). The Forensic Data Bank: Documenting Skeletal Trends in the United States. In: Reichs, K.J. (eds), *Forensic Osteology: Advances in the Identification of Human Remains*. Charles C Thomas. 441-458.

Pelin, C., Duyar, I., Kayahan, E.M., Zaˇgyapan, R., Aˇgıldere, A.M., Erar, A. (2005). Body height estimation based on dimensions of sacral and coccygeal vertebrae. *Journal of Forensic Science,* 50(2), 294-297.

Perini, T.A., de Oliveira, G.L., Ornellas, J.S., de Oliveira, F.P. (2005). Technical error of measurement in anthropometry. *Revista Brasileira de Medicina do Esporte,* 11, 86–90.

Pitcher, R.D., Wilde, J.C., Douglas, T.S., van As, A.B. (2009). The use of the Statscan digital X-ray unit in paediatric polytrauma. *Pediatric Radiology,* 39(5), 433-437.

Pittayapat, P., Thevissen, P., Fieuws, S., Jacobs, R., Willems, G. (2010). Forensic coral imaging quality of hand-held dental X-ray devices. Comparison of two image receptors and two devices. *Forensic Science International,* 194(1), 20-27.

Rathnayaka, K., Momot, K.I., Noser, H., Volp, A., Schuetz, M.A., Sahama, T. (2012). Quantification of the accuracy of MRI generated 3D models of long bones compared to

CT generated 3D models. *Medical Engeneering and Physics*, 34, 357–363.

Rejtarová, O., Hejna, P., Rejtar, P., Bukac, J., Slí- zová, D., Krs, O. (2009). Sexual dimorphism of ossified costal cartilage. Radiograph scan study on Caucasian men and women (Czech population). *Forensic Science International*, 191 (1-3), 110.e1 -5.83.

Richtsmeier, J.T., Paik, C.H., Elfert, P.C., Cole, T.M., Dahlman, H.R. (1995). Precision, repeatability and validation of the localization of cranial landmarks using computed tomography scans. *Cleft-Palate Craniofacial Journal*, 32(3), 217-227.

Robinson, C., Eisma, R., Morgan, B., Jeffery, A., Graham, E.A.M., Black, S. *et al.* (2008). Anthropological measurement of lower limb and foot bones using multi-detector computed tomography. *Journal of Forensic Science*, 53(6). 1289-1295.

Rocha, M.A. (1995). Les collections oste´ologiques humaines identifie´es du Muse´e Anthropologique de l'Universite´ de Coimbra. *Antropologia Portuguesa* 13, 7–38.

Rosário Junior, A.F., Souza, P.H.C., Coudyzer, W., Thevissen, P., Willem, G., Jacobs, R. (2012). Virtual autopsy in forensic sciences and its applications in the forensic odontology. *Revista Odonto Ciência*, 27(1), 5-9.

Rutty, G.N., Robinson, C.E., BouHaidar, R., Jeffery, A.J., Morgan, B. (2007). The role of mobile computed tomography in mass fatality incidents. *Journal of Forensic Science*, 52, 1343–1349.

Saint-Martin, P., Rerolle, C., Dedouit, F., Bouilleau, L., Rousseau, H., Roug´e, D. (2013). Age estimation by magnetic resonance imaging of the distal tibial epiphysis and the calcaneum. *International Journal of Legal Medicine*, 127, 1023–1030.

Sansoni, G., Trebeschi, M., Docchio, F. (2009). State-of-the-art and applications of 3D imaging sensors in industry, cultural heritage, medicine, and criminal investigation. *Sensors*, 568-601.

Scheuer, L., Black, S. (1995). The St. Bride's documented skeletal collection. Unpublished

archive held at the Calvin Wells Laboratory at the Department of Archaeological Sciences: University of Bradford.

Schmidt, S., Schiborr, M., Pfeiffer, H., Schmeling, A., Schulz, R. (2013). Sonographic examination of the iliac crest for forensic age estimation in living persons. *Science & Justice,* 53, 395-401.

Schmutz, B., Rathnayaka, K., Wullschleger, M.E., Meek, J., Schuetz, M.A. (2010). Quantitative fit assessment of tibial nail designs using 3D computer modelling. *Injury,* 41(2), 216–219.

Schmutz, B., Wullschleger, M.E., Noser, H., Barry, M., Meek, J., Schuetz, M.A. (2011). Fit optimisation of a distal medial tibia plate. *Computer Methods in Biomechanics and Biomedical Engineering*, 14(4), 359–1364.

Schulz, R., Muhler, M., Mutze, S., Schmidt, S., Reisinger, W., Schmeling, A. (2005). Studies on the time frame for ossification of the medial epiphysis of the clavicle as revealed by CT scans. *International Journal of Legal Medicine,* 119, 142–145.

Schulz, R., Schiborr, M., Pfeiffer, H., Schmidt S, Schmeling A. (2013). Sonographic assessment of the ossification of the medial clavicular epiphysis in 616 individuals. *Forensic Science, Medicine and Pathology,* 3, 351-357.

Schulz, R., Schiborr, M., Pfeiffer, H., Schmidt, S., Schmeling, A. (2014). Forensic age estimation in living subjects based on ultrasound examination of the ossification of the olecranon. *Journal of Forensic and Legal Medicine,* 22, 68-72.

Serin, J., Rérolle, C., Pucheux, J., Dedouit, F., Telmon, N., Savall, F. (2016). Contribution of magnetic resonance imaging of the wrist and hand to forensic age assessment. *International Journal of Legal Medicine*, 130, 1121–1128.

Sholts, S.B., Flores, L., Walker, P.L., Wärmländer, S.K.T.S. (2011). Comparison of coordinate measurement precision of different landmark types on human crania using a 3D laser

scanner and a 3D digitiser: implications for applications of digital morphometrics. *International Journal of Osteoarchaeology,* 21, 535–543.

Sholts, S.B., Wärmländer, S.K.T.S., Flores, L.M., Miller, K.W.P., Walker, P.L. (2010). Variation in the measurement of cranial volume and surface area using 3D laser scanning technology. *Journal of Forensic Science*, 55, 871-876.

Simonis, C., Friess, M., Détroit, F. (2009). Skull shapes, maps, and micro-scribes [abstract]. *American Journal of Physical Anthropology,* 48, 240.

Spies, A.J., Steyn, M., Bussy, E., Brits, D. (2020). Forensic imaging: the sensitivities of the various imaging modalities in detecting skeletal trauma in simulated cases of child abuse using a pig model. *Journal of Forensic and Legal Medicine,* 1-8.

Spradley, M.K. (2016). Metric methods for the biological profile in forensic anthropology: sex, ancestry, and stature. *Academic Forensic Pathology,* 6(3), 391-399.

Spradley, M.K., Jantz, R.L., Robinson, A., Peccerelli, F. (2008). Demographic change and forensic identification: problems in metric identification of Hispanic skeletons. *Journal of Forensic Anthropology,* 53, 21–28.

Sree Ram, M.N., Malay Jos, M., Debnath, J., Khana, S.K. (1998). Review article: 3 dimensional CT. *Medical Journal Armed Forces India*, 54(3), 239–242.

Stull, K.E. (2013). An osteometric evaluation of age and sex differences in long bones of South African children from Western Cape. Unpublished thesis: University of Pretoria.

Stull, K.E., L'Abbè, E.N., Ousley, S.D. (2017). Subadult sex estimation from diaphyseal dimension. *American Journal of Physical Anthropology*, 163, 64-74.

Stull, K.E., L'Abbè, E.N., Steiner, S. (2014b). Measuring distortion of skeletal elements in Lodox Statscan-generated images. *Clinical Anatomy*, 26(6), 780-786.

Stull, K.E., Tise, M.L., Ali, Z., Fowler, D.R. (2014a). Accuracy and reliability of measurements obtained from computed tomography 3D volume rendered images. *Forensic Science*

International, 238, 133-140.

Swift, B., Rutty, G.N. (2006). Recent advances in postmortem forensic radiology: CT and MRI applications. *Open Forensic Science,* 4, 355–404.

Thali, M.J., Yen, K., Schweitzer, W., Vock, P., Boesch, C., Ozdoba, C. (2003). Virtopsy, a new imaging horizon in forensic pathology: virtual autopsy by postmortem multislice computed tomography (MSCT) and magnetic resonance imaging (MRI)-a feasibility study. *Journal of Forensic Science,* 48, 386–403.

Thali, M.J., Braun, M., Buck, U. (2005). VIRTOPSY—scientific documentation, reconstruction and animation in forensic: individual and real 3D data based geometric approach including optical body/object surface and radiological CT/MRI scanning. *Journal of Forensic Science,* 50(2), 428-442.

Thali, M.J., Dirnhofer, R., Vock, P. (2009). *History of virtopsy. How it all began. The Virtopsy Approach 3d: 3D Optical and Radiological Scanning and Reconstruction in Forensic Medicine.* CRC Press/Taylor and Francis, Florida, United States. 11.

Thali, M.J., Jackowski, C., Oesterhelweg, L., Ross, S.G., Dirnhofer, R. (2007). Virtopsy–the swiss virtual autopsy approach. *Legal Medicine (Tokyo)*, 9, 100-104.

Torimitsu, S., Makino, Y., Saitoh, H., Sakuma, A., Ishii, N., Yajima, D. (2016). Sex estimation based on scapula analysis in a Japanese population using multidetector computed tomography. *Forensic Science International*, 262, 285.e1-285.e5.

Ubelaker, D.H. (2008). Issues in the global applications of methodology in forensic anthropology. *Journal of Forensic Science*, 53(3), 606-607.

Ulijaszek, S.J., Kerr, D.A. (1999). Anthropometric measurement error and the assessment of nutritional status. *British Journal of Nutrition*, 82, 165–177.

Urbanová, P., Hejna, P., Jurda, M. (2015). Testing photogrammetry-based techniques for three-dimensional surface documentation in forensic pathology. *Forensic Science*

International, 250, 77-86.

van Rijn, R.R., Sieswerda-Hoogendoorn, T. (2012). Educational paper: imaging child abuse: the bare bones. *European Journal of Pediatrics*, 171, 215-224.

Verhoff, M.A., Ramsthaler, F., Krahahn, J., Deml, U., Gille, R.J., Grabherr, S. (2008). Digital forensic osteology possibilities in cooperation with the Virtopsy project. *Forensic Science International*, 174, 152e6.

Walsh, M., Reeves, P., Scott, S. (2004). When disaster strikes ; the role of the forensic radiographer. *Radiography*, 10(1), 33-43.

Wang, Y.Z., Huang, Y., Zhou, X.R., Deng, Z.H. (2012). Stature estimation based on the length of tibia and fibula measured by digital X-ray in Chinese Han teenagers. *Fa Yi Xue Za Zhi*, 28(6), 413-7, 425.

Weber, G.W., Sebire, N.J. (2011). Post-mortem Investigation of Sudden Unexpected Death in Infancy: Role of Autopsy in Classification of Death. In: Turk, E.E. (eds), *Forensic Pathology Reviews*. Springer Science + Business Media, London, 6, 27-46.

Whiley, S.P., Mantokoudis, G., Ott, D. (2012). A review of full-body radiography in nontraumatic emergency medicine. *Emergency Medicine International*, 108–129.

Wiersema J, Love JC, Naul LG. 2009. The Influence of the Daubert Guidelines on Anthropological Methods of Scientific Identification in the Medical Examiner Setting. In: Steadman DW, ed. Hard Evidence: Case Studies in Forensic Anthropology. New Jersey, Prentice Hall. p. 80-90.

Williams, F.L., Richtsmeier, J.T. (2003). Comparison of mandibular landmarks from computed tomography and 3D digitizer data. *Clinical Anatomy*, 16, 494-500.

Zech, W., Näf, M., Siegmund, F., Jackowski, C., Lösch, S. (2016). Body height estimation from post-mortem CT femoral F1 measurements in a contemporary Swiss population. *Legal Medicine*, 19, 61-66.

Zhan, M.J., Cui, J.H., Zhang, K., Chen, Y.J., Deng, Z.H. (2019). Estimation of stature and sex from the skull measurements by multidetector computed tomography in Chinese. *Legal Medicine*, 41, 101625.

Zhang, Q., Rodriguez, A., Banner, Jørkov, M.L.S. (2019). Stature estimation from the postmortem CT femoral maximum length in contemporary Danish population. *Journal of Forensic Sciences*, 65(3), 930-938.

APPENDIX A

University of the Witwatersrand Human Research Ethics Committee (Medical) - Clearance Certificate No. M190765

UNIVERSITY OF THE WITWATERSRAND JOHANNESBURG

R14/49 Ms B Mamabolo (with Dr A Alblas)

HUMAN RESEARCH ETHICS COMMITTEE (MEDICAL)
CLEARANCE CERTIFICATE NO. M190765

NAME: (Principal Investigator)	Ms B Mamabolo (with Dr A Alblas)
DEPARTMENT:	School of Anatomical Sciences Medical School University
PROJECT TITLE:	The accuracy and repeatability of Lodox Statscan Osteometric Measurements
DATE CONSIDERED:	Ad hoc
DECISION:	Approved unconditionally
CONDITIONS:	
SUPERVISOR:	Dr D Brits
APPROVED BY:	Dr CB Penny, Chairperson, HREC (Medical)
DATE OF APPROVAL:	2019/08/27

This clearance certificate is valid for 5 years from date of approval. Extension may be applied for.

DECLARATION OF INVESTIGATORS

To be completed in duplicate and **ONE COPY** returned to the Research Office Secretary on the 3rd Floor, Phillip Tobias Building, Parktown, University of the Witwatersrand, Johannesburg.
I/we fully understand the conditions under which I am/we are authorized to carry out the above-mentioned research and I/we undertake to ensure compliance with these conditions. Should any departure be contemplated, from the research protocol as approved, I/we undertake to submit details to the Committee. **I agree to submit a yearly progress report**. When a funder requires annual re-certification, the application date will be one year after the date when the study was initially reviewed. In this case, the study was initially reviewed in **July** and will therefore reports and re-certification will be due early in the month of **July** each year. Unreported changes to the application may invalidate the clearance given by the HREC (Medical).

Principal Investigator Signature _____ Date _____

PLEASE QUOTE THE CLEARANCE CERTIFICATE NUMBER IN ALL ENQUIRIES

APPENDIX B

Stellenbosch University Human Research Ethics Committee (Medical)- Clearance Certificate No. N19/05/068

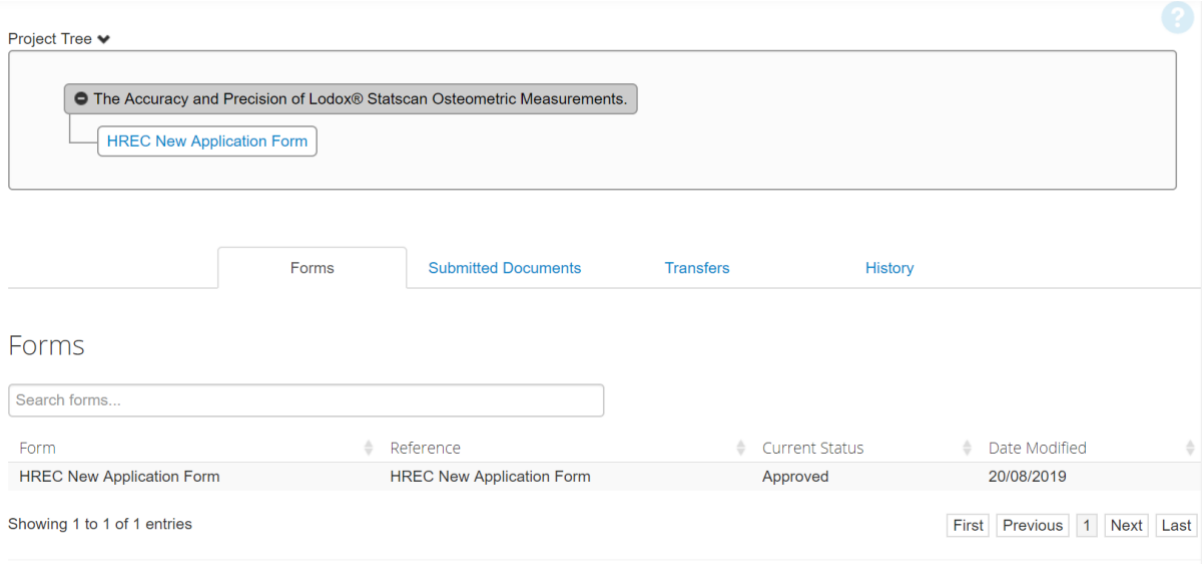

APPENDIX C

Normality test results of the measurements collected from Lodox Statscan images and from corresponding dry bone.

Table 1 Table displaying the Shapiro-Wilk test results for the skull measurements collected from Lodox images and corresponding dry bone.

Measurement	Dry bone	Lodox
ZYGB	0.060	0.004*
FOL	0.000*	0.022
FOB	0.008*	0.489
HMB (R)	0.389	0.501
mRB (R)	0.758	0.657
HMB (L)	0.981	0.532
mRB (L)	0.851	0.444
MRh (L)	0.171	0.914
ML (L)	0.118	0.018

*R- Right; L- Left; *p<0.05*

ZYGB- Bizygomatic breath; FOL- Length of foramen magnum; FOB- Breadth of foramen magnum; HMB- Height of mandibular body; mRB- Minimum ramus breadth; MRh- Maximum ramus height; ML- Mandibular length.

Table 2 Table displaying the Shapiro-Wilk test results (p-value) for the pectoral girdle and upper limb measurements collected from Lodox images and corresponding dry bone.

Measurements	**Dry bone**	**Lodox**
MLC^x (R)	0.599	0.764
MDC^x (R)	0.599	0.057
mDC^x (R)	0.009*	0.040*
HS^y (R)	0.125	0.067
BS^x (R)	0.153	0.003*
MLC^x (L)	0.688	0.703
MDC^x (L)	0.035*	0.753
mDC^x (L)	0.130	0.779
HS^y (L)	0.208	0.406
BS^x (L)	0.062	0.009*
MLH^y (R)	0.661	0.289
EBH^x (R)	0.075	0.580
MVDhH (R)	0.536	0.814
MDH (R)	0.822	0.527
mDH (R)	0.495	0.378
MLR (R)	1.00	0.943
MDR (R)	0.394	0.881
mDR (R)	0.240	0.594

*R- Right; L- Left; *p<0.05*

MLC- Maximum length of clavicle; MDC-Maximum diameter of clavicle at midshaft; mDC-Minimum diameter of clavicle at midshaft; HS- Height of scapula; BS- Breadth of scapula; MLH- Maximum length of humerus; EBH- Epicondylar breadth of humerus; MVDhH- Maximum vertical diameter of the head of humerus; MDH- Maximum diameter of humerus at midshaft; mDH- Minimum diameter of humerus at midshaft; MLR- Maximum length of radius; MDR- Maximum diameter of radius at midshaft; mDR- Minimum diameter of radius at midshaft.

Table 2 *Continued*

Measurements	Dry bone	Lodox
MDRh (R)	0.361	0.851
MLU (R)	0.642	0.566
MDU (R)	0.094	0.062
mDU (R)	0.326	0.810
PLU (R)	0.000*	0.413
MLH (L)	0.549	0.720
EBH (L)	0.067	0.147
MVDhH (L)	0.765	0.672
MDH (L)	0.960	0.362
mDH (L)	0.266	0.675
MLR (L)	0.731	0.679
MDR (L)	0.791	0.196
mDR (L)	0.924	0.299
MDRh (L)	0.240	0.584
MLU (L)	0.772	0.669
MDU (L)	0.725	0.403
mDU (L)	0.024*	0.606
PLU (L)	0.302	0.818

*R- Right; L- Left; *p<0.05*

MDRh- Maximum diameter of radial head; MLU-Maximum length of ulna; MDU- Maximum diameter of ulna at midshaft; mDU- Minimum diameter of ulna at midshaft; PLU- Physiological length of ulna; MLH; Maximum length of humerus; EBH- Epicondylar breadth of humerus; MVDhH- Maximum vertical diameter of the head of humerus; MDH- Maximum diameter of humerus at midshaft; mDH- Minimum diameter of humerus at midshaft; MLR- Maximum length of radius; MDR- Maximum diameter of radius at midshaft; mDR- Minimum diameter of radius at midshaft.

Table 3 Table displaying the Shapiro-Wilk test results (p-value) for the pectoral girdle and upper limb measurements collected from Lodox images and corresponding dry bone.

Measurement	Dry bone	Lodox
AHS	0.725	0.000*
ABS	0.000*	0.011*
TDSS1	0.807	0.179
MInh (R)	0.057	0.065
MIB (R)	0.049	0.085
WIB (R)	0.056	0.962
ASISS (R)	0.013*	0.013*
MInh (L)	0.060	0.098
MIB (L)	0.060	0.052
WIB (L)	0.758	0.000*
ASISS (L)	0.770	0.003*
MLF (R)	0.551	0.117
BLF (R)	0.464	0.294
EBF (R)	0.178	0.803
MDFh (R)	0.052	0.795
TSDF (R)	0.294	0.055

*R- Right; L- Left; *p<0.05*

AHS- Anterior height of sacrum; ABS- Anterior breadth of sacrum; TDSS1- Transverse diameter of sacral segment 1; Minh- Maximum innominate height; MIB- Maximum innominate breadth; WIB- Minimum innominate breadth; ASISS- Anterior superior iliac spine to symphysion; MLF- Maximum length of the femur; BLF- Bicondylar length of femur; EBF- Epicondylar breadth of femur; MDFh- Maximum diameter of the femur head; TSDF- Transverse subtrochanteric diameter of femur.

Table 3 *Continued*

Measurement	Dry bone	Lodox
MDF (R)	0.242	0.744
mDF (R)	0.096	0.871
LT (R)	0.122	0.029
MPeBT (R)	0.948	0.888
DeBT (R)	0.115	0.754
MT (R)	0.662	0.893
mT (R)	0.704	0.758
MLFib (R)	0.649	0.324
MDFib (R)	0.682	0.686
MLF (L)	0.479	0.405
BLF (L)	0.506	0.397
EBF (L)	0.677	0.014
MDFh (L)	0.006	0.894
TSDF (L)	0.058	0.089
MDF (L)	0.173	0.861
mDF (L)	0.060	0.067
LT (L)	0.395	0.134
MPeBT (L)	0.195	0.749
DeBT (L)	0.112	0.397

*R- Right; L- Left; *p<0.05*

MDF- Maximum midshaft diameter of femur; mDF- Minimum midshaft diameter of femur; LT- Length of tibia; MPeBT- Maximum proximal epiphyseal breadth of tibia; DeBT- Distal epiphyseal breadth of tibia; MT- Maximum midshaft diameter of tibia; mT- Minimum midshaft diameter of tibia; MLFib- Maximum length of the fibula; MDFib-Maximum diameter of the fibula at midshaft; MLF- Maximum length of femur; BLF- Bicondylar length of femur; EBF- Epicondylar breadth of femur; MDFh- Maximum diameter of femur head; TSDF- Transverse subtrochanteric diameter of femur.

Table 3 *Continued*

Measurement	**Dry bone**	**Lodox**
MT (L)	0.315	0.683
mT (L)	0.945	0.734
MLFib (L)	0.777	0.759
MDFib (L)	0.993	0.342

*R- Right; L- Left; *p<0.05*

MT- Maximum midshaft diameter of tibia; mT- Minimum midshaft diameter of tibia; MLFib- Maximum length of the fibula; MDFib-Maximum diameter of the fibula at midshaft.

APPENDIX D

Bland-Altman Plots of measurements, whose paired t-test/Wilcoxon signed rank test results showed significant difference between Lodox and dry bone.

A1

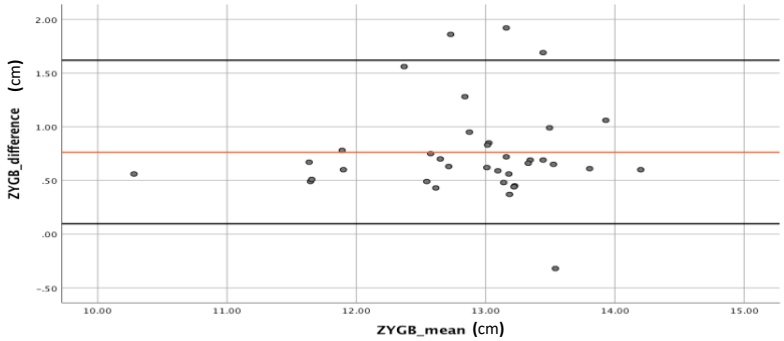

B1

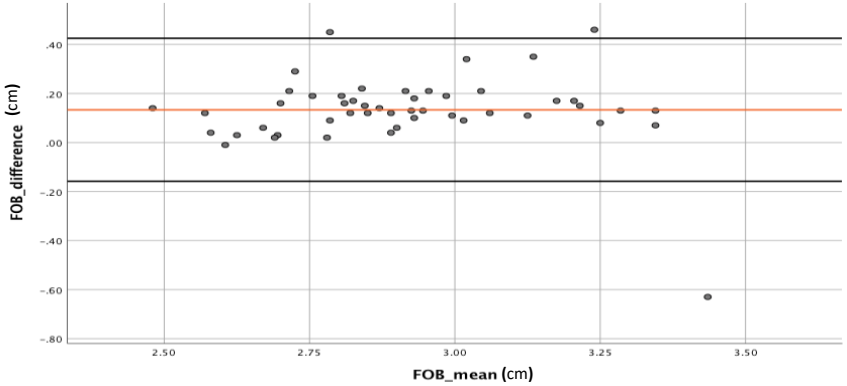

C1

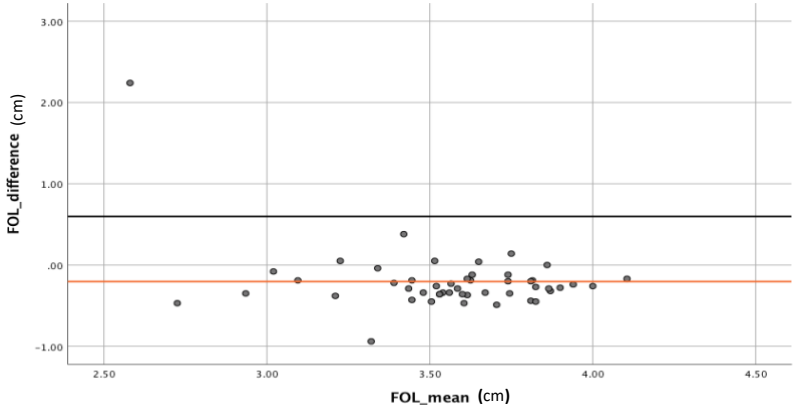

Figure 1 Bland-Altman plots representing the agreement of the skull measurements for the A1) bizygomatic breadth, B1) foramen magnum breadth and C1) foramen magnum length, taken from the dry bone and Lodox images. The graph shows the mean (red line) and the limits of agreement (with a 95% confidence interval, represented by the solid black lines). In the case of C1), the lower limits of agreement and upper limits of agreement, respectively, could not fit into the scale of the graph.

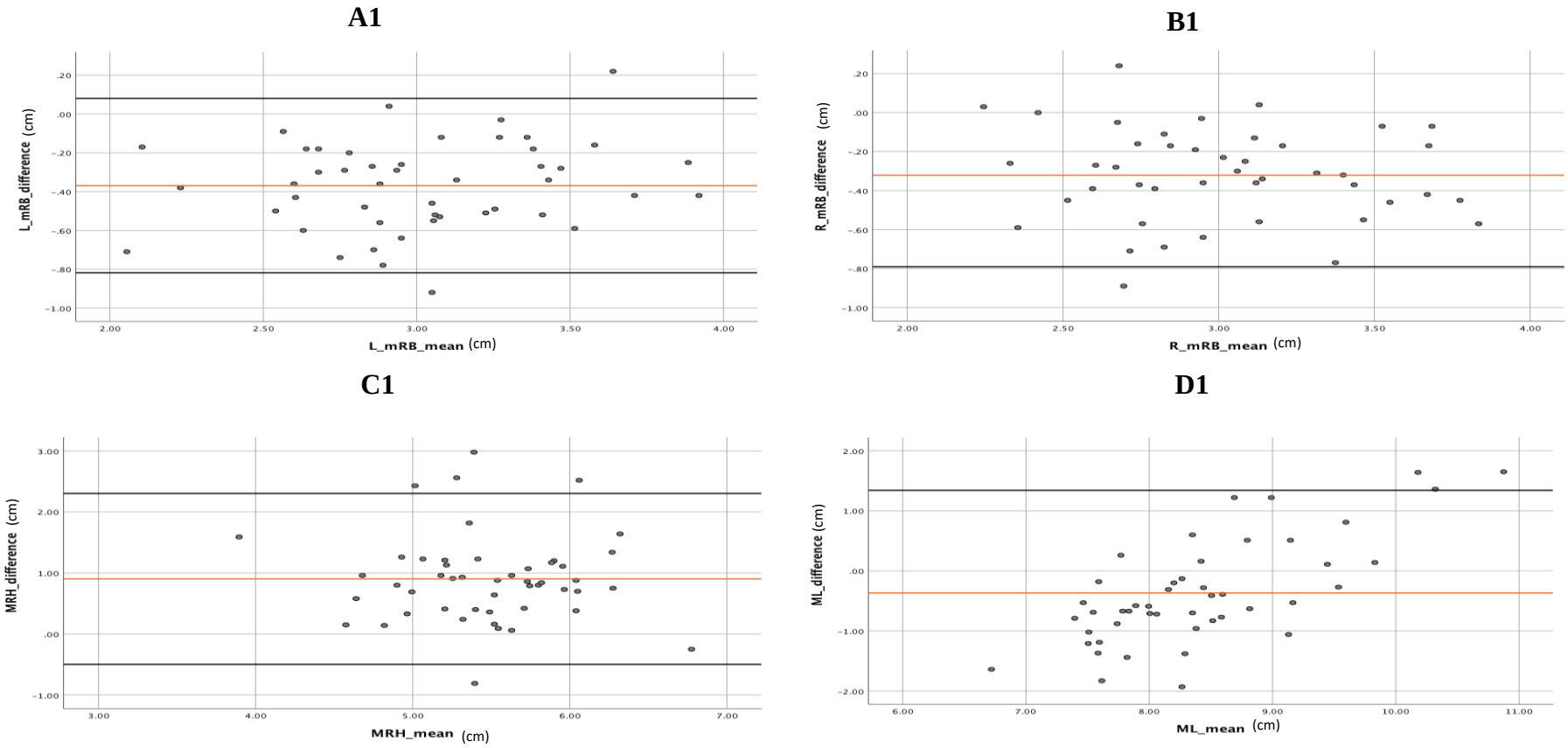

Figure 2 Bland-Altman plots representing the agreement of the mandibular measurements for the A1) minimum ramus breadth on the left and B) right side, C1) maximum ramus height and D1) mandibular length, taken from the dry bone and Lodox images. The graph shows the mean (red line) and the limits of agreement (with a 95% confidence interval, represented by the solid black lines). In the case of B1) the lower limits of agreement and upper limits of agreement, respectively, could not fit into the scale of the graph.

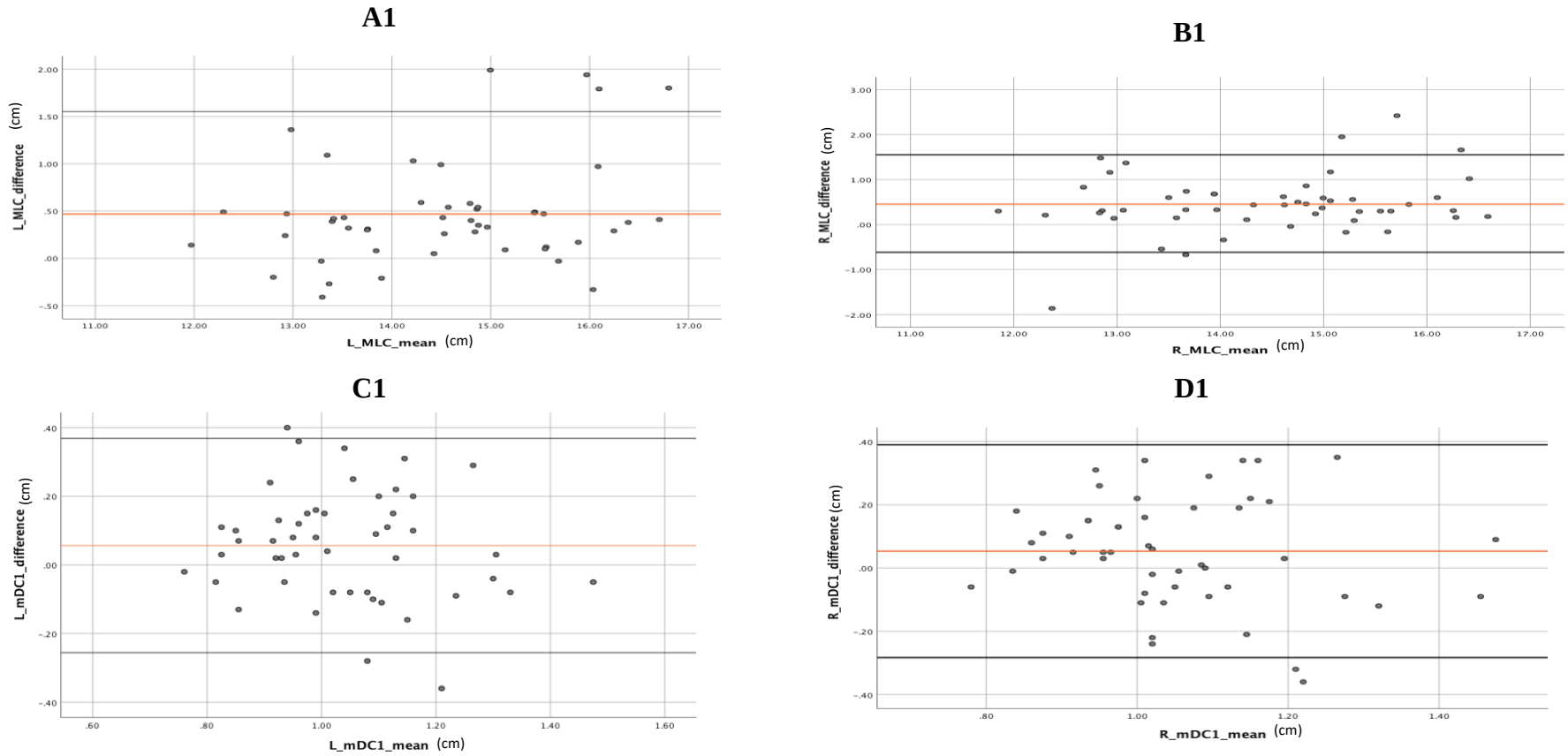

Figure 3 Bland-Altman plots representing the agreement of the pectoral girdle measurements for the A1) maximum length of the clavicle on the left and B1) right side, C1) minimum midshaft diameter of the clavicle on the left and D1) right side, taken from the dry bone and Lodox images. The graph shows the mean (red line) and the limits of agreement (with a 95% confidence interval, represented by the solid black lines). In the case of A1) the lower limits of agreement and upper limits of agreement, respectively, could not fit into the scale of the graph.

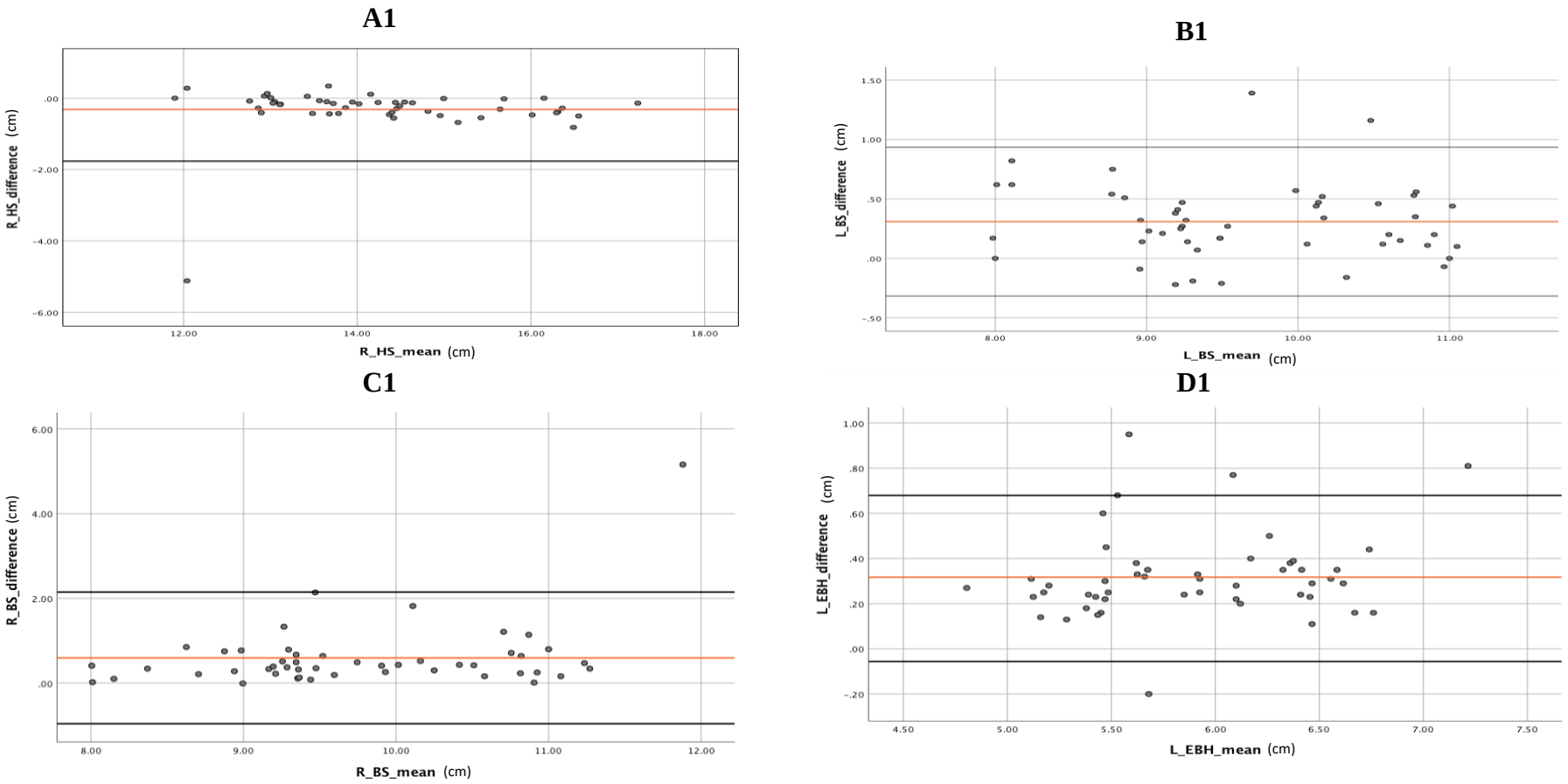

Figure 4 Bland-Altman plots representing the agreement of the pectoral girdle and upper limb measurements the A1) height of the scapula on the right side, B1) breadth of scapula on the left and C1) right side and the D1) epicondylar breadth of humerus on the left side, taken from the dry bone and Lodox images. The graph shows the mean (red line) and the limits of agreement (with a 95% confidence interval, represented by the solid black lines). In the case of A1) the lower limits of agreement and upper limits of agreement, respectively, could not fit into the scale of the graph.

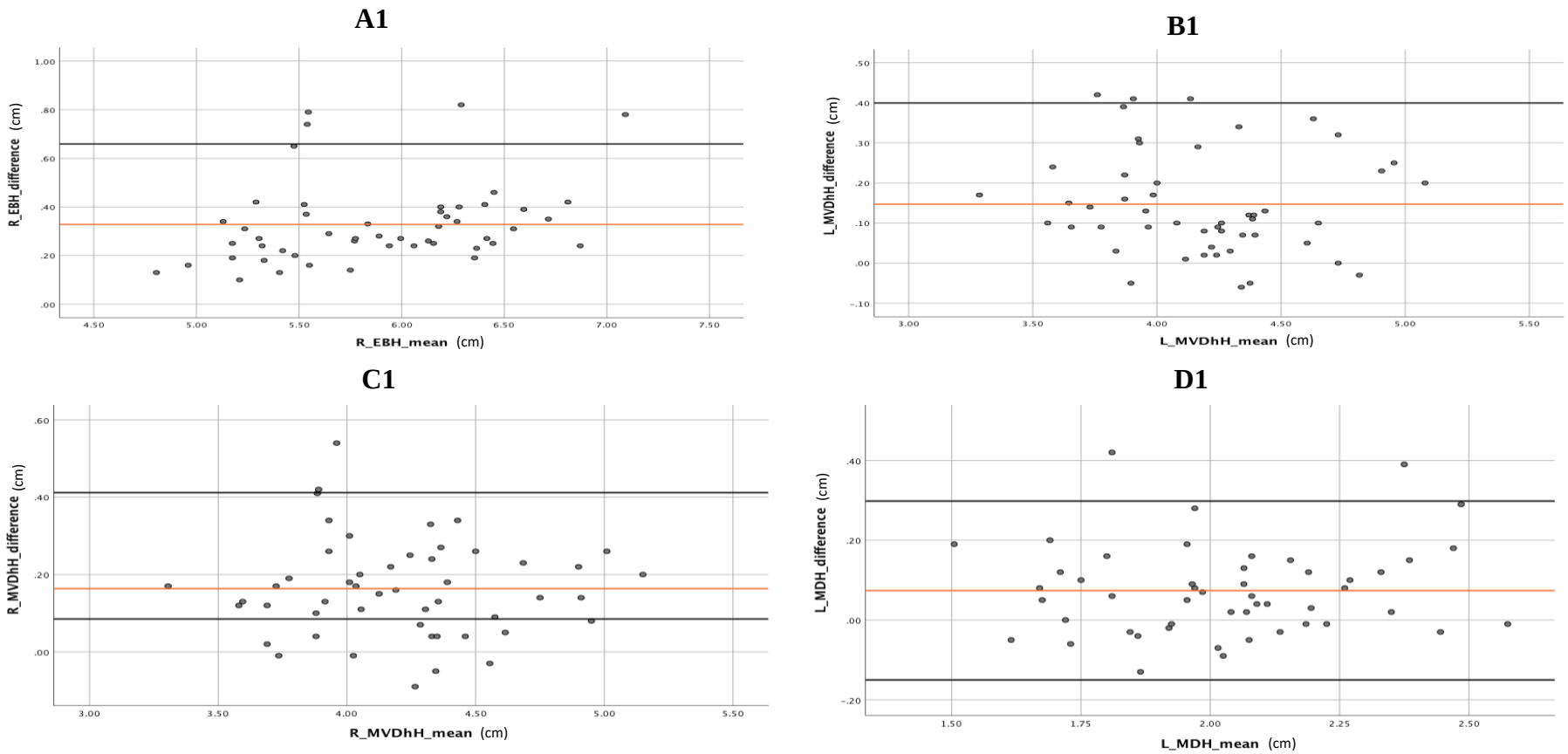

Figure 5 Bland-Altman plots representing the agreement of the upper limb measurements for the A1) epicondylar breadth of the humerus on the right side, B1) maximum vertical diameter of the head of the humerus on the left and C1) right side and the D1) maximum diameter of the humerus at midshaft on the left side, taken from the dry bone and Lodox images. The graph shows the mean (red line) and the limits of agreement (with a 95% confidence interval, represented by the solid black lines). In the case of A1) and B1) the lower limits of agreement and upper limits of agreement, respectively, could not fit into the scale of the graph.

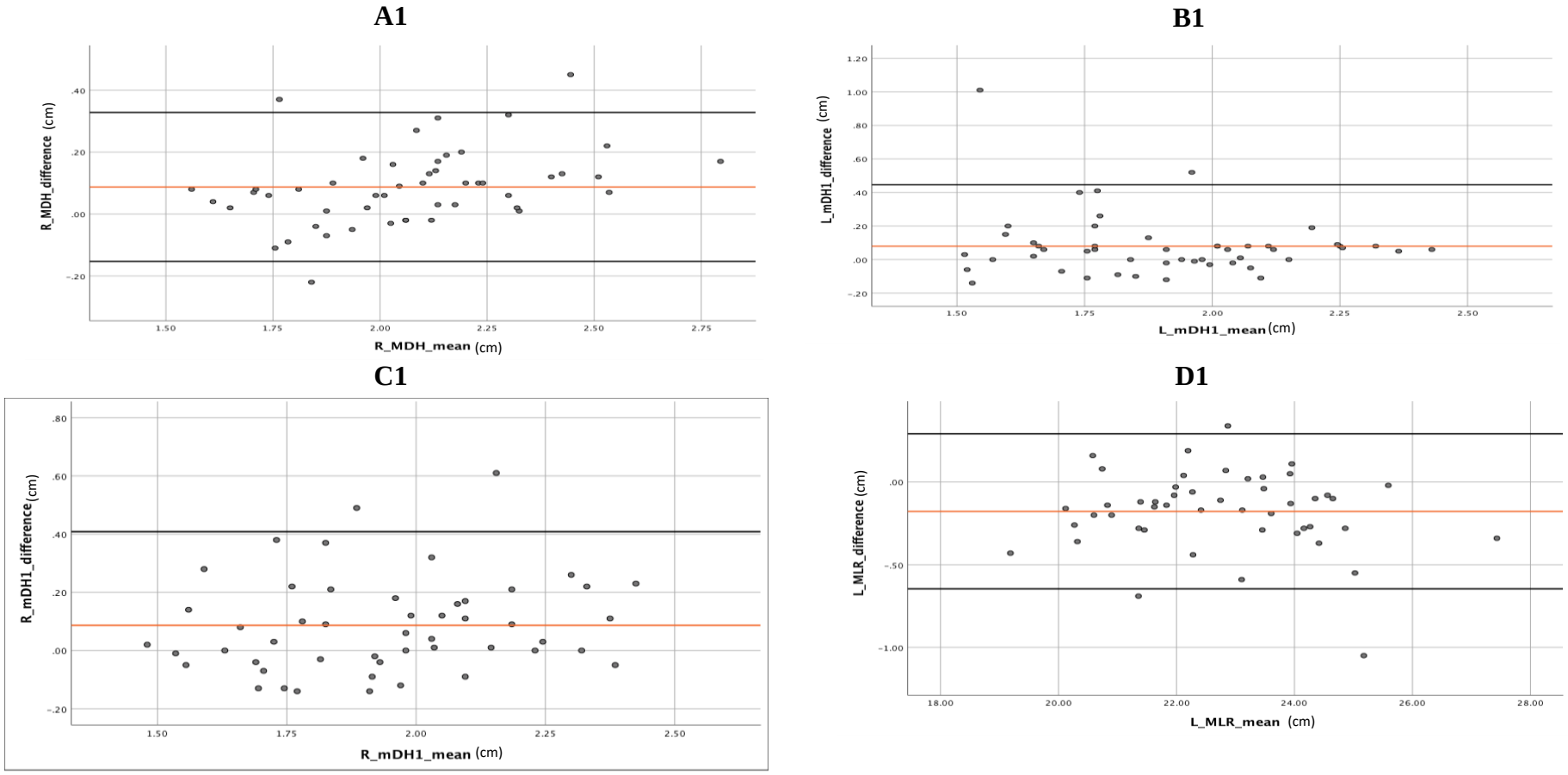

Figure 6 Bland-Altman plots representing the agreement of the upper limb measurements for the A1) maximum diameter of the humerus at midshaft on the right side, B1) minimum diameter of the humerus at midshaft on the left and C1) right side and the D1) maximum length of radius on the left side, taken from the dry bone and Lodox images. The graph shows the mean (red line) and the limits of agreement (with a 95% confidence interval, represented by the solid black lines). In the case of B1) and C1) the lower limits of agreement and upper limits of agreement, respectively, could not fit into the scale of the graph.

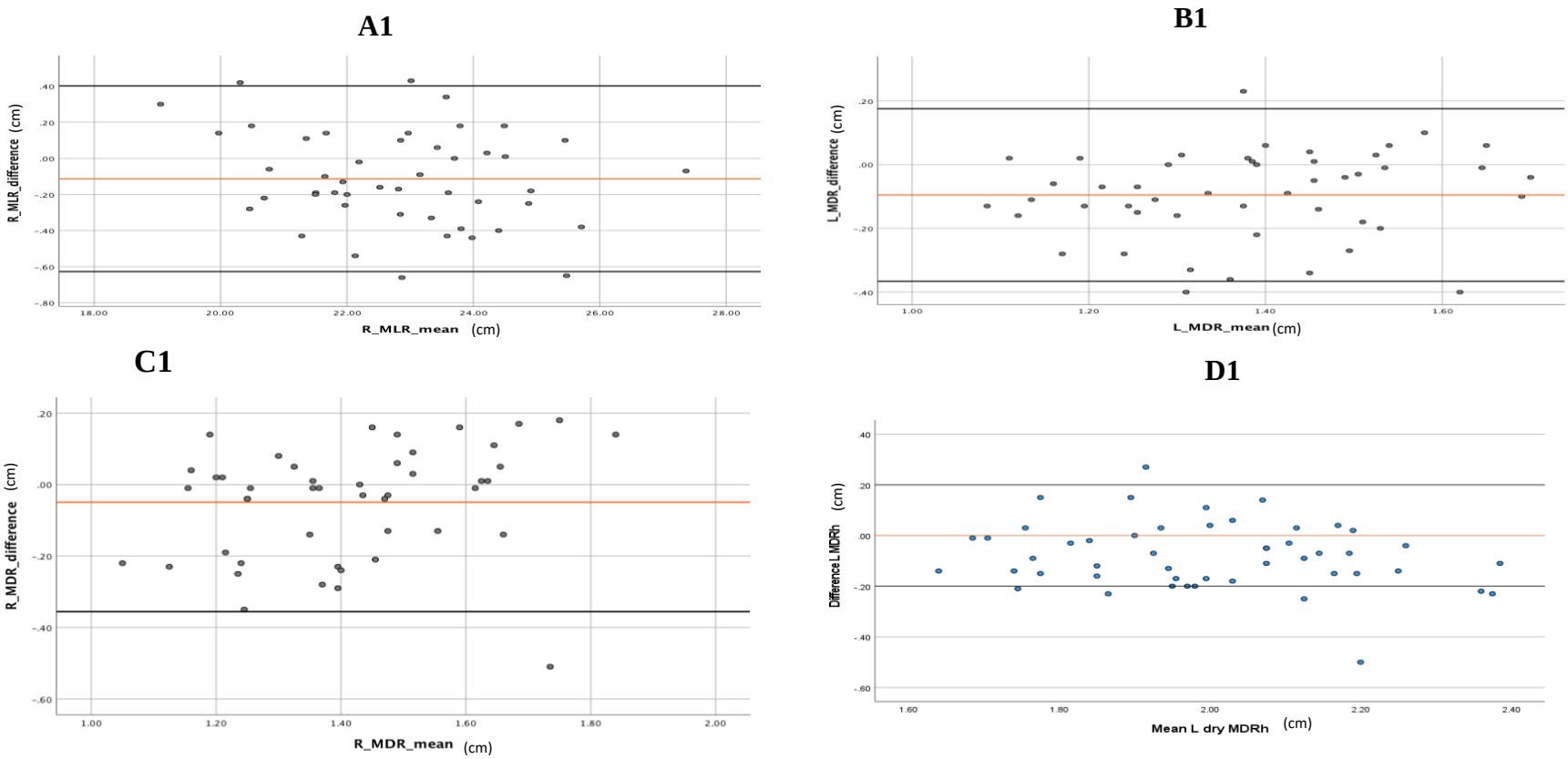

Figure 7 Bland-Altman plots representing the agreement of the upper limb measurements for the A1) maximum length of radius on the right side, B1) maximum diameter of the radius at midshaft on the left and C1) right side and the D1) maximum diameter of the radial head on the left side, taken from the dry bone and Lodox images. The graph shows the mean (red line) and the limits of agreement (with a 95% confidence interval, represented by the solid black lines). In the case of ai) the lower limits of agreement and upper limits of agreement, respectively, could not fit into the scale of the graph.

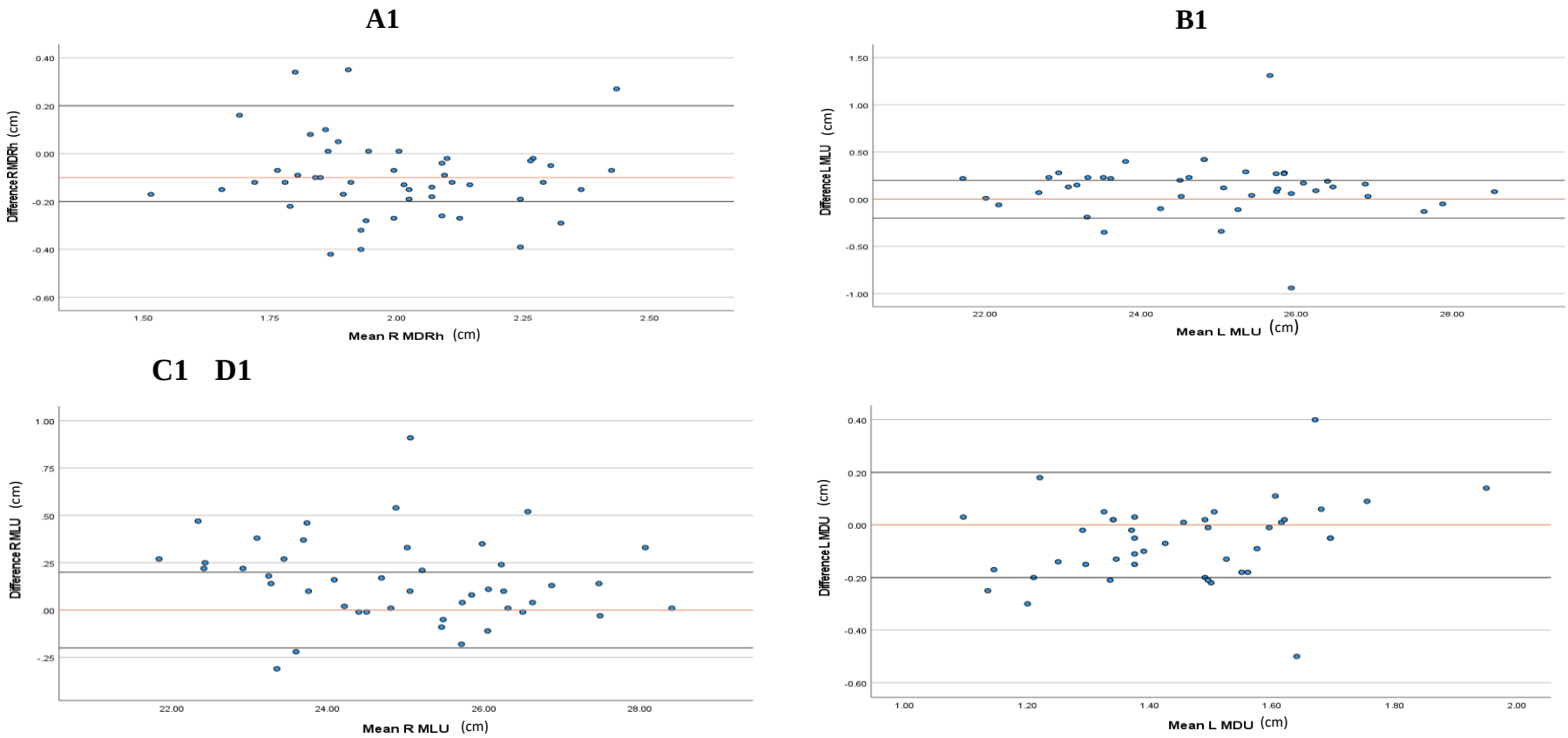

Figure 8 Bland-Altman plots representing the agreement of the upper limb measurements for the A1) maximum diameter of the radial head on the right side, B1) maximum length of the ulna on the left and C1) right side and the D1) maximum diameter of ulna at midshaft on the left side, taken from the dry bone and Lodox images. The graph shows the mean (red line) and the limits of agreement (with a 95% confidence interval, represented by the solid black lines). In the case of ai) the lower limits of agreement and upper limits of agreement, respectively, could not fit into the scale of the graph.

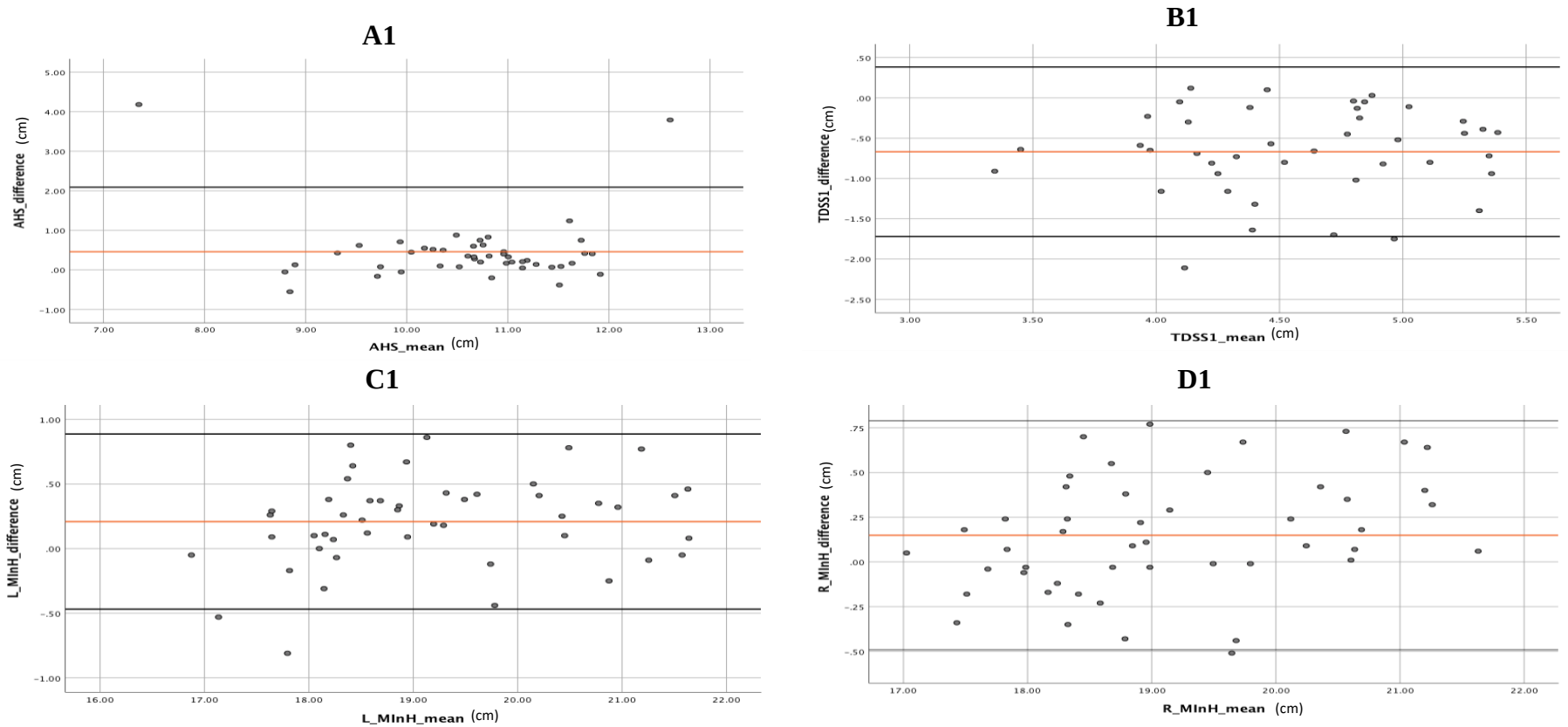

Figure 9 Bland-Altman plots representing the agreement of the pelvic girdle measurements for the A1) anterior height of sacrum, B1) transverse diameter of sacral segment 1, C1) maximum innominate height on the left and D1) right side, taken from the dry bone and Lodox images. The graph shows the mean (red line) and the limits of agreement (with a 95% confidence interval, represented by the solid black lines). In the case of A1) the lower limits of agreement and upper limits of agreement, respectively, could not fit into the scale of the graph.

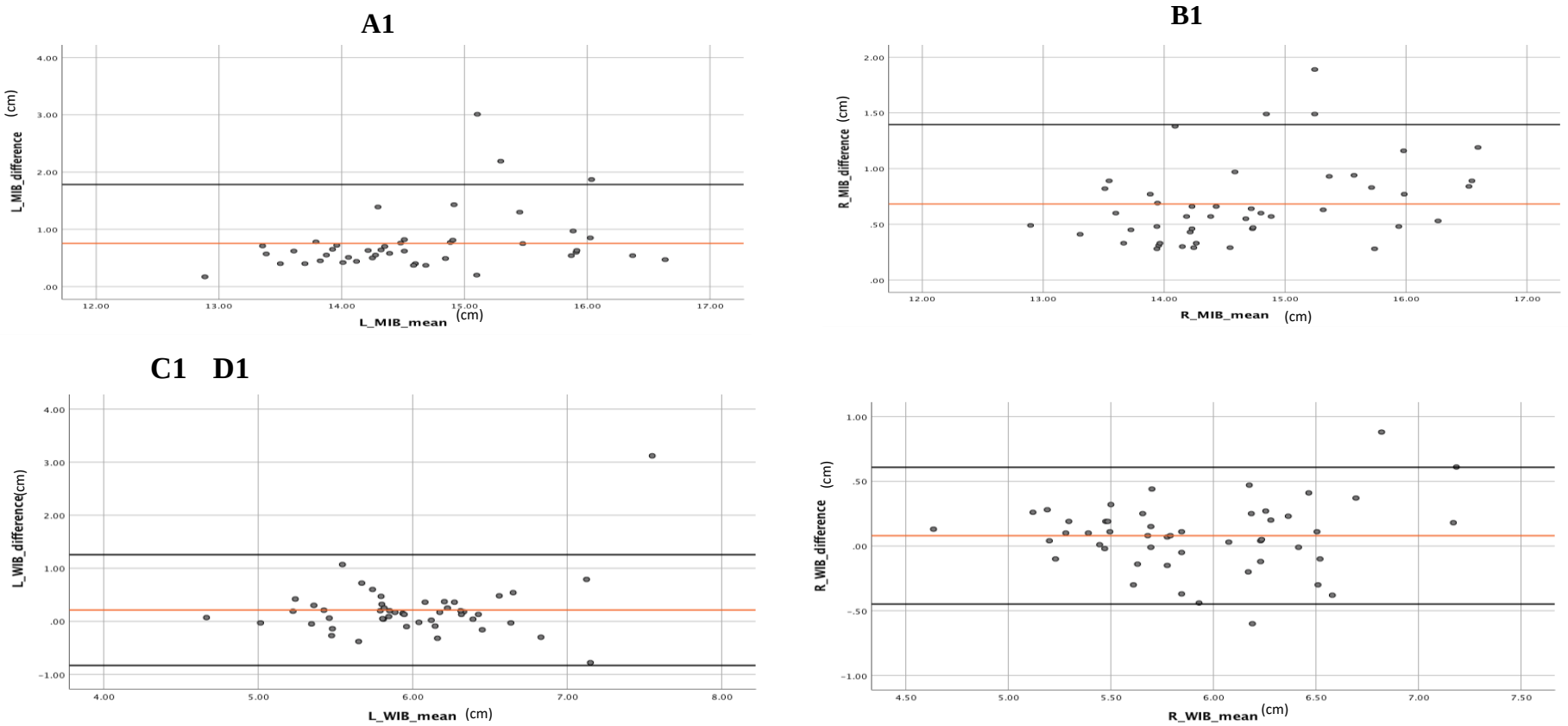

Figure 10 Bland-Altman plots representing the agreement of the pelvic girdle measurements for the A1) maximum iliac breadth on the left and B1) right side, C1) minimum iliac breadth on the left and D1) right side, taken from the dry bone and Lodox images. The graph shows the mean (red line) and the limits of agreement (with a 95% confidence interval, represented by the solid black lines). In the case of A1) and A2) the lower limits of agreement and upper limits of agreement, respectively, could not fit into the scale of the graph.

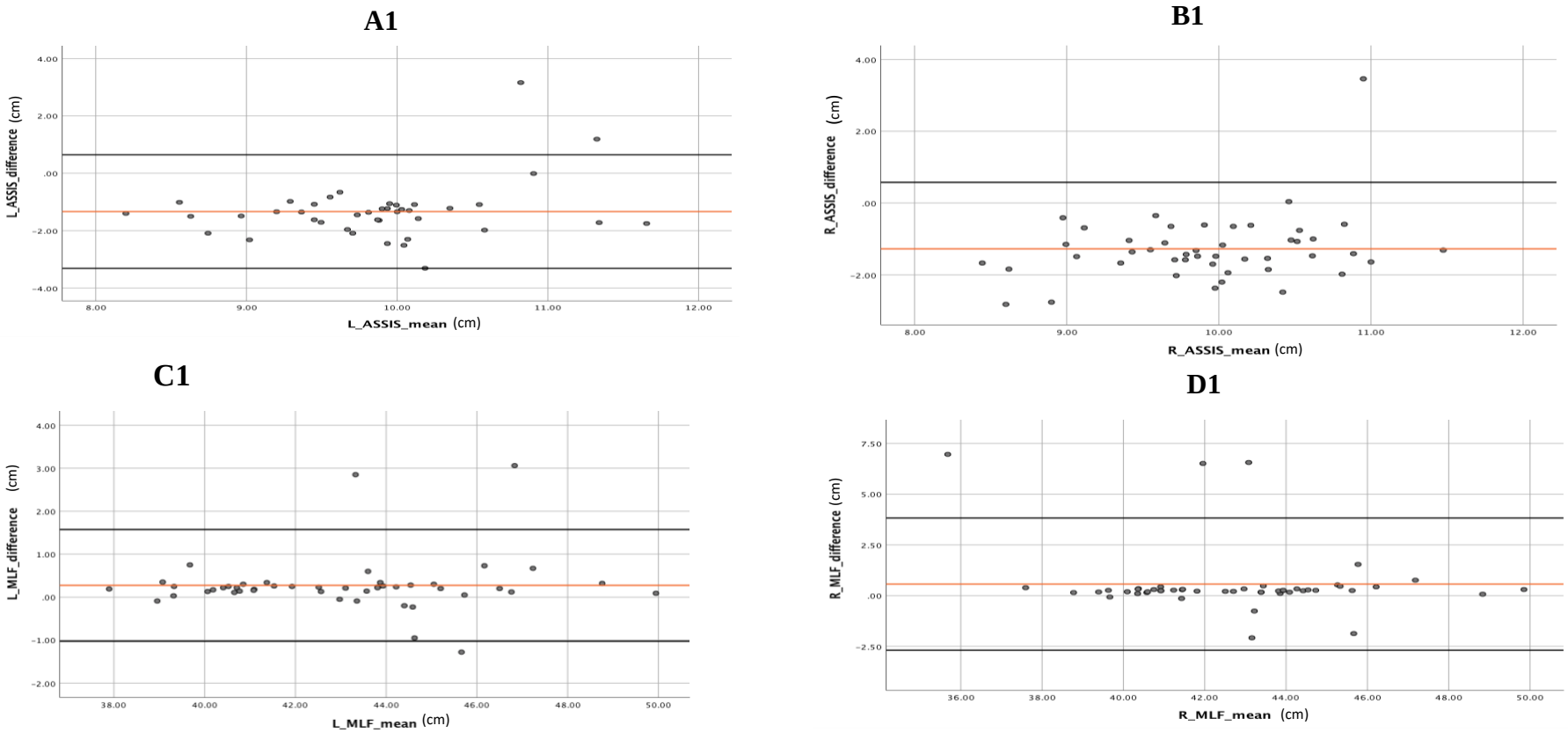

Figure 11 Bland-Altman plots representing the agreement of the pelvic girdle and lower limb measurements for the A1) anterior superior iliac spine to the symphysion on the left and B1) right side, C1) maximum length of the femur on the left and D1) right side, taken from the dry bone and Lodox images. The graph shows the mean (red line) and the limits of agreement (with a 95% confidence interval, represented by the solid black lines). In the case of B1) the lower limits of agreement and upper limits of agreement, respectively, could not fit into the scale of the graph.

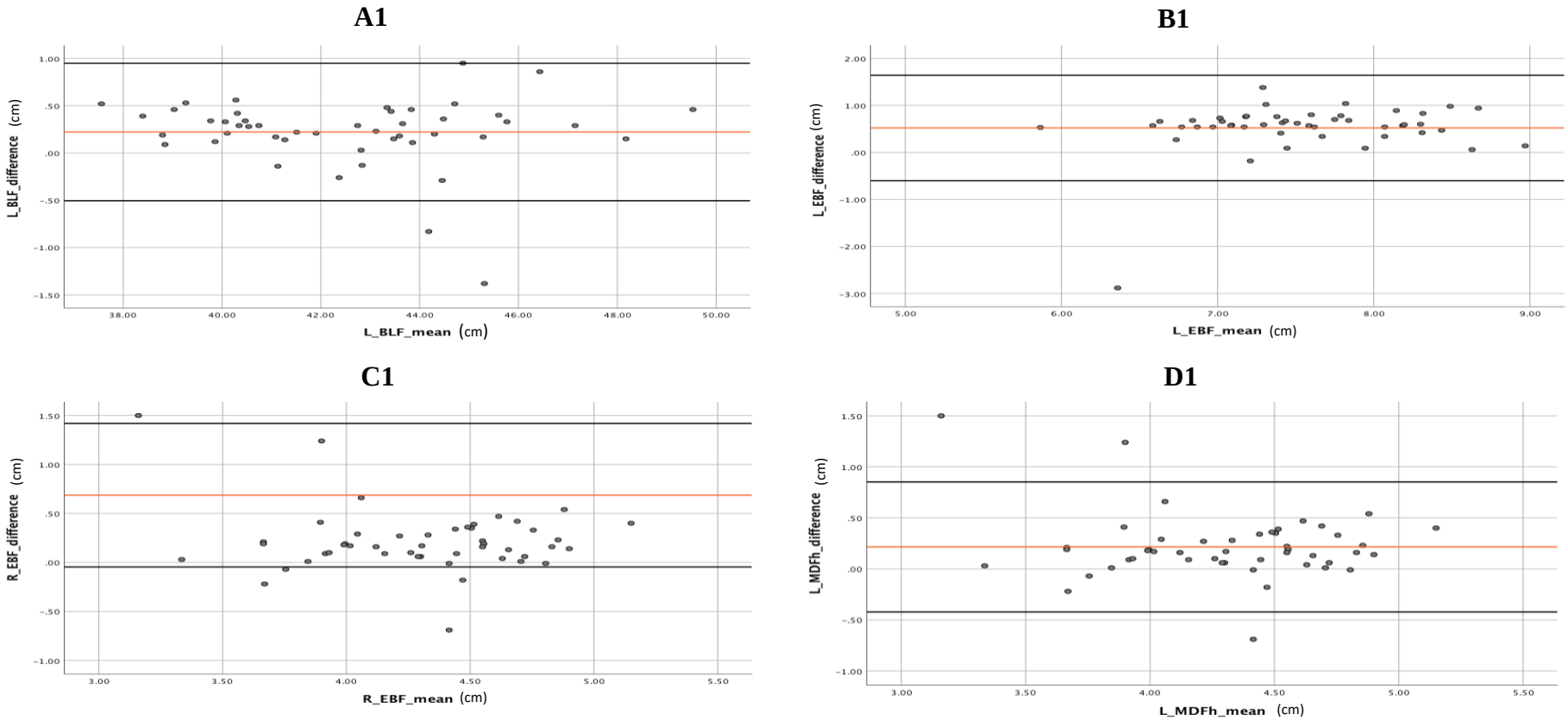

Figure 12 Bland-Altman plots representing the agreement of the lower limb measurements for the A1) bicondylar length of femur on the left side, B1) epicondylar breadth of the femur on the left and C1) right side and the D1) maximum diameter of the head of femur on the left side, taken from the dry bone and Lodox images. The graph shows the mean (red line) and the limits of agreement (with a 95% confidence interval, represented by the solid black lines).

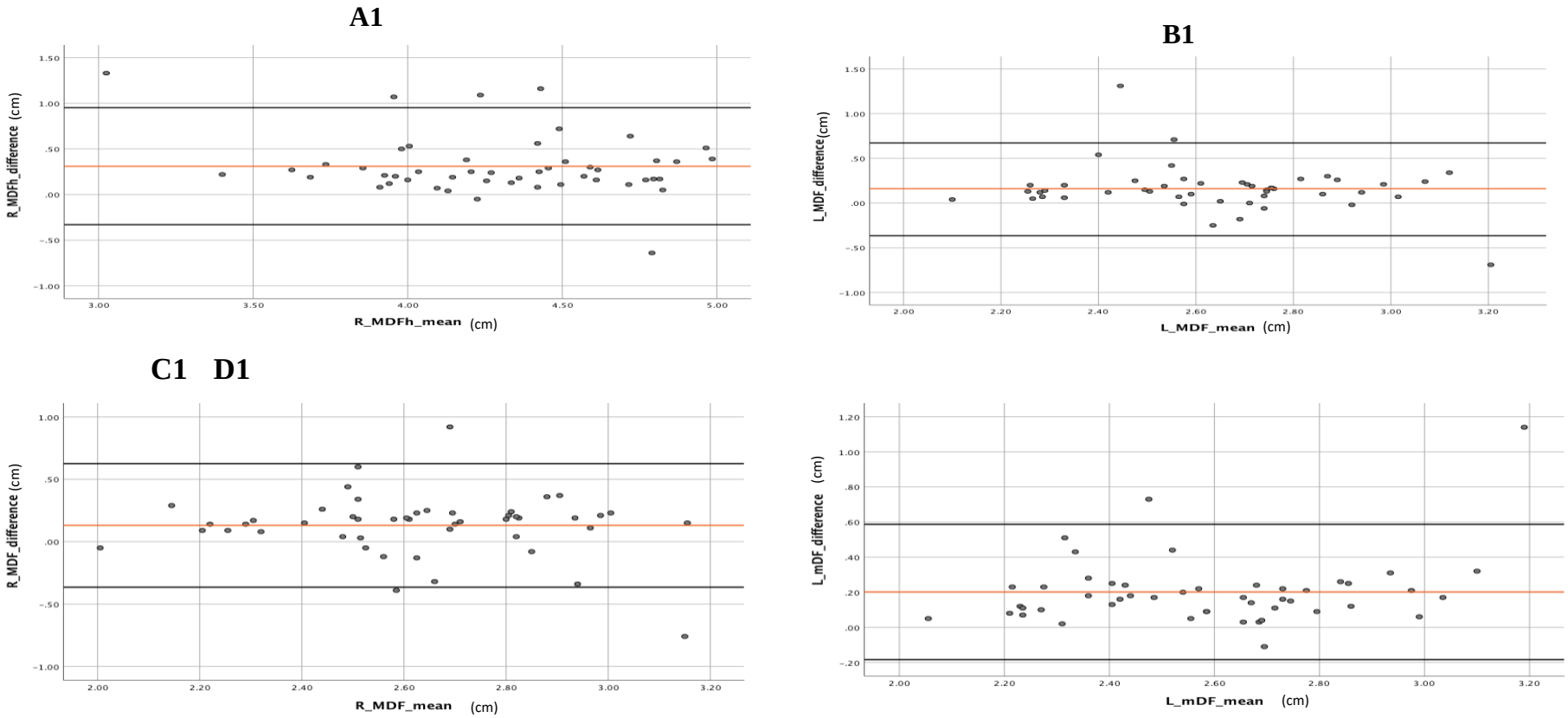

Figure 13 Bland-Altman plots representing the agreement of the lower limb measurements for the A1) maximum diameter of the head of femur on right side, B1) maximum midshaft diameter of femur on the left and C1) right side and the D1) minimum diameter of the femur on the left side, taken from the dry bone and Lodox images. The graph shows the mean (red line) and the limits of agreement (with a 95% confidence interval, represented by the solid black lines).

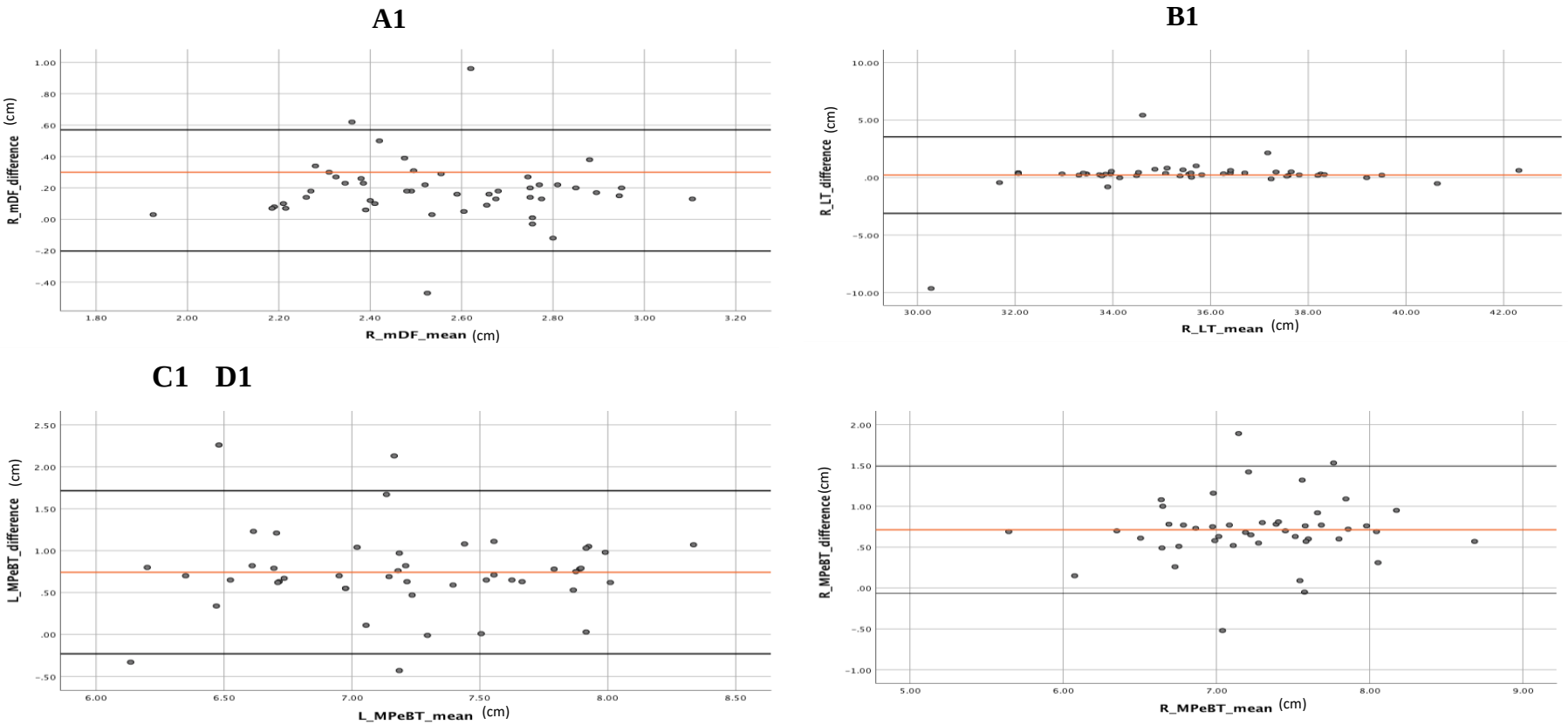

Figure 14 Bland-Altman plots representing the agreement of the lower limb measurements for the A1) minimum midshaft diameter of femur on right side, B1) length of tibia on the right side,C1) maximum proximal epiphyseal breadth of tibia on the left and D1) right side, taken from the dry bone and Lodox images. The graph shows the mean (red line) and the limits of agreement (with a 95% confidence interval, represented by the solid black lines).

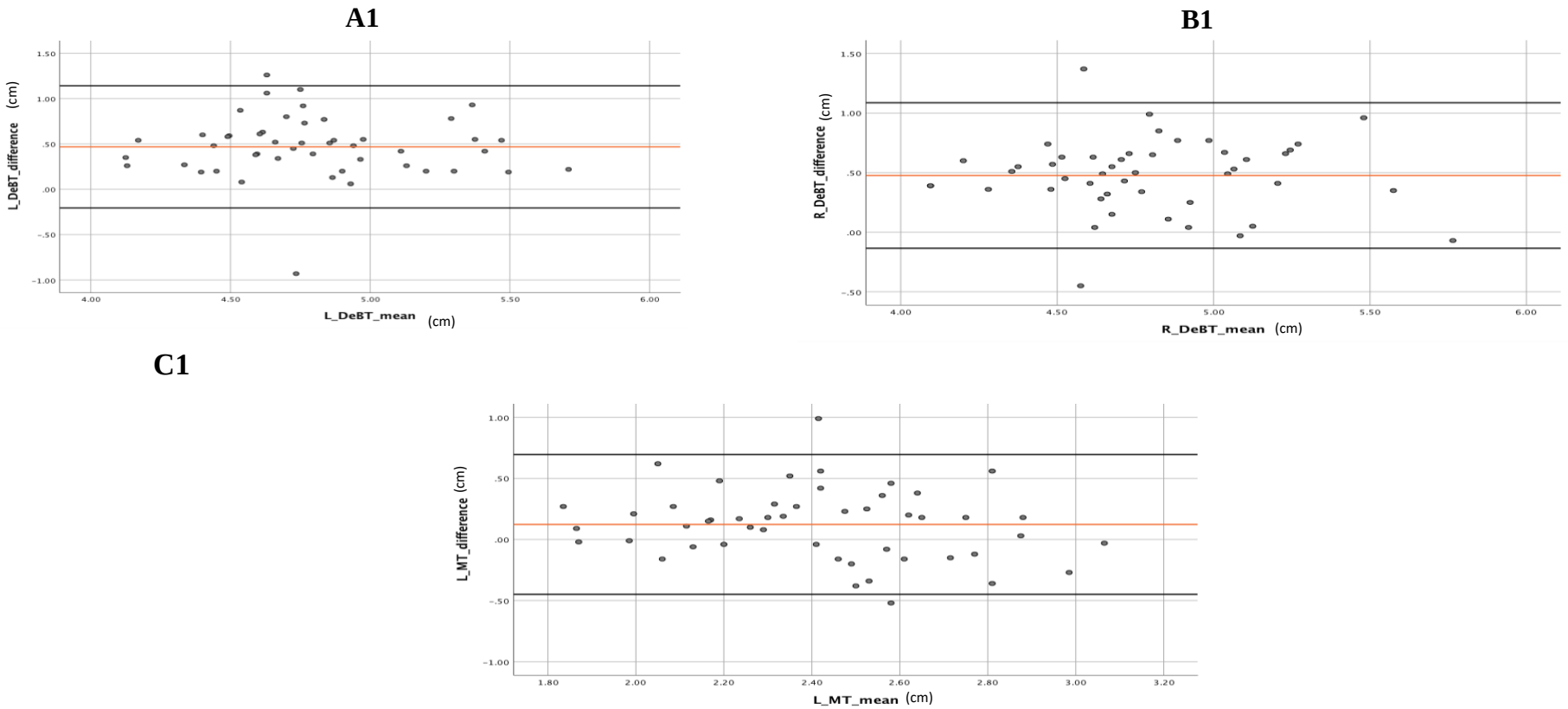

Figure 15 Bland-Altman plots representing the agreement of the lower limbl measurements for the A1) distal epicondylar breadth of tibia on the left and B1) right side and the C1) maximum midshaft diameter of tibia on the left side, taken from the dry bone and Lodox images. The graph shows the mean (red line) and the limits of agreement (with a 95% confidence interval, represented by the solid black lines).

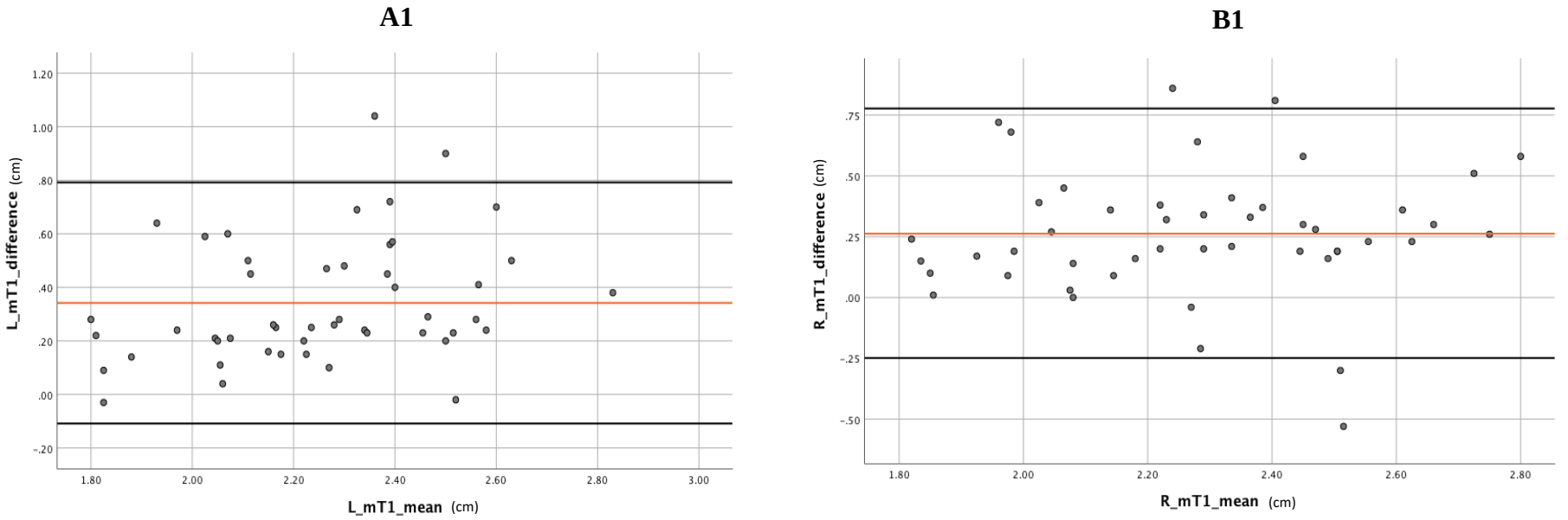

Figure 16 Bland-Altman plots representing the agreement of the lower limbl measurements for the A1) minimum midshaft diameter of tibia on the left and B1) right side, taken from the dry bone and Lodox images. The graph shows the mean (red line) and the limits of agreement (with a 95% confidence interval, represented by the solid black lines).

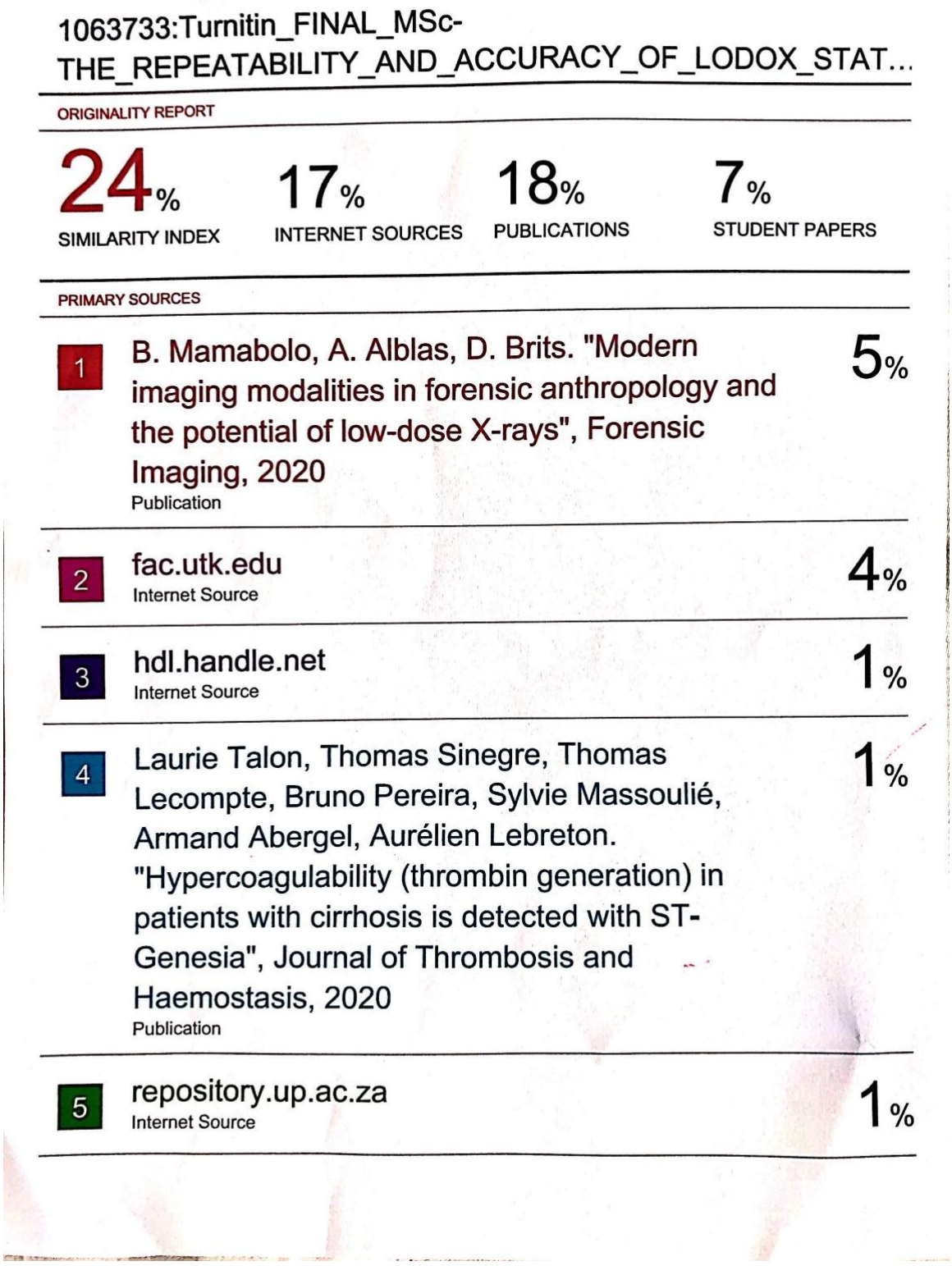

1063733:Turnitin_FINAL_MSc-THE_REPEATABILITY_AND_ACCURACY_OF_LODOX_STAT...

ORIGINALITY REPORT

24%	17%	18%	7%
SIMILARITY INDEX	INTERNET SOURCES	PUBLICATIONS	STUDENT PAPERS

PRIMARY SOURCES

1	B. Mamabolo, A. Alblas, D. Brits. "Modern imaging modalities in forensic anthropology and the potential of low-dose X-rays", Forensic Imaging, 2020 Publication	5%
2	fac.utk.edu Internet Source	4%
3	hdl.handle.net Internet Source	1%
4	Laurie Talon, Thomas Sinegre, Thomas Lecompte, Bruno Pereira, Sylvie Massoulié, Armand Abergel, Aurélien Lebreton. "Hypercoagulability (thrombin generation) in patients with cirrhosis is detected with ST-Genesia", Journal of Thrombosis and Haemostasis, 2020 Publication	1%
5	repository.up.ac.za Internet Source	1%